DOCTOR OF PHILOSOPHY

An in vivo study of chromatin compaction in human cells

Visvanathan, Ashwat

Award date:
2013

DOCTOR OF PHILOSOPHY

An in vivo study of chromatin compaction in human cells

Ashwat Visvanathan

2013

University of Dundee

PhD Thesis

Presented in partial fulfillment of the degree of

Doctor of Philosophy to the University of Dundee

An In Vivo Study of Chromatin Compaction in Human Cells

Ashwat Visvanathan

School of Life Sciences
University of Dundee
Scotland

Supervised by Prof. Angus I. Lamond

September 2012

Table of Contents

List of Figures

List of Tables

Acknowledgements

I would first like to thank Prof. Angus Lamond for having accepted me as PhD student and having given me the freedom to work on the project. I would also like to thank him for the best lab environment that I have experienced to date. I would like to thank David Lleres who had helped me though the start of my project in the lab, with helpful discussions and training me in the FLIM technique. Most of this work would not have been possible, if not for the technique set up in the lab by him. I would like to thank Saskia Hutten for all the help ranging from finding antibodies to reminding me, the voltage settings to run a gel. I thank Mark Larance, Yasmeen Ahmad, Tony Ly and Dalila Bensaddek for all the help with the proteomics experiments. The best work environment does not come without the people in the lab, I thank the other lab members, past and present, Severine Boulon, Belinda Ryan, Andrea Pawallek, Fabio Avolio, Ursula Ryder, Moto Ono, Kayo Ono, Silvana van Koningsbruggen, Bart Engles, Armel Nicholas, Kate Bird, Aki Endo and Pesky Jens for all their help over the past four years.

Many thanks to Sonia Rocha, Susan Wyllie, Daniel Klotz and John James for help with experiments. I thank Paul Crocker, Arno Muller and Tom Owen Huges for having accepted me into the Wellcome Trust 4 year PhD program. I thank Inke Natke and Tom Owen Huges for being on my thesis committee and for all their help and suggestions regarding the project. I thank the Wellcome Trust for the generous funding of the project. I thank Gail Guild, Carol Urquhart and Nikki Forbes for handling all the administrative work regarding the project.

I would like to thank all my teachers, especially Prasanna Rajesh, Fathima Benazir and Prof S Shanmugasundaram, who inspired me to study biology and eventually do a PhD. I thank all my friends for all their help over the past four years.

I would finally like to thank my parents, Janarth, the rest of my extended family and my spiritual master Swami Nithyananda for all the help, in numerous ways, some of which they were aware of and some, that they were not.

Declaration

I, hereby, declare that (a) I am the author of this thesis; (b) that unless otherwise stated, all references cited have been consulted; (c) that the work in this thesis is an account of my work during the PhD; and (d) that it has not been previously accepted for a higher degree.

Ashwat Visvanathan

Abstract

Chromatin was one of the first sub-cellular structures to be described in early microscopy studies (Heitz 1928). Chromatin is formed from DNA, RNA, histones and other associated proteins. Within the nucleus, chromatin is arranged as compacted heterochromatin and decompacted euchromatin. During cell division, interphase chromatin compacts to form the mitotic chromosomes. The arrangement of chromatin within cells, with respect to its compaction state, has a number of implications for processes like transcription, DNA replication, DNA repair and more recently, in vision of nocturnal animals.

Most work on the study of chromatin compaction has been done with in vitro assembled nucleosome arrays. Chromatin has been shown to compact when the concentration of polyvalent cations increases, possibly due to negation of the repulsive forces of the negatively charged poly-phosphate DNA backbone. However, these in vitro studies do not necessarily reflect the in vivo chromatin environment. An example of this difference can be seen in the formation of the 30nm fibre in nucleosome arrays, which has not been found within mammalian nuclei, where it adopts a 'beads on a string' structure, even in more compact regions.

The work in this thesis studies chromatin compaction in mammalian cells using three different approaches. In the first part, I have performed experiments to study charge-based compaction of chromatin in intact nuclei. Studies on permeabilised

cells indicate that compaction of chromatin increases with an increase in concentration of polyvalent cations. This increase in chromatin compaction is charge and concentration dependent. The results show that the concentration required for maximal compaction in cells is similar to that required for nucleosome arrays assembled in vitro. Increasing the free intracellular concentration of Ca^{2+} also led to compaction of chromatin in intact cells.

In the second part of the thesis, I use ATP depletion, in vivo, as a model system to induce chromatin compaction in HeLa cells. Either inhibition of transcription, or inhibition of kinases, does not prevent this increase of chromatin compaction caused by ATP depletion. The ATP dependent change in compaction is also seen in mitotic chromosomes. There is a difference in charge distribution within the cell on ATP depletion, with an increase in Ca^{2+} and changes in localisation of $spermine^{4+}$, which could explain the increase in chromatin compaction.

In the third and final results section, I used a quantitative proteomics approach to systematically identify changes in the abundance of chromatin-associated proteins in HeLa cells, when chromatin is decompacted by Trichostatin A (TSA) treatment. TSA causes increased acetylation of lysine residues in histones, which leads to a loss of positive charge, and concominant decompaction of chromatin. Using MS based proteomics, I have identified a list of proteins that could potentially mediate TSA-dependent chromatin compaction.

Abbreviations

APC – Adenomatous Polyposis Coli

ATP – Adenosine triphosphate

BSA – Bovine Serum Albumin

CD – Chromodomain

dATP – Deoxyadenosine Triphosphate

dCTP – Deoxcytidine Triphosphate

dGTP – Deoxyguanosine Triphosphate

DMEM – Dulbecco's Modified Eagle's Medium

DMSO – Dimethyl sulphoxide

DNA – Deoxyribonucleic acid

DRB – 5,6-Dichloro-1-beta-D-RibofuranosylBenzimidazole

dTTP – Deoxythymidine Triphosphate

EDTA – EthyleneDiamine Tetra-Acetic acid

EGFP – Enhanced Green Fluorescent Protein

FISH – Fluorescent In Situ Hybridisation

FITC – Fluorescene Iso ThioCyanate

FLIM – Fluorescence Lifetime Imaging Microscopy

FRAP – Fluorescence Recovery After Photo-bleaching

FRET – Fluorescence/Foster Resonance Energy Transfer

G419 - genticin

HAT – Histone Acetyl Transferase

HDAC – Histone Deacetylase Complex

HMG – High Mobility Group

HP1 – Heterochromatin Protein 1

HPLC – High Pressure Liquid Chromatography

HRP – Horse Radish Peroxidase

MALDI – Matrix-Assisted Laser Desorption Ionisation

MS – Mass Spectrometry

PAF – PCNA Associated Factor

PBS – Phosphate Buffered Saline

PcG – Polycomb Group

ppm – part per million

PRC – Polycomb Repressor Complex

RNA – Ribonucleic acid

SAR – Scaffold attachment region

SILAC - Stable Isotope Labelling using Amino acids in Cell culture

SNRNP – Small Nuclear Ribonucleo Protein

TBP – TATA Binding Protein

TBS – Tris Buffered Saline

TEAB – Triethylaamine Bicarbonate

TSA – Trichostatin A

UV – Ultra Violet

v/v – volume/volume

w/v – weight/volume

Chapter 1

Introduction

1.1 Chromatin

DNA is the physiological carrier of genetic information for all living organisms. DNA is a polymer of deoxy-ribonucleotides with a negatively charged phosphate backbone and is unable to fold upon itself due to the inherent electrostatic repulsion from the phosphate backbone (Bloomfield 1996). All known eukaryotes store their DNA inside nuclei in the form of chromatin, wherein the DNA associates with proteins. Chromatin is an array of nucleosomes, which are composed of histones, DNA, RNA and other associated proteins. One of the functions of chromatin is in organisation of long genomic DNA, two metres for human cells, within the confined space of the nucleus, which is smaller by several orders of magnitude.

The basic unit of chromatin, the nucleosome, consists of an octamer of core histones with 147bp of DNA wrapped around in 1.7 left handed superhelical turns (Fig 1). The octamer is formed from two copies of the histones H2A, H2B, H3 and H4. The core histones have many positively charged lysine and arginine residues which can neutralize ~60% of the negative charge in DNA's phosphate backbone (Strick, Strissel et al. 2001).

The formation of the nucleosome by association of the DNA with the histone octamer results in a 5-10 fold compaction of DNA (Kornberg and Thomas 1974). The nucleosomes are attached to adjacent nucleosomes via a segment of DNA (~10-80bp) called linker DNA. The nucleosomes are not static complexes, but rather dynamic assemblages, where the nucleosome can dissociate or move/slide along the

DNA (Widom 1998; Hansen 2002). This poly-nucleosome chain, also referred to as 'beads on a string chromatin', can form a compact fibre that is approximately 30nm in width, thereby producing a compaction of about 50 fold. The 30nm fibre can be stabilised by linker histones and cations like Mg^{2+}, which has been well documented *in vitro* (Hansen 2002). In vivo evidence of the 30nm fiber was shown in starfish sperm by electron microscopy studies (Horowitz, Agard et al. 1994) and in isolated avian erythrocyte nuclei (Scheffer, Eltsov et al. 2011). The latter show that the observed structure was a two start left handed helix with approximately 6.5 nucleosomes per turn. However, cryo-EM studies of compacted mitotic chromosomes shows no evidence for the presence of the 30nm fiber (Eltsov, Maclellan et al. 2008).

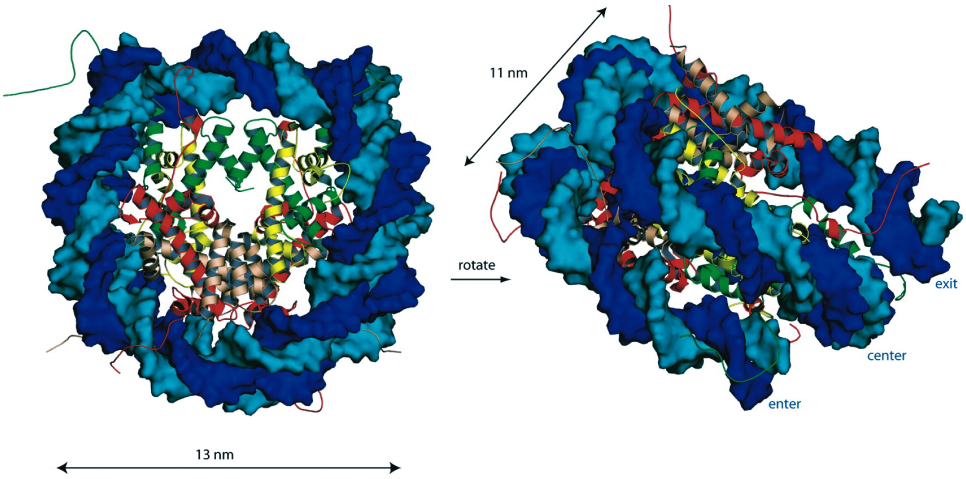

Fig 1 – The Atomic Structure of the Nucleosome Core Particle. Each strand of DNA is shown in different shade of blue. The DNA makes 1.7 turns around the histone octamer to form an overall particle with a disk-like structure. The histones H2A (red), H2B (pink), H3 (green) and H4 (yellow) are seen in the center of the disk-like structure. Figure adapted from (Khorasanizadeh 2004)

Electron spectroscopy imaging of chromatin from interphase cells shows the presence of the 10nm 'beads on a string' chromatin even in condensed chromatin domains defined as heterochromatin (Ahmed, Dehghani et al. 2010). There are, however, no reports confirming the presence of the 30nm fiber in interphase cells.

The accessibility of DNA to other regulatory proteins varies with its association with histones. The association of histones with DNA and subsequently with other non-histone proteins leads to different structural and functional states of chromatin. Changes in histone DNA interactions can be brought about by different mechanisms, such as

- changes in modification states of the histones (predominantly to their tail regions) (Kouzarides 2007).
- Nucleosome remodeling by protein complexes, that typically require energy from the hydrolysis of ATP (Clapier and Cairns 2009)
- Presence of histone variants. (Talbert and Henikoff 2010).

The chromatin from specific chromosomes has been shown to be organised as territories in interphase cells. These territories normally remain in defined domains throughout interphase.

1.2 Chromosome territories

Initial experimental evidence for the presence of chromosomal territories came from Stack et al., (Stack, Brown et al. 1977), who proposed that chromosomes remain in distinct territories through interphase. Later work from the Cremer group (Cremer and Cremer 2010) provided evidence that chromosomes were organised in territories within the interphase nucleus. Their experiments showed that micro-irradiation of a confined region of interphase nuclei led to DNA damage on specific chromosomes as revealed in a metaphase spread of the treated cells. The damage was not distributed over many chromosomes, as visualised by staining with antibodies against UV-damaged DNA. These experiments provided compelling evidence that interphase chromosomes were confined to specific territories and not intermingled throughout the nucleus.

Subsequently, chromosome-painting techniques were developed (Telenius, Pelmear et al. 1992) wherein fluorescent probes complementary to sequences of specific chromosomes would bind DNA of the given chromosome. This led to the visualisation of compartmentalised chromosomes in the interphase nucleus. The arrangement of the chromosome territories in the human lymphocyte nucleus was found to be non-random, with gene rich chromosomes, e.g. chromosome 19, consistently found in the nuclear interior, while the gene poor chromosome 18 was found closer to the nuclear periphery (Croft, Bridger et al. 1999). This arrangement is conserved among various primate species (Tanabe, Muller et al. 2002). The same trend was found to be true for all other chromosomes in humans, rodents, cattle and

birds as well (Cremer and Cremer 2010). This radial organisation was not observed in bovine pre-implantation embryos and its appearance was correlated with major gene activation and fully established in blastocysts (Koehler, Zakhartchenko et al. 2009). Spherical nuclei of lymphocytes showed radial arrangement that correlated with gene density. However, similar analysis on fibroblast cells with a flat ellipsoidal nucleus showed a radial arrangement that correlated with chromosome size, but gene density correlation was present at the sub-chromosomal level (Bolzer, Kreth et al. 2005).

Chromosomes have been shown to be distributed within nuclei, with formation of spatial clusters among specific chromosomes. These preferential positioning patterns among chromosomes have been shown in mouse tissue (Parada, McQueen et al. 2004) and in human lymphocytes (Khalil, Grant et al. 2007). Chromosome territories appear with manifold shapes composed of higher order chromatin domains when visualised by chromosome painting (Khalil, Grant et al. 2007). The outer surface of a given chromosome territory does not generally compartmentalise either gene dense, or transcriptionally active, chromatin. However, certain gene dense and/or transcriptionally active regions, like the *Hox* gene locus, are known to loop out of their chromosome territories (Chambeyron, Da Silva et al. 2005).

Differences in chromosome territory structure have been seen between the active (Xa) and inactive (Xi) X chromosomes. From initial staining patterns the Xi chromosome, known as the Barr body, seemed to be more compact than Xa (Lyon 1962). However, distinct differences in shape and structure exist between the active

and inactive forms, with surprisingly little difference in their total volume (Eils, Dietzel et al. 1996)

An example of chromosome territory reorganisation is seen in the rod cells of the retina in nocturnal mammals. The condensed heterochromatin is located at the centre of the nucleus in post-mitotic differentiated rod cells (Solovei, Kreysing et al. 2009). In diurnal mammals this arrangement is not seen and the heterochromatin is found localised to the nuclear periphery and around the nucleolus. The change in rod cells of nocturnal animals is thought to facilitate the nucleus to act as a micro-lens and help channel the photons to the photoreceptors.

Heterochromatin is often associated with the nuclear envelope, with silenced genes also associated with this sub compartment (Grewal and Jia 2007). This supports a concept of silenced genes being located closer to the nuclear periphery with the more active genes found more towards the interior of the nucleus (Schneider and Grosschedl 2007). Studies tethering genes to the outer compartments of the nucleus has shown to silence genes in certain studies while having no effect in others. In these experiments genes were tethered to the nuclear periphery, by fusion of LacO repeats close to the genes. These cells also expressed LacI protein fused to nuclear envelope associated proteins like lamin (Kumaran and Spector 2008) and Lap2β (Finlan, Sproul et al. 2008). The LacI protein binds the Lac O repeats and causes the chromatin to be localised to the nuclear periphery. The former study looked at the expression from an inducible promoter and showed no changes in the expression when tethered to the nuclear periphery while the latter study looked at endogenous

genes in the vicinity of the Lac O repeats and observed a reduction in their expression.

1.3 Heterochromatin and euchromatin

Heterochromatin was defined even before the discovery of DNA as the regions of the nucleus that stained strongly with basic dyes (Heitz 1928). Heterochromatin and euchromatin are terms used to describe the compaction state of chromatin (Fig 2). Heterochromatin was seen to be located along the nuclear periphery and surrounding the nucleolus, which can be seen clearly in light and electron micrographs (Comings 1980; Grewal and Jia 2007). The term heterochromatin is now used to include transcriptionally silent regions. Constitutive heterochromatin is, as the name indicates, always compact and is known to be enriched in repetitive, gene poor and late replicating regions (Woodcock and Ghosh 2010).

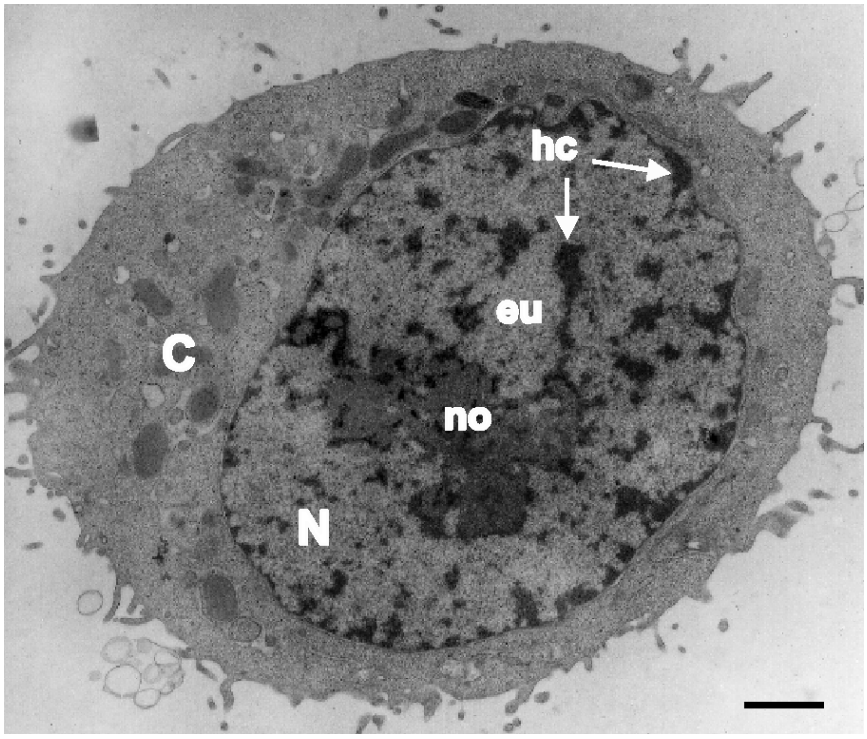

Fig 2 – Electron micrograph of a cell showing the cytoplasm (C), nucleus (N), nucleolus (no), euchromatin (eu) and heterochromatin (hc) (Scale bar 1µm). Image adapted from the book 'Principles of nuclear structure and function' by Peter R Cook, 2001.

Facultative heterochromatin can undergo reversible transitions from compact and inactive to more open and active states. It had been suggested that facultative heterochromatin can be defined as condensed, transcriptionally inactive regions that can decondense and allow transcription within temporal, spatial and parental/heritable contexts (Trojer and Reinberg 2007). Studies have shown chromatin decondensation of developmentally activated loci (Chambeyron, Da Silva et al. 2005; Wegel, Vallejos et al. 2005). This opposite is seen during embryogenesis and lymphocyte differentiation where the amount of facultative heterochromatin increases as expression of a number of genes is progressively shut down (Brown, Guest et al. 1997; Brown, Baxter et al. 1999). It was recently shown that tissue specific promoters when activated in their given tissue type move into the center of the nucleus, while the un-activated promoter DNA remained associated to the heterochromatin along the nuclear periphery in *C.elegans* (Meister, Towbin et al. 2010). The opposite is seen when the reverse occurs and differentiated cells are reprogrammed to become stem cells. These changes are normally accompanied by changes in expression of histone variants, post-translational histone modifications and the presence of other chromatin-associated proteins. Another important feature of heterochromatin is its propensity to spread to adjacent regions. Euchromatic genes brought into juxtaposition with heterochromatin by chromosomal rearrangements exhibit gene silencing, HP1 has been shown to be involved in this process (Hines, Cryderman et al. 2009). Heterochromatin may also have functional significance in rod photoreceptors in nocturnal but not diurnal animals, where the heterochromatin is concentrated in the centre of the nuclei and may act as a collecting lens to adjust to very low light conditions (Solovei, Kreysing et al. 2009).

1.4 Factors influencing higher order structure and dynamics of chromatin

Higher order chromatin structure is organised in an unstructured manner and the principles that define its organisation have been difficult to decipher. This is apparent in the names of some recent reviews such as “Chromatin higher-order structure: chasing a mirage?” (van Holde and Zlatanova 1995), “Higher-order structures of chromatin: the elusive 30 nm fiber” (Tremethick 2007), and “Chromatin fiber structure: where is the problem now?” (van Holde and Zlatanova 2007).

Variability of the ‘orderliness’ arises even at the most basic level of the various nucleosome variants, post-translational histone modifications and differences in the length of linker DNA. For example, the length of linker DNA between nucleosome core particles varies not only between species, but also between tissues of the same organism, and within a single nucleus (van Holde 1989). To compound the effect is the presence of various chromatin binding proteins and chromatin remodeling enzymes that can alter nucleosome spacing. Transmission electron microscopy of nuclei reveals a coarse differentiation between strongly stained heterochromatin either located close to the nuclear periphery or at the nucleolus (Comings 1980; Grewal and Jia 2007).

One can expect a number of chromatin states to be present within the nucleus. There are 130 known individual histone modifications (Tan, Luo et al. 2011).

Combined with the various other binding proteins and chromatin remodeling complexes the number of possible chromatin states increases.

Recent work has shown that these individual histone modifications may be working in concert, so as to provide a kind of 'histone code'. It was recently shown that the histone variant H2A.Z, H3 lysine9 tri-methylation and the protein HP1 might be acting in conjunction with each other in compacting chromatin (Fan, Rangasamy et al. 2004). The binding of HP1 to H3K9Me3 can in turn be inhibited by the phosphorylation of H3 serine 10, which would make the later a more 'dominant' modification (Hirota, Lipp et al. 2005). In other cases like the ATP-dependent chromatin remodeling protein, BPTF, which carries adjacent PHD and bromodomains, binding is enhanced with the presence of a second histone modification (Rando 2012). Certain protein complexes like the TIP60 complex involved in DNA repair have as many as 10 distinct histone modification-binding domains which increases the potential to bind chromatin carrying a combination of histone modifications (Rando 2012). Such examples have led to the possibility of a histone code that may be present in chromatin, where different combinations of histone modifications result in different structural and functional states. These modifications can also be passed on from the parent cell to the daughter cells, thereby maintaining the chromatin epigenetically. Their deregulation has been shown to be involved in diseases like cancer (Sharma, Kelly et al. 2010).

1.4.1 Histone modifications

There are at least 8 types of histone modifications including acetylation, methylation, phosphorylation, ubiquitylation, sumoylation, ADP ribosylation, deamination and proline isomerization (Kouzarides 2007). Recently, Minjia Tan et al., (Tan, Luo et al. 2011) discovered a novel modification - lysine crotonylation and 67 novel histone modification sites, taking the number of different histone modifications to 130. Most of the work has focused on the covalent modifications of acetylation, phosphorylation and methylation and their associated processes (Fig 3).

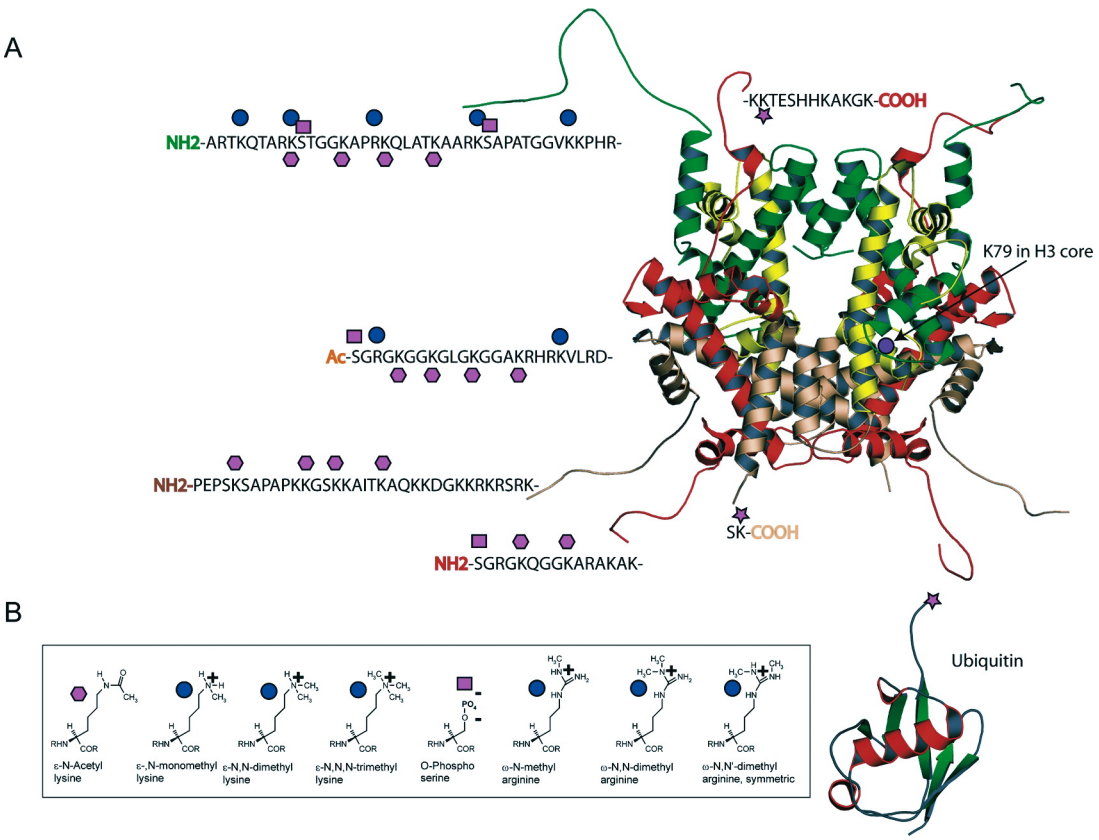

Fig 3 – (A) figure showing the methyl, acetyl, phospho and ubiquitin modification sites for histone H3, H4, H2A and H2B. The covalent modifications of the amino acids are shown are shown in (B). Image adapted from (Khorasanizadeh 2004)

Modifications may affect higher order chromatin structure by affecting either the contact between histones and DNA, or by recruiting other modifying/structural proteins. Of the know modifications, acetylation has been shown to affect chromatin structure, possibly by neutralising the charge of lysine (Lleres, James et al. 2009; Allahverdi, Yang et al. 2011). Phosphorylation of histones also has the ability to modulate higher order structure (Bannister and Kouzarides 2011).

Acetylation – Acetylation of histones has been shown to be associated with activation of transcription, DNA synthesis and DNA repair, all of which require an open chromatin structure (Kouzarides 2007). Acetylation of histones in the chromatin has been shown to de-compact chromatin with the loss of condensed heterochromatic regions (Lleres, James et al. 2009). This effect is attributed to the loss of +ve charge in the modified lysine resulting in diminished nucleosome – nucleosome association. In particular the effect of H4K16 acetylation has been shown to have the highest effect on the inhibition of compaction of nucleosome arrays in vitro. Histone 4 acetylation at lysine 16 leads to a loss of the positive charge of the acetylated lysine. This in turn, is likely to weaken the interaction between the amino terminus of H4 and an acidic patch on the surface of the histone H2A (Shogren-Knaak, Ishii et al. 2006). The presence of this single modification can inhibit the formation of the more compact 30mn fiber in reconstituted nucleosomes (Fischle, Wang et al. 2003). Acetylation of H4K16 in vitro, showed much higher inhibition of formation of the 30nm chromatin fiber when compared with combined acetylation of H4K5, H4K8 and H4K12 in a 12 nucleosome array (Chodaparambil, Barbera et al. 2007; Allahverdi, Yang et al. 2011). This shows that the effect of the

modification on specific residues may have different roles in modulating higher order structure.

Acetylation is catalysed by acetyl transferases, which are divided into three families known as GNAT, MYST, and CBP/p300 (Sterner and Berger 2000). The enzymes can modify more than one lysine, however some limited specificity can be seen. Most of the characterised sites for acetylation in histones are confined to the histone tails. The modification can be recognised as a binding site by bromo-domain containing proteins which includes $TAF_{II}250$, a subunit of the TFIID complex that initiates transcription (Jacobson, Ladurner et al. 2000).

De-acetylation is correlated with transcriptional repression. There are four classes of histone de-acetylases – the class I and class II de-acetylases, the class III NAD^+ dependent enzymes of the Sir family and class IV with a single member, HDAC11 (Bannister and Kouzarides 2011). These enzymes like the acetylases do not show much specificity and will deacetylate a wide range of substrates.

Phosphorylation – Phosphorylation of histones, similar to acetylation is a modification that can alter the charge of chromatin. Phosphorylation leads to increasing the negative charge on chromatin while acetylation reduces the positive charge of the histones. Histone phosphorylation has been associated with a variety of cellular processes, including transcriptional regulation, apoptosis, cell cycle progression, DNA repair, chromosome condensation, and developmental gene

regulation (Kouzarides 2007). Interestingly, phosphorylation has been implicated in both gene activation and formation of mitotic chromosomes, which require opposite compaction states and likely involve other modifications states acting in combination (Banerjee and Chakravarti 2011).

Phosphorylation has been shown to occur on serine, threonine, tyrosine and histidine residues of histones. One of the most well studied histone phosphorylation sites is Histone 3 serine10. Phosphorylation of this residue is a known mechanism for the release from chromatin of HP1, which binds tri-methyl H3K9 (Hirota, Lipp et al. 2005). This modification is also associated with mitotic chromosomes, along with H3S28 phosphorylation (Hsu, Sun et al. 2000). It has also been associated with the activation of NFKB regulated genes and immediate early genes, such as *c-fos* and *c-jun* (Macdonald, Welburn et al. 2005). Concomitant with the phosphorylation is also the binding of the 14-3-3 proteins which then leads to acetylation of histones (Macdonald, Welburn et al. 2005).

During DNA repair one of the earliest recognized responses is the phosphorylation of the histone variant of H2A, γ-H2AX (Rogakou, Pilch et al. 1998). This phosphorylation in budding yeast has been shown to recruit the ATP-dependent remodeling complex, INO80, and thereby facilitating double strand break repair (Van Attikum, Fritsch et al. 2004).

Methylation – lysines or arginines can either be mono, di or tri methylated. Unlike acetylation and phosphorylation, they do not alter the charge on the histone. They can be detected by chromodomain and PHD domain containing proteins. Lysine methylation is associated with both transcriptional activation and repression (Bannister and Kouzarides 2005). There are a number of methylases that can modify histones and are more specific in activity than histone acetyl transferases, (Kouzarides 2007).

The methylation sites associated with the activation of transcription are H3K4, H3k36 and H3K79. Tri-methyl H3K4 localizes to the 5' end of active genes, whereas tri-methyl H3K36 localises to the 3' end of genes (Joshi and Struhl 2005). Methylation of Histone3 lysine9 and lysine27 has been directly implicated in epigenetic inheritance and repression of transcription (Lachner, O'Sullivan et al. 2003). The HP1 protein binds to methylated H3K9 and is known to condense chromatin and thereby promote gene silencing. In a similar manner, the polycomb repressor complex binds methylated H3K27. HP1 can be removed with the phosphorylation of the serine residue at the 10^{th} position of histone H3 (Hirota, Lipp et al. 2005).

It has been shown that the histone variant H2A.Z and the protein HP1 might be acting in conjunction with each other in compacting chromatin (Fan, Rangasamy et al. 2004). This has led to the proposal of a histone code that may be present in chromatin modulating its structure and activity.

Ubiquitination – Ubiquitination of histone H2B has been shown to inhibit chromatin compaction in defined nucleosome arrays (Fierz, Chatterjee et al. 2011). H2B (K120) ubiquitination is mediated by RNF20/RNF40 and is associated with activation of transcription (Shiloh, Shema et al. 2011). It has been implicated in transcription and DNA repair processes. Modification of H2A (K119) is mediated by Bmi/Ring1A found in the polycomb complex and is associated with transcriptional repression. Ubiquitination is also implicated in DNA repair. DNA damage induced by UV results in modification of H3 and H4 and is required for the recruitment of the XPC repair protein (Wang, Zhai et al. 2006)

Other modifications of histones include Sumoylation, ADP ribosylation and proline isomeristion. These modifications have not been as well characterised as the other mentioned modifications and have been implicated in modulation of transcription (Kouzarides 2007).

1.4.2 Histone variants

A number of histone variants of H3, H2A and H1 exist in cells with most eukaryotes encoding only a single copy of the histones H4 and H2B (Talbert and Henikoff 2010). The variants replace the usual histones normally found on nucleosomes with varied functions. Functional significance has been attributed to a number of these variants. The most studied variants are described below.

Histone 3 -

The canonical H3 variants are denoted as H3.1 and H3.2, differing by a single amino acid. H3.3 differs by only four amino acids in most organisms from the canonical H3 variants. In HeLa cells canonical H3 variants are incorporated into chromatin during replication and DNA repair, whereas H3.3 undergoes either replication-coupled, or replication-independent, assembly and occurs predominantly at active genes (Talbert and Henikoff 2010). H3.3 is also incorporated into the male pro-nucleus during its de-condensation before the first round of zygotic replication (Orsi, Couble et al. 2009).

CENP-A is a centromere specific variant of Histone H3. Centromere specific variants are required for the assembly of the kinetochore (Talbert and Henikoff 2010). CENP-A chromatin is found in condensed heterochromatin. They have 50-60% identity with canonical H3 with no conservation of the histone tails. They do not show sequence specificity, but prefer AT-rich DNA (Churchill and Suzuki 1989).

Histone H2A –

The human canonical H2A variants vary at ten or more positions, with frequent variation at the last six residues (Talbert and Henikoff 2010). The global variants of H2A include H2A.Z and γH2A.X.

H2A.Z is encoded by two genes in humans and vary by three residues. H2A.Z is found in nucleosomes at transcription start sites where they have been shown to help in the recruitment of RNA polymerase II (Hardy, Jacques et al. 2009). Another function attributed to this histone variant is in centromere structure. Higher compaction can be brought about by the histone variant H2A.Z, whose X-ray crystal structure shows a larger acidic patch (Suto, Clarkson et al. 2000) at the nucleosome surface which appears to strengthen nucleosome-nucleosome interaction of the chromatin surrounding the centromeres (Greaves, Rangasamy et al. 2007). H2A.Z has also been attributed to have roles in gene activation and silencing, nucleosome turnover, DNA repair, heterochromatin, boundary element and chromatin fibre formation, suppression of antisense RNAs, embryonic stem cell differentiation and antagonizing DNA methylation (Talbert and Henikoff 2010).

γH2A.X differs from the canonical H2A by the presence of a C-terminal motif Ser-Gln-(Glu/Asp)- hydrophobic residue. The motif can become rapidly phosphorylated at serine by the kinases – ATM, ATR and DNA-PK to form YH2A.X in response to double stranded breaks. γH2A.X helps recruit DNA repair proteins, histone modifying enzymes and chromatin remodeling complexes (Altaf, Auger et al. 2009). γH2A.X is also known to be involved in meiotic silencing of unpaired chromatin and cell cycle

regulated roles on the inactive X chromosome (Talbert and Henikoff 2010). A common feature to the associated processes involves chromatin remodeling.

Histone H1 –

H1 has been shown to be required for compacting chromatin. H1 depleted arrays do not readily form the 30nm fibre (Schwarz and Hansen 1994), possibly due to the loss of charge neutralisation. Modest depletion of H1 from cells leads to a reduction in the nucleosome repeat length in some tissues, while severe depletion being fatal in mice and drosophila(Fan, Nikitina et al. 2003); (Lu, Wontakal et al. 2009). There is a strong linear relationship between H1 concentration and nucleosome repeat length (Woodcock 2006).

There are 7 somatic variants of histone H1 - H1.1, H1.2, H1.3, H1.4 and H1.5 which are reported to be expressed in a replication dependent manner, whereas H1.0and H1X are replication independent (Terme, Sese et al. 2011). H1.0 is known to accumulate in terminally differentiated cells (Terme, Sese et al. 2011). In mice, knocking out of one of the subtypes leads to the compensatory up-regulation of other variants (Fan, Sirotkin et al. 2001). In a study on T47D derived breast cancer cell line, it was shown that knockdown of H1.2 and H1.4 lead to changes in cell cycle progression with a decrease in cells in S phase, while knockdown of other histone variants H1.1, H1.3 and H1.5 had no effect (Sancho, Diani et al. 2008). Histone H1 variants are differentially expressed upon differentiation with H1.0 levels being increased, while abundance of H1.3 and H1.5 decreases (Terme, Sese et al. 2011).

1.4.3 Proteins associated with compaction of chromatin

A number of proteins associate with nucleosomes and can play a role in modulation of chromatin structure. This association of the proteins with chromatin can be influenced by the accessibility and post-translational modification state of the nucleosomes. Some of the proteins that are known to associate with chromatin and influence chromatin structure dynamics include High Mobility Group (HMG) proteins, Heterochromatin Protein 1 (HP1), Polycomb Repressor Complex (PRC) and ATP dependent remodeling proteins.

HMG Nuclear Proteins

HMG proteins are classified into three classes as the HMGA, HMGB the HMGN. HMG proteins have a similar biochemical and biophysical properties and show the presence of a long negatively charged carboxy-terminal tail that serves a regulatory function (Gerlitz, Hock et al. 2009). The HMG proteins are known to have a role in embryonic development, regulation of transcription and modulation of DNA repair. The three families HMGA, HMGB and HMGN are distinguished from each other by their unique DNA binding motifs.

HMGA family proteins preferentially bind to A/T rich B form DNA (Reeves and Nissen 1990). One of the best characterized roles of the HMGA proteins is in the co-ordination of the formation of DNA protein complexes at A/T rich promoters for transcriptional activation (Fashena, Reeves et al. 1992). The HMGA proteins have also been shown to recruit histone acetylases to promoter regions (Merika and

Thanos 2001). HMGA proteins can cause structural alterations of DNA without requiring ATP (Reeves and Beckerbauer 2001). During the G2/M phase of the cell cycle HMGA proteins are known to be phosphorylated by cdc2 kinase leading to decreased affinity of the protein for DNA, it is likely to be associated with marked changes in chromosomal structure (Nissen, Langan et al. 1991; Reeves, Langan et al. 1991). HMGA1 protein has been shown to co-localise with H1 and Topo II at Scaffold attachment regions (SARs), which are thought to constitute the structural backbone of the metaphase chromosome. It has been proposed that the competition between H1 and HMGA1 to bind to these regions alters the compaction state of the chromosome. Hence reduced affinity to HMGA1 to these regions due to modification by cdc2 during G2/M might lead to the binding of H1 and the subsequent compaction of the chromatin (Zhao, Kas et al. 1993). However, other studies indicate that HMGA might be involved in compaction as they are seen associated and are essential components in heterochromatin domains in cells that have undergone senescence (Narita, Krizhanovsky et al. 2006). Being amongst the most highly modified proteins in the nucleus, different modifications might be responsible for the two contradictory functions.

HMGB proteins are characterized by two tandem DNA binding boxes called HMG box domains, followed by an unstructured 30 acidic amino acid tail. The HMG boxes bind the minor groove of DNA and introduce a bend of 90° or more (Reeves 2010). HMGB proteins are known to be involved in transcription, replication, V(D)J recombination, DNA repair and other activities (Reeves 2010). HMGB proteins affect transcription by recruiting chromatin remodelers and other transcription factors to

DNA. It has been observed to be bound to apoptotic chromatin and might be responsible for regulating the condensation of chromatin. HMGB is released from necrotic cells, thereby signaling to the surrounding tissue, inducing them to divide, migrate, activate inflammation and/or start an immune response. It is also released from immune cells and is a late mediator of sepsis (Wang, Bloom et al. 1999).

HMGN proteins contain a nuclear localisation signal, a nucleosome binding domain and an acidic tail called the chromatin-unfolding domain (Bustin 2001). These proteins are found only in vertebrates and are linked to cellular differentiation. They are found in abundance during mouse embryogenesis with a progressive reduction through development and differentiation. However, this reduction in protein levels does not occur in continuously renewing cell types and over expression inhibits differentiation (Korner, Bustin et al. 2003; Furusawa, Lim et al. 2006). HMGN proteins primarily function by promoting chromatin de-compaction, and thereby aid in DNA related processes like transcription, replication and DNA repair. The process mediating compaction is however not known (Reeves 2010). HMGNs are also the only non-histone proteins known to specifically bind inside the nucleosome between the gyres of DNA and the histone octamer core (Bustin 2001)

Heterochromatin Protein 1 (HP1)

HP1 is a non-histone chromosomal protein predominantly found in the condensed heterochromatin regions of the chromatin. The protein is conserved and found in

almost all eukaryotes. It contains two highly conserved domains, an N-terminal Chromodomain(CD) that binds methylated H3K9 and a chromoshadow domain (CSD) that has been implicated in a number of protein-protein interactions, including dimerisation . A hinge region (Hin) of variable length joins the two domains. Humans have three isoforms of the protein named – HP1α, HP1β and HP1γ, with the fly counterparts being HP1a, HP1b and HP1c (Kwon and Workman 2011).

HP1α and HP1β are known to localise to heterochromatin, whereas HP1γ has been seen predominantly in euchromatin and functions in gene specific silencing (Ayyanathan, Lechner et al. 2003). Studies have revealed an interaction between the hydrophobic pocket of the HP1 CD and methylated lysine 9 of histone H3 (H3K9me) (Jacobs and Khorasanizadeh 2002; Lomberk, Bensi et al. 2006). The three proteins also undergo post translational modifications like acetylation, phosphorylation, methylation, ubiquitination, sumoylation and formylation some of which are known to define localisation and function of the protein (Kwon and Workman 2011). Hyper-phosphorylation of HP1 is associated with heterochromatin formation, while phosphorylation of the Ser83 of HP1γ defines a subpopulation that is specifically associated with euchromatin (Lomberk, Bensi et al. 2006). Recent studies have also shown a role for HP1 proteins in the DNA damage response. The proteins are recruited to DNA damage lesions, which requires the chromoshadow domain in nematodes, loss of HP1 renders them highly sensitive to DNA damage (Luijsterburg, Dinant et al. 2009).

The Polycomb Group (PcG) complex

The Polycomb Group (PcG) complex has been implicated in chromatin compaction and gene regulation. The PcG complex has been shown to regulate a number of genes that are crucial regulators of genomic programming and differentiation. They were initially shown to act at the same target genes as Trithorax and related proteins with antagonistic effects (Schwartz and Pirrotta 2008).

There are two principal complexes, PRC1 and PRC2. The PRC2 complex methylates lysine27 of histone3, which is then bound by PRC1 through a chromodomain (Schwartz and Pirrotta 2008). A second histone modification associated with PcG complexes is the ubiquitylation of histone H2A K119 mediated by the dRING (RING1B in mammals) component of PRC1. Loss of H2A ubiquitination leads to a loss of the repressive activity although H3K27 tri-methylation still persists (Wang, Wang et al. 2004).

Compaction of chromatin in vitro can be observed by electron microscopy where nucleosome arrays can be compacted in the presence of PRC1 (Grau, Chapman et al. 2011). This study identified the subunit responsible for the compaction of chromatin. Surprisingly, when the mouse and drosophila PRC1 complex subunits were tested for the compaction of chromatin, the compacting proteins form mouse (M33) and Drosophila (PSC) were not homologues of each other. Structure/function analysis of the two proteins showed the presence of a highly basic region with a predicted, disordered secondary structure that causes compaction of the nucleosome array (Grau, Chapman et al. 2011), possibly by charge neutralisation of chromatin.

ATP dependent chromatin remodelers

Snf2 family ATPases cause changes of nucleosome positioning with the hydrolysis of ATP. They are required for various processes like chromatin assembly, DNA replication, DNA repair and recombination, chromosome segregation and gene regulation (reviewed in (Clapier and Cairns 2009)). The ATP dependent chromatin remodelers exist as multi sub-unit complexes. All complexes have a large core polypeptide that has a region homologous to the helicase-related Snf2 family ATPase. They can be classified into four families as SWI／SNF, ISWI, CHD and INO80 (Ghaemmaghami, Huh et al. 2003; Clapier and Cairns 2009; Weiss, Schrimpf et al. 2010; Hargreaves and Crabtree 2011) based on the ATPase and its flanking regions, with a total of 17 proteins in yeast and 37 proteins in human genomes. Remodeling complexes are also highly abundant in the nucleus (Ghaemmaghami, Huh et al. 2003; Weiss, Schrimpf et al. 2010) with some complexes being more abundant than others. The remodeling complexes have domains such as the bromodomain, chromodomain and the plant homeodomain, which are known to interact with specific histone modifications and than could facilitate the localisation of the corresponding chromatin remodeling complexes to specific regions (Clapier and Cairns 2009). Chromatin remodelers are regulated by specific proteins and by post translational modifications like phosphorylation, acetylation and PARylation (Clapier and Cairns 2009).

1.5 Biological implications of chromatin compaction

A number of factors have been implicated with the compaction of chromatin, as described in the sections above. However, the compaction state of chromatin affects its suitability for a number of cellular processes. Chromatin compaction has been shown to have implications is transcription, mitosis and even sight of nocturnal mammals.

Transcription has been shown to be more active in regions in de-compacted chromatin. However, the question of weather the compaction state is a cause or consequence of transcription has not been conclusively shown. It has been shown in plants that transcription of some genes preceded de-compaction of chromatin (Wegel, Vallejos et al. 2005). However it has also been show in vitro that with higher levels of Mg^{2+}, which leads to more compacted chromatin, causes abrogation of transcription (Hansen and Wolffe 1992). Recent work has also shown that the Histone H3 Lysine 27 methylation by the PRC2 complex was more efficient when nucleosomes were separated with a shorter linker sequence, indicating that PRC1 bound heterochromatin originates from partially compacted chromatin (Yuan, Wu et al. 2012). This could indicate that formation of heterochromatin could be preceded by other events, possibly inhibition of transcription.

However, studies on the Hox locus genes in mice have shown transcription from the hox genes coincided with the specific loci being translocated outside the chromosome territories, arguing that decompacted chromatin was required for

transcription (Chambeyron, Da Silva et al. 2005). Similar conclusions were reached with experiments tethering genes to the nuclear envelope, known to have more condensed chromatin, leading to lower levels of transcription from genes with endogenous promoters (Finlan, Sproul et al. 2008). However, tethering genes with strong inducible promoters did not influence levels of transcription (Kumaran and Spector 2008). Thus, chromatin compaction could affect transcription form different promoters to differing extents. Differentiation of cells has also been shown to be shown be associated with the presence of more compact chromatin (Brown, Guest et al. 1997; Brown, Baxter et al. 1999).

The compaction of all of chromatin also happens with each cell cycle during mitosis. This is reversed after mitosis with the retention of the differentially compacted state of the interphase nucleus. A number of epigenetic factors have been implicated in the maintenance of these heterochromatin and euchromatin regions (Kouzarides 2007). Heterochromatin is mainly seen associated with the nuclear membrane. However, in the rod cells of nocturnal animals, the opposite orientation has been observed with the condensed heterochromatin localised to the interior of the nucleus (Solovei, Kreysing et al. 2009). This arrangement has been implicated in the ability of these animals to more effectively collect light, thereby acting as a micro lens.

The effects of chromatin compaction have been implicated in a number of biological processes, ranging from transcription to eyesight. The processes required for the maintenance of compaction states chromatin have not been well studied. Most

evidence of chromatin compaction has been derived from in vitro experiments. The read out for most of these experiments has been the formation of the 30nm fibre, which has not been shown to exist in mammalian cells (Tremethick 2007). This indicates that the results and conclusions derived from in vitro experiments may not necessarily hold true in vivo.

A number of proteins have been shown to be associated with chromatin of different compaction states. The mechanism of these proteins has not been well elucidated. Some of the proteins involved with compaction have bee shown to have unstructured charged regions, and thus implicated in maintenance of chromatin compaction by charge neutralization (Grau, Chapman et al. 2011). However the role of charge in maintenance of chromatin in vivo is not known, although well studied in vitro.The role of proteins implicated in chromatin compaction discussed have been shown mainly by association and any direct evidence comes from in vitro studies.

Chromatin compaction thus influences a number of biological processes and the factors influencing it will also affect the down stream processes. Most of our knowledge of the factors influencing chromatin compaction comes from in vitro experiments, which may or may not hold true to chromatin in vivo. Thus, identification of factors influencing chromatin compaction in vivo will consequently lead to the identification of factors that affect processes like transcription, mitosis and DNA repair amongst others.

1.6 Salt-Induced chromatin Compaction

DNA, being a polymer of deoxyribonucleotides with a negatively charged phosphate backbone, is unable to fold upon itself due to the inherent electrostatic repulsion (Bloomfield 1996). DNA complexes with positively charged histones, which can neutralise approximately 60% of the backbone charge (Strick, Strissel et al. 2001). The tails of the histones are required for the intra and inter array nucleosome-nucleosome interactions and are also required for regulation of transcription and replication (Hansen 2002). Studies have shown that the tails act independently and the effect is cumulative, with the H4 and H3 tails being more effective in bringing about compaction in nucleosome arrays (Gordon, Luger et al. 2005).

Most studies involving charge based compaction have been performed in well defined nucleosome arrays (Simpson, Thoma et al. 1985), prepared in vitro by assembly of their DNA and histone components. The condensation of nucleosome arrays in vitro is characterized by two transitions. The first is the intra-array nucleosome association to form a 30mn fibre, followed by aggregation of the fibres to form higher order structures (Korolev, Allahverdi et al. 2010). The common methods for measuring chromatin compaction of nucleosome arrays include differential centrifugation assay and calculation of sedimentation velocity. The differential centrifugation assay involves the nucleosome arrays being suspended in the buffer of choice, incubated at room temperature and then centrifuged at 13,000g in a micro centrifuge and then calculation of the percentage of the sample present in the supernatant (Schwarz and Hansen 1994). Upon complete intra-array

nucleosome association brought about by increasing buffer polyvalent cation concentration, 100% of the arrays are pelleted.

Analysis of sedimentation velocity gives another measure of compaction of the nucleosome array. In completely saturated 12 nucleosome arrays, it was observed that the sedimentation coefficient increases upon increasing the ionic concentration of the buffer. The increase in sedimentation coefficient correlates directly with the compaction of the chromatin (Schwarz and Hansen 1994). The study also found that regularly spaced nucleosomal arrays equilibrate between unfolded and highly folded conformations in <2mM Mg^{2+} (between 29S-55S). The highly folded conformations (55S) correspond to the formation of the 30nm fibre. The highly folded fibres then self-associate at Mg^{2+} concentrations above 2mM (>>55S) (Schwarz and Hansen 1994) (Fig 4).

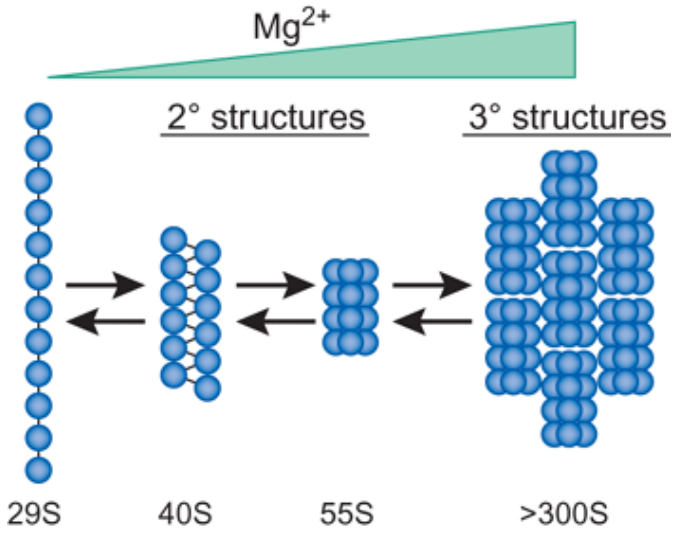

Fig 4 – Schematic showing the different states of a nucleosome array with increasing Mg concentration (Caterino and Hayes 2007).

Most of the initial studies on nucleosome arrays were done with increasing concentrations of monovalent and bivalent cations. However, polyvalent cations like spermidine and spermine, with charges of +3 and +4 are found in physiological conditions.

In a study by Korolev et al., (Korolev, Allahverdi et al. 2010) the effect of cations with charges ranging from +1 to +4 was analysed. It was found that increasing the valency of the cation led to a drastic reduction in the concentration of the cation required for the formation of the 55S structure.

It has been shown that histone tails facilitate chromatin compaction (Gordon, Luger et al. 2005). Recent studies have looked specifically into the roles of Histones H3 and H4 tails in chromatin compaction with increasing magnesium concentration. The histone H3 tails can form intra-array and inter-array nucleosome interactions. Intra-array nucleosome interactions predominantly occur in low ionic concentrations and increasing the polyvalent cation concentration results in inter-array associations. The nucleosome array is though to be present in the extended 'beads on a string' conformation at low ionic concentrations. As the Mg^{2+} concentration is gradually increased, there is an increase in intra-array nucleosome interactions leading to the formation of the 30nm fibre. Further increase in Mg^{2+} leads to inter-array interactions with the formation of higher order structures in vitro. Formation of the 30nm fiber typically occurs at a concentration of 2mM Mg^{2+} (Zheng, Lu et al. 2005).

The ability of these histone tails to form inter-array interactions/associations is also a measure of their ability to form tertiary structures and thereby aid chromatin compaction. In studies conducted by Pu-Yeh Kan et al., (Kan, Lu et al. 2007; Kan, Caterino et al. 2009), both histone tails showed no inter-array associations when Mg^{2+} concentrations were between 0mM and 2mM. At higher concentrations of Mg^{2+} inter-array interaction were observed, saturating at 6-8mM Mg2+ (Kan, Lu et al. 2007; Kan, Caterino et al. 2009). It has also been shown that increased concentrations of Mg^{2+} inhibit transcription by RNA Pol III on vitro chromatin templates (Hansen and Wolffe 1992).

Most knowledge about salt dependent compaction is from reconstituted arrays, systems, most of which lack the linker histone H1 (Schwarz and Hansen 1994). The data, however valuable, do not accurately represent the nuclear environment of chromatin, which has a number of other macromolecules associated with the chromatin. To study the role of cations in a more native environment, we have studied compaction using the FLIM-FRET technique with varying polyvalent cation concentrations.

1.7 Fluorescence Lifetime Imaging Microscopy (FLIM) for the quantification of chromatin compaction

Fluorescence is the emission of light by a substance after its having absorbed either visible light, or other electromagnetic radiation. FLIM refers to the measurement of time between the excitation of a fluorophore (fluorescent substance) and its subsequent emission of a photon (Bastiaens and Squire 1999; Wallrabe and Periasamy 2005; Treanor, Lanigan et al. 2006; Lleres, Swift et al. 2007). When a fluorophore is excited by the absorption of a quantum of light, a valence electron is boosted to an orbit of higher energy. This excited fluorophore, with its energy stored in its valence electron, then returns to its ground state by emitting the absorbed energy as light (Fig 5 A). In fluorescence, the emitted photon is of a lower energy and hence longer wavelength to the energy absorbed from the exciting radiation (Lakowicz 2006). An example is Enhanced Green Fluorescent Protein (EGFP), which has excitation maxima at 488nm and emission maxima at 509nm (Reichel, Mathur et al. 1996). The energy loss, observed as the increase in wavelength of the emitted photon, is transferred to the environment. The average time spent by a molecule in the excited, higher energy state is referred to as fluorescence lifetime and is typically in the nanosecond time scale (Lakowicz 2006) (Fig 5 A). The fluorescence lifetime of a fluorophore is dependent on the local physical environment. Changes to the fluorescence lifetime of a given fluorophore can occur due to factors like Fluorescence Resonance Energy Transfer (FRET) (Lakowicz 2006) and collisional quenching (Vishwanath, Zhong et al. 2006) (Fig 5 B). FRET occurs when the presence

of a second fluorophore with appropriate spectral properties that enable it to absorb energy from the excited fluorophore. The primary excited fluorophore is referred to as the donor and the energy accepting fluorophore, the acceptor. For two fluorophores to act as a FRET pair, the spectral range of donor emission should overlap the spectral range of acceptor absorption. For transfer of energy between the two fluorophores, they have to be in close proximity. The distance between the acceptor and donor should be less than 10nm (Forster 1949). Thus only when fluorophores are in close proximity, will FRET be possible. The efficiency of FRET can be calculated using the equation :

$$\mathbf{E = R_o^6/(R_o^6 + r^6)}$$

Where 'E' denotes FRET efficiency, 'Ro', also known as the Foster distance, is the distance at which 50% of the energy is transferred between the donor and the acceptor and 'r' is the actual distance between the donor and the acceptor (Forster 1949). Ro is a constant and depends on a number of factors, including the fluorescence quantum yield of the donor in the absence of acceptor, the refractive index of the solution, the dipole angular orientation of each molecule, and the spectral overlap integral of the donor and acceptor (Forster 1949). FRET occurs over greater than interatomic distances, without conversion to thermal energy, and without any molecular collision. As the FRET efficiency is inversely propotional to the distance between the fluorophores, the closer they are, higher will be the FRET efficiency.

Collisional quenching refers to the decrease in fluorophore quantum yield (the ratio of emitted to absorbed photons) that occurs when an excited fluorophore returns non-radiatively to the ground state due to physical interactions (collisions) with an agent (quencher) (Vishwanath, Zhong et al. 2006). Thus, in a highly crowded molecular environment, there will be a higher rate of collisions and this will lead to increased collisional quenching. Collisional quenching also leads to a decrease in the lifetime of the fluorophore.

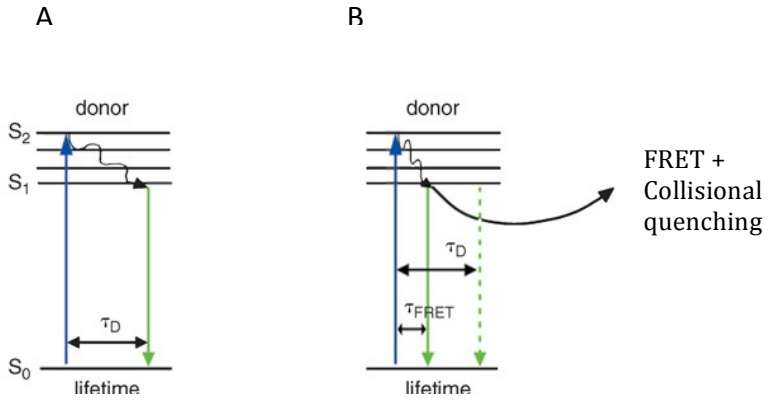

Fig 5 – Jablonski diagram showing the different energy states associated with a fluorophore. The blue line indicates the increase in energy by absorption and the green line indicates emission with τ representing lifetime. S_0 represents the ground state while S_1 andS_2 indicate excited energy states of the fluorophore. (A) Jablonski diagram showing the fluorophore energy states in the absence of quenching. (B) Jablonski diagram showing the fluorophore energy states with a reduction in fluorescence lifetime in the presence of FRET and collisional quenching.

Quantification of chromatin compaction was done in a $HeLa^{H2B\text{-}2FP}$ cell line co-expressing histone H2B tagged to either EGFP, or mCherry, fluorescent proteins at their N and C termini respectively (Lleres, James et al. 2009). EGFP and mCherry fluorescent proteins can participate in a FRET reaction, as donor and acceptor

fluorophores, respectively (Shaner, Campbell et al. 2004). The labeled histones have been shown to be incorporated into nucleosomes (Kimura H Fau - Cook and Cook 2001). Hence, depending on the level of compaction, the proximity between the histones and thereby the fluorophores, will vary. In regions of low chromatin compaction the nucleosomes will be further away from other nucleosomes and thus will result in low FRET interactions and regions with compacted chromatin will show high FRET efficiency. In a similar manner, as the chromatin compacts one can assume that the molecular environment will be more crowded and result in higher levels of collisional quenching, which, along with FRET, leads to lower lifetime values.

Fluorescence lifetime can be obtained using either time domain or frequency domain measurements. In time domain measurements, the sample is excited with a short pulse of excitation light, which is normally shorter than the decay time of the sample. The time dependent fluorescence emission intensity is measured following the pulse. The lifetime is then calculated from the slope of the resulting emission intensity. The alternative method is the frequency domain or phase modulation method, wherein the intensity of the incident light is modulated, typically in a sine wave manner (Lakowicz 2006). When a fluorescent molecule is excited in this manner, it is forced to respond with the same modulation frequency in its emission. The lifetime of the fluorescence will cause the emitted light to lag the in time relative to the excitation light. The fluorescence lifetime can be calculated form this phase shift. The lifetime of the fluorophore also causes a decrease in the peak to peak height of the emitted light relative to the excitation light (Fig 6). This results due to the fact that some of the fluorophores excited at the peak of excitation light still

continue to emit while the excitation in minimal, hence giving a higher than expected intensity of emitted light. This is called demodulation and can also be used to calculate the fluorescence lifetime.

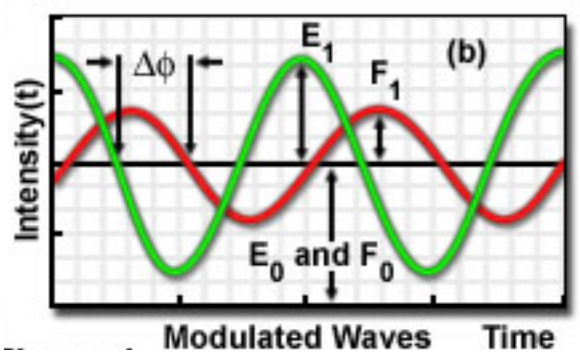

Fig 6 – shows the difference in phase (Δφ) and amplitude (E_1, F_1) between the fluorescence excitation (green) and emission (red) profiles. From these measured valued, the fluorescence lifetime can be calculated by using a standard reference.

Lifetime measurements for the experiments described in this thesis were obtained in the time domain using the time correlated single photon counting technique (TCSPC) (Lleres, James et al. 2009). This technique is based on the detection of a single photon after a short excitation pulse from a laser capable of producing femtosecond pulses at a high repetition rate. Two-photon excitation was achieved using a Ti:Sapphire laser (Coherent) that provided sub-200-femtosecond pulses at repetition rate of 90MHz. Upon release of the excitation pulse, a signal is sent to the constant function discriminator (CFD) which accurately measures the arrival time of the pulse at the sample. This signal is passed to the time to amplitude converter (TAC). The TAC generates a voltage ramp on arrival of the signal from the CFD. The voltage ramp, is a voltage that increases linearly with time in the nanosecond time

scale. The emitted photon, from the fluorophore being imaged, is detected with a photomultiplier tube. The arrival time of the emitted photon is calculated by another CFD, which sends a signal to stop the voltage ramp in the TAC. The voltage in the TAC is now proportional to the time delay between excitation and emission signals. The voltage can be amplified if needed and is converted to a numerical value by an analog to digital converter. This value corresponds to the lifetime of a single photon from the imaged fluorophore. After every cycle, the voltage in the TAC is reset for the next cycle. The use of a low level intensity of excitation light with a high pulse rate results in a low probability of emission of a photon per cycle. The probability of a photon emitted per excitation pulse is much less than 1. Therefore the probability of detecting more than one photon per excitation pulse is also very low. The repetition rate of 90MHz, there will be 11ns of dead time between each pulse. This dead time of 11ns is much longer than the lifetime of the fluorophore. The average lifetime measured for H2B-GFP is approximately 2.3ns. This will prevent the emission from one excitation pulse being recorded after the subsequent excitation cycle.

This process is repeated a number of times for a given pixel. The obtained data per pixel (number of photons against the lifetime) is plotted as a histogram, which is the decay curve of the fluorophore under the given conditions.

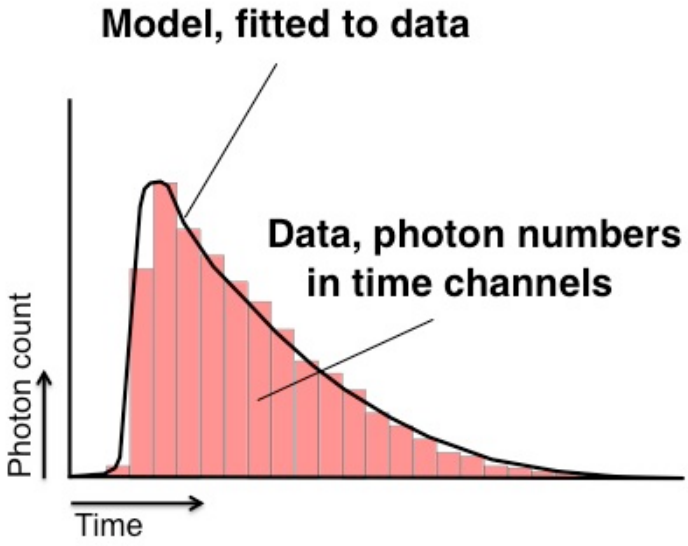

Fig 7 – Fitting of a curve on the data obtained for each pixel to determine fluorescence lifetime.

From the histogram, the fluorescence lifetime is obtained by fitting the curve with an appropriate model while taking into account the instrument response function. A single exponential model was used to fit the data. The instrument response function takes into account, the shape of the laser pulse. The process is done for every single pixel in the imaged area and a lifetime map for the sample is obtained (Lakowicz 2006). Thus, the lower the lifetime of a pixel, the higher the FRET and collisional quenching, which indicates that the histones are closer together and more compact.

For experiments in this thesis, measurements were carried out using a multiphoton-enabled confocal microscope, the Bio-Rad Radiance2100MP equipped with a Coherent Cameleon Diode-Pumped Laser. Photon counting was controlled by the SPCM software of the SPC-830 module (Becker & Hickl) (Becker 2008). The lifetime values from the obtained data were calculated a using the SPCImage software.

1.8 Mass spectrometry

Mass spectrometry is a technique used to measure the mass to charge (m/z) ratio of charged molecules. From the measured m/z values, the composition of the peptides and other chemical compounds can be elucidated. In a typical MS procedure, the sample to be analysed is vaporised and ionised in the ion source, the mass analyzer then sorts the ions by their masses to charge ratios with the help of electromagnetic fields. Finally, a detector quantifies the abundance of each ion and the result is obtained as a graphical output.

The elucidation of the structure of large polar biomolecules like peptides was made possible by the invention of ionisation techniques like electrospray ionisation (Fenn, Mann et al. 1989) and matrix-assisted laser desorption ionisation (MALDI) (Karas and Hillenkamp 1988). The experiments described in this thesis were performed using the electrospray technique.

Electrospray ionisation mass spectrometry (ESI-MS) was developed for use in biological mass spectrometry by Fenn et al., (Fenn, Mann et al. 1989). Electrospray ionization accomplished the transfer of ions from solution to the gas phase and is extremely useful for the analysis of large, non-volatile, chargeable molecules such as peptides and nucleic acid polymers. In this method, the analyte, in a solvent is pumped at a low flow rate through a needle at a high voltage to electrostatically disperse or electrospray, small, micrometre sized droplets containing the analyte. There is a counter flow of heated nitrogen gas, which causes the solvent in the

droplet to vaporize. These droplets rapidly evaporate and thereby imparts the charge onto the analyte molecule. As the process takes place in atmosphere, the process is gentle and usually occurs without fragmentation of the analyte, which is beneficial for the elucidation of the structure of peptides. The analyte, now in the gas phase, is transferred to the mass spectrometer.

The peptide mixtures to be analysed can be complex. Prior to ionization, peptides are first separated by reverse phase High Pressure Liquid Chromatography (HPLC) using a C18-bonded silica analytical column. The C18 chains covalently attached to the silica of the column will bind peptides with hydrophobic residues. The hydrophobicity of a peptide is determined by the number of hydrophobic amino acids. The separation of peptides is then accomplished by gradually decreasing the polarity of the eluent. By this, the lower the hydrophobicity a peptide, the faster it is eluted and eventually fed into the electrospray. The complex peptide mixture can thus be separated for better resolution.

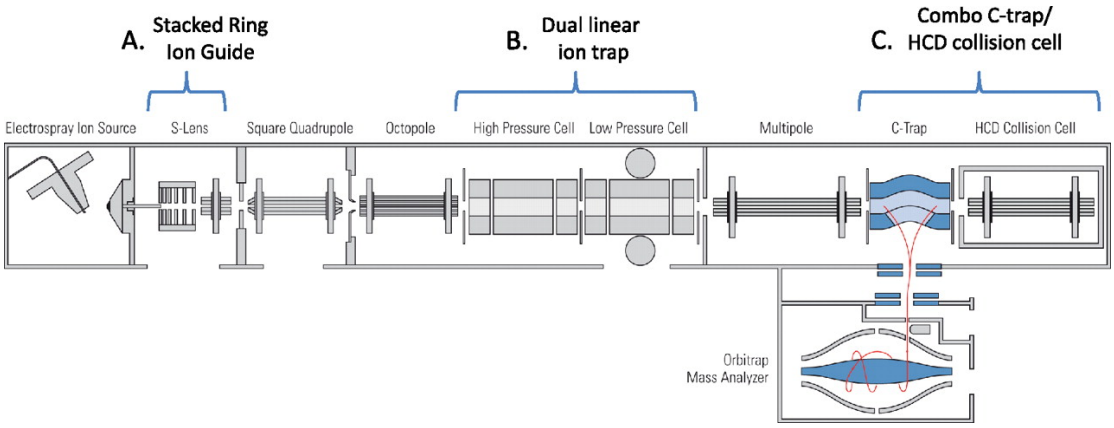

Fig 8 - Schematic of the LTQ Orbitrap Velos MS instrument (Olsen, Schwartz et al. 2009)

The LTQ Orbitrap Velos (Olsen, Schwartz et al. 2009) is the MS instrument used in this thesis (Fig 7). This includes a nano electrospray from which the ions pass through the ion transfer tube and into the S lens. The S lens is also known as the stacked ring ion guide and is made of a set of stainless steel apertures to which a radio frequency voltage is applied. The apertures are arranged in two sequences, with the first having an inner diameter of 7.5mm to accommodate all the ions from the electrospray ion flux. The second set has an inner diameter of 5mm and thereby helps to focus the ion beam. As the focusing of the beam is done using an electrostatic field, molecules that have no charge on them will thus not be focused and hence will be lost. This is advantageous as only charged species and be analysed using this mass spectrometer. The S lens also transports the ions from atmospheric pressure to a vacuum within the mass spectrometer.

The focused ion beam thus passes through the transmission quadrupole. Passage through the quadrupole is facilitated by an electromagnetic field, generated by varying charges on each of the four components of the quadrupole. The unwanted transport of droplets and solvent clusters into the ion optics, downstream of the S lens, is minimised by a curve in the transmission quadrupole ion guide found between the S lens and the octopole. This occurs as the charged ions will be guided through the curve by the electromagnetic field, whilst the other particles will be lost. The ions then pass through the octopole which works in a manner, similar to the quadrupole and acts as a passage to the ions. The quadrupole and octopole facilitate the movement of the ions from regions of higher atmospheric pressure to lower pressure found in the ion traps. The ions at this point can either pass through the

two chambers of the linear ion trap into the C trap, or be isolated and fragmented in the linear ion trap.

For the first scan, ions are collected in the C trap and injected into the Orbitrap, for mass/charge analysis. The Orbitrap is a type of ion trap in which the ions are electrostatically trapped in an orbit around a spindle shaped electrode. The ions then oscillate along the length of the ion trap and are detected by a detector electrode. The frequency of the oscillations correlate with the mass/charge of the trapped ions. From the first MS scan, the molecules to be fragmented are identified by their mass/charge ratios. For the MS/MS or second scan the chosen ions/peptides can then be selected in the high-pressure compartment of the linear ion trap and fragmented. They are then sent into the low-pressure chamber of the ion trap and then ejected sequentially by mass to charge into the detectors. The dual pressure system of the linear ion trap along with the Orbitrap on the LTQ Orbitrab Velos provides increased resolution, sensitivity and fast cycle times.

The data obtained from the Mass spectrometer for the fragmented peptides can be searched using Andromeda database search engine to identify peptides. The peptides were identified by searching against the International Protein Index (IPI) human protein database containing 89,422 proteins, to which 175 commonly observed contaminants and all the reverse sequences were added (Cox and Mann 2008; Cox, Matic et al. 2009).

1.9 Stable Isotope Labelling using Amino acids in Cell culture (SILAC)

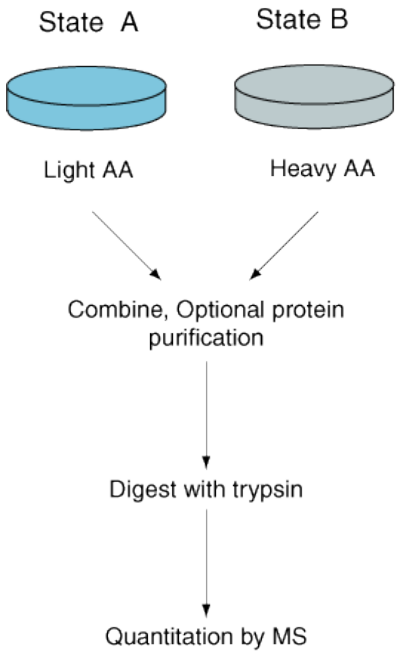

Fig 9 – Schematic showing the workflow of a typical SILAC experiment

SILAC is a method for quantitative peptide analysis. It involves the growing two or three population of cells in media that contain specific amino acids with different molecular weights due to the presence of stable isotopes of carbon, nitrogen or hydrogen (Ong, Blagoev et al. 2002). The presence isotope-labeled forms of the amino acids, argenine and lysine, in media supplied to growing cells leads to their incorporation into cell proteins. Arginine and lysine are essential amino acids for HeLa cells (Eagle 1955). Hence two or more populations of cells can be labeled with amino acids that differ in their molecular masses. Peptides generated for analysis from labeled proteins is done by treating the proteins with trypsin. Trypsin typically cleaves proteins after every arginine or lysine residue, hence, all peptides generated by tryptic digestion will contain labeled amino acids. This results in a shift in the molecular mass of identical proteins/peptides obtained from two cell populations.

Complete labeling of proteins in a population can typically be brought about after 5 cell doublings.

Populations of cells labeled with either light, or heavy, amino acids, can be subjected to different treatments/conditions. The cells can then be mixed, the proteins purified and digested and then analysed using the mass spectrometer. Identical peptides from two or more conditions will travel together in the reverse phase high pressure liquid chromatography, due to their similar physical characteristics like charge and hydrophobicity and eventually injected into the mass spectrometer for analysis. The resulting spectra for the peptides from two or more conditions will appear grouped together in the mass spectra, however, they will be distinguishable from the differences in their masses due to the presence of labeled amino acids. The ratio between the intensities of the quantified peptides is representative of the protein abundance in the different conditions. The intensities of two or more peptides mapping to a protein are then combined to obtain a final ratio, representative of the changes in protein abundance in the different conditions. Changes in the proteins expressed between the different conditions can thus be ascertained. This method has been used to study the changes in protein expression levels, localisation, interaction partners and post translational protein modification states between cells subjected to different treatments/conditions (Mann 2006; Trinkle-Mulcahy, Andersen et al. 2006; Boisvert, Ahmad et al. 2012).

Proteomic studies have also been used to study chromatin associated proteomes. Chromatin associated proteins which differ in the different phases of the cell cycle

have been identified using a mass spectrometry based approach (Khoudoli, Gillespie et al. 2008). In another study by the groups of Juri Rappsilber and William C. Earnshaw, the protein composition of mitotic chromosomes was analysed (Ohta, Bukowski-Wills et al. 2010). They used SILAC based Mass spec approaches to identify proteins that were associated with the mitotic chromosomes. The proteins that were stably associated with the chromosome and also those which exchange with the cytosol were identified in their study. They identified a number of previously uncharacterised proteins, 30 predicted chromosomal proteins were confirmed by GFP tagged expression from a set of 34 analysed proteins (Ohta, Bukowski-Wills et al. 2010). This high success rate of identification shows that SILAC based mass spectrometry is a good tool for the identification of chromatin bound proteins.

Chapter 2

Materials and methods

2.1 Cell culture

2.1.1 Medium preparation

HeLa cells were grown in Dulbecco's Modified Eagle's Medium (DMEM) (Invitrogen ♯41966-052) supplemented with 10% Foetal Bovine Serum (Invitrogen ♯10106-169) and 100 U/mL penicillin-streptomycin (Invitrogen ♯15140-122). For the HeLa H2B-EGFP stable cell line, the above media was supplemented with Blasticidin (Invitrogen ♯25-0205) at a final concentration of 5μg/ml and for HeLa H2B-2FP was supplemented with Blasticidin (Invitrogen ♯25-0205) and G418 (Roche ♯146-4981)at final concentrations of 5μg/ml and 200 μg/ml respectively.

Complete media

500 ml Dulbecco's Modified Eagle's Medium (DMEM) (Invitrogen ♯41966-052)

50 ml Foetal Bovine Serum (Invitrogen ♯10106-169)

5ml penicillin-streptomycin (Invitrogen ♯15140-122)

For SILAC experiments, HeLa cells were grown in DMEM minus leucin, Arginine and Lysine (Invitrogen D9443) supplemented with 10% dialysed foetal Bovine serum (Invitrogen ♯26400-044), L-leucine (Sigma-Aldrich ♯L8000) and penicillin-streptomycin (Invitrogen ♯15140-122). L-arginine (Sigma-Aldrich ♯A3784) and L-lysine (Sigma-Aldrich ♯L5501) were added to the "light," and L-arginine 13C/15N (Cambridge Isotope Laboratory ♯CNLM-539-H-0.5) and L-lysine 13C/15N (Cambridge Isotope Laboratory ♯CNLM-291-H-0.25) to the "heavy" media. The amino acid concentrations are based on the formula for normal DMEM (Invitrogen).

SILAC media

500ml DMEM minus leucin, arginine and lysine (Invitrogen D9443)

50 ml dialysed fetal calf serum (Invitrogen ♯26400-044)

5ml penicillin-streptomycin (Invitrogen ♯15140-122)

74mg L-lysine (Sigma-Aldrich ♯L5501) or L-lysine 13C/15N (Cambridge Isotope Laboratory ♯CNLM-291-H-0.25)

42mg L-arginine (Sigma-Aldrich ♯A3784) or L-arginine 13C/15N (Cambridge Isotope Laboratory ♯CNLM-539-H-0.5)

52.5mg L-leucine (Sigma-Aldrich ♯L8000)

2.1.2 General growth conditions

The cell lines were grown in 75cm^2 flasks with filter caps (Grenier ♯658175) in a humidified incubator set at 5% CO_2 and 37°C. The cells were grown and upon reaching 70-100% confluency, the cells were split using 1ml of Trypsin (Invitrogen ♯25300-054) per flask for about 3 minutes and neutralised with 9ml of their standard growth medium. Subsequently the cells were diluted to desired concentrations and plated for experiments or maintained in the flask by diluting 1:10 with standard growth medium. All tissue culture work was performed within a laminar flow chamber.

Cells that were labeled with SILAC media had an additional step incorporated, wherein, after trypsinisation of the cells; the cells were harvested with 9ml of PBS (Invitrogen ♯10010-056) and spun down for 4 minutes at 170g (1000rpm,Beckman GS-15 centrifuge, S4180 rotor). The supernatant was discarded and the pellet was

resuspended with the respective growth media and then plated to the desired concentration. The cells were grown for a minimum of three passages with a plating dilution of 1:10 to facilitate complete labeling of proteins before performing experiments.

2.2 Permeabilisation of cells

Cell permeabilisation was carried out on cells grown in glass-bottomed petri dishes (Willcowells ♯GWSt-3522).

The cells were grown to about 70% confluency and washed once in PBS (Invitrogen 14190) at room temperature.

The cells were incubated in permeabilisation buffer for 7minutes at room temperature. The cells were then washed in the permeabilisation buffer lacking digitonin for 3X3min.

FLIM images of the cells were then acquired with the cells in the permeabilisation buffer lacking digitonin with increasing concentrations of polyvalent cations or with addition of RNAse as indicated in the respective experiments.

Permeabilisation buffer

1ml 1M HEPES (Formedium) (pH-7.4)

20mM (final concentration)

5.3ml 1M potassium acetate (Sigma-Aldrich ♯P1190)

110mM (final concentration)

6.25µl 2%w/v digitonin (Calbiochem ♯11024-24-1)

0.00125%w/v (final concentration)

Made up to 50ml using distilled water.

2.3 Calcium measurements

Calcium measurements were preformed using the cell permeable calcium specific dye, Fluo4-AM (Invitrogen ♯F-14201).

Cells were seeded onto glass-bottomed petri dishes (Willcowells ♯GWSt-3522). The cells were grown to about 70% confluency.

The media was removed and the cells were washed once with serum free DMEM (Invitrogen ♯41966-052).

2µl of 50mM Fluo4-AM in DMSO was mixed with 2µl of 1M Pluronic F-127 (Invitrogen ♯P6867) and added to 1ml of serum free DMEM which was then added to the cells and incubated for 40minutes at 37°C. Pluronic F-127 is a surfactant that helps loading the dye into the cells.

On entering the cells, esterases within the cell cleave the Fluo4-AM to Fluo4, which is now active and becomes impermeable to the cellular membrane, thereby trapping it within the cell.

The cells were then washed once with CO_2 independent medium lacking phenol red (Invitrogen ♯ME090085P1) and imaged with the same media.

Fluo4 was imaged with excitation at 488nm and emission at 525nm, which is similar to GFP fluorescence. Live cell imaging was accomplished within a 37°C chamber attached to the microscope.

All images were acquired with a wide-field fluorescence microscope (DeltaVision Spectris; Applied Precision) and a CoolMax charge-coupled device camera (Roper Scientific). Imaging was performed using a 60x oil immersion, NA 1.4 Plan-Apochromat objective.

2.4 Drug treatments

Cells were grown petri dishes to about 70% confluency. The cells were related with various drugs to cause effects as listed below. The cells were imaged or harvested to be used in other experiments.

2.4.1 ATP depletion

The cells were treated with a final concentration of 10mM sodium azide (Sigma-Aldrich ♯S2002) and 50mM 2-deoxy glucose (Sigma-Aldrich ♯D8375), which causes the depletion of ATP in cells by inhibiting the oxidative and glycolytic pathways (Schwoebel, Ho et al. 2002). The chemicals were dissolved directly in imaging media or a 10X stock was made with PBS and added to media.

2.4.2 Staurosporine

The cells were treated to a final concentration 0.5µM of staurosporine (Sigma-Aldrich ♯S4400) for 2 hours. The addition of staurosporine causes the inhibition of a number of kinases. The stock solution was 1M Staurosporine in DMSO and was stored at -20°C.

2.4.3 Calcium ionophore (A23187)

The cells were treated with a final concentration of 10µM of calcium ionophore (Sigma-Aldrich ♯C7522) from a stock solution of 2mM in DMSO stored at -20°C. The addition causes an increase in concentration of free intracellular calcium.

2.4.4 Transcription inhibition

For inhibition of transcription, cells were treated with 5,6-Dichloro-1-beta-D-ribofuranosylbenzimidazole (DRB) at a final concentration of 25µg/ml for 1hour. Inhibition of transcription was visualised by staining nascent RNA using Click-iT® RNA Alexa Fluor® 488 Imaging Kit (Invitrogen ♯C10329) following manufacturers instructions.

2.4.5 Trichostatin A (TSA)

Cells were treated with TSA at a final concentration of 200ng/ml for indicated periods. The stock solution was at a concentration of 1mg/ml dissolved in Ethanol.

2.4.6 RNAse treatment

Cells treated with RNAse were first permeabilised using the above-mentioned protocol. RNAse was then added at a final concentration of 10 µM/ml.

2.5 Gel Electrophoresis and Immunoblotting

Cells were grown on petri dishes to a confluency of about 80%, the cells were treated depending on the respective experiments.

The cells were then scraped and resuspended in denaturing lysis buffer and denatured at 65°C for 5 min.

For Western blotting analysis, the proteins were resolved using a precast 4-12% polyacrylamide Bis-Tris gel (Invitrogen ♯NP0321).

10µg of protein was loaded into individual wells of the gel and were run at 200V for 50min in tris-acetate SDS running buffer (Invitrogen ♯LA0041) or MOPS SDS running buffer (Invitrogen ♯NP0001).

The gel was transferred to nitrocellulose membrane using the iBlot system (Invitrogen ♯IB801001) using the standard 7 min protocol.

The nitrocellulose membrane was then incubated with shaking in blocking buffer for 1h at room temperature.

The membranes were then incubated with primary antibody diluted 1:1000 in blocking buffer overnight at 4^{o}C with shaking.

The membranes were washed in TBS and 0.1% Tween 20 for 3x10 min at room temperature followed by incubation with secondary antibody conjugated with Horse Radish Peroxidase (HRP) diluted 1:15,000 in blocking buffer for 1h at RT.

It was then washed in TBS and 0.1% Tween 20 for 3x10 min at room temperature.

For visualisation, enhanced chemiluminescence reagent (ECL; GE Healthcare ♯RPN2132) was applied to the membrane and incubated for 5 minutes and the chemiluminescence was imaged with the LAS-3000 imaging system from Fuji.

Denaturing Lysis buffer

1ml 10% SDS (Sigma-Aldrich ♯L4390)

2% (final concentration)

0.5ml 1M HEPES (Formedium)

10mM (final concentration)

100µl EDTA (Sigma-Aldrich ♯E6758)

1mM (final concentration)

5ml 2.5M Sucrose (Sigma-Aldrich ♯S7903)

250mM (final concentration)

1 Complete ULTRA protease inhibitor (Roche ♯05892970001)

5 PhosStop phosphatase inhibitor (Roche ♯04906845001)/10ml

Made up to 50ml with distilled water.

Tris buffered saline (TBS)

30ml 5M Nacl (Sigma –Aldrich ♯S7653)

150mM (final concentration)

100ml 1M Tris-HCl pH-7.4 (Sigma –Aldrich ♯T5941)

100mM (final concentration)

Final volume was made up to 1L using distilled water.

Blocking buffer

5g BSA (Sigma –Aldrich ♯A2153)

0.1ml Tween 20 (Sigma –Aldrich ♯P1379)

0.02mg sodium azide (NaN_3) (Sigma –Aldrich ♯S2002)

100ml Tris Buffered Saline (pH-7.4)

filtered using Stericup 0.2 mm (Millipore ♯SCVPU02RE) and stored at 4^oC.

2.5.1 Antibodies used for western blotting

Acetyl H4 lysine5 (Cell Signaling #9672)

Epiplakin (Santa Cruz biotechnology ♯sc-87102)

PCNA associated factor (Abcam ♯ab56773)

Histone H1.0 (Abcam ♯ab11079)

Histone H3 (Cell Signaling #9715)

Anti-APCII anti-serum (Nathke, Adams et al. 1996)

2.6 siRNA knockdown of Adenomatous polyposis coli (APC) protein

Knockdown of APC and its validation was done by Daniel Klotz from the Inke Nathke group (University of Dundee) as part of a collaborative project (Dikovskaya, Khoudoli et al. 2012). The materials and method for the experiment are as follows.

HeLa cells were cultured in complete media. For siRNA-mediated APC protein or mock depletion, cells were transfected with 10 nM of appropriate non-targeting or APC-targeting siRNAs (Dharmacon) using Interferrin (Polyplus) according to the manufacturer's instructions and cultured further for 72 hours.

2.7 Cell fixation, immunostaining and microscopy

The following procedure was used to look at the changes in the localisation of spermine upon ATP depletion. Spermine is a small molecule and can bind to DNA due to the inherent charge. The immunostaining was done after denaturing the DNA so as to allow access to the DNA, which could possibly be prevented after chromatin compaction and fixation treatments.

Cells were grown on glass coverslips to a confluency of about 70% on coverslips and fixed for 5 min in 3.7% paraformaldehyde in PHEM buffer.

The cells fixed on the coverslips were then permeabilised for 10 minutes with 1% Triton X-100 in phosphate-buffered saline (PBS) (Invitrogen ♯10010-056).

The coverslips were washed three times with PBS for duration of 5 minutes each.

The coverslips were transferred into wells containing 2X SSC at room temperature, which was the placed into a water bath at 80°C and was incubated for 45 minutes.

The coverslips were then sequentially incubated in 70% ethanol, 100% ethanol, 0.1M NaOH, 70% ethanol and 100% ethanol for 10 minutes each at room temperature.

The coverslips were then washed in 0.5% Tween 20 (Sigma –Aldrich ♯P1379) in PBS for 10 minutes at room temperature.

The cells were then blocked with blocking buffer for 30 min.

The blocking solution was removed and then incubated with primary antibody against Spermine (Abcam ♯ab26975) diluted 1:100 in the blocking solution for 1 hour.

The cover slips were washed three times with PBS for duration of 5 minutes each.

The coverslips were then incubated with secondary antibodies, diluted in blocking buffer for 45 min.

The cover slips were then washed three times with PBS for 5 minutes each.

The cells were then stained with DAPI (0.3 µg/ml; Sigma ♯D9542).

A final set of washes was repeated with PBS and cells were mounted in Vectashield media (Vector Laboratories ♯H1000).

All images were acquired with a wide-field fluorescence microscope (DeltaVision Spectris; Applied Precision) and a CoolMax charge-coupled device camera (Roper Scientific).

Imaging was performed using a 60x oil immersion, NA 1.4 Plan-Apochromat objective.

SoftWorX software (Applied Precision) was used for image acquisition and data deconvolution.

PHEM buffer (pH 6.9)

60 mM PIPES (Sigma –Aldrich ♯P6757)

25 mM HEPES (Formedium)

10 mM EGTA (Sigma –Aldrich ♯3889)

2 mM MgCl2 (Sigma –Aldrich ♯M8266)

2X SSC

1.753g NaCl (Sigma –Aldrich ♯S7653)

0.882g Sodium citrate (Sigma –Aldrich ♯C0909)

in 100ml distilled water and pH adjusted to 7.

Blocking buffer

1% donkey serum

0.1% Triton X-100 (Sigma –Aldrich ♯X100) in PBS

2.8 FLIM-FRET microscopy

FLIM-FRET experiments were carried out on a HeLa H2b-2FP cell line stably expressing EGFP and mCherry tagged histone H2B as previously described by Lleres et al., (Lleres, James et al. 2009).

Cells were cultured on glass bottom dishes (Willcowells ♯GWSt-3522) with complete DMEM until they were 70% confluent.

Custom made CO_2 independent medium lacking phenol red (Invitrogen ♯ME090085P1) replaced complete DMEM for the duration of imaging.

Fluorescence Lifetime Imaging Microscopy (FLIM) was performed using an inverted laser scanning multi-photon microscope Radiance 2100MP (Bio-Rad Laboratories) equipped with temperature-controlled environmental chamber constructed with black walls to exclude external sources of light during the sensitive period of FLIM measurement.

Measurements were acquired at 37°C, with a 60× oil immersion lens (1.4 NA).

Two-photon excitation was achieved using a Chameleon Verdi-pumped ultrafast tunable (720–930 nm) laser (Coherent) to pump a mode-locked frequency-doubled Ti:Sapphire laser that provided sub-200-femtosecond pulses at a 90-Mhz repetition rate with an output power of 1.4 W at the peak of the tuning curve (800 nm).

The region of interest was scanned at 600 lines per second with the laser intensity adjusted to the highest sub-saturating limit.

Fluorescence lifetime measurements were acquired over 60s.

Enhanced detection of the scattered component of the emitted (fluorescence) photons was afforded by the use of fast single-photon response (5783P; Hamamatsu Photonics) direct detectors.

The fluorescence lifetime imaging capability was provided by TCSPC electronics (SPC-830; Becker & Hickl GmbH). TCSPC measures the time elapsed between laser pulses and the fluorescence photons.

Fluorescence lifetimes were calculated for all pixels in the field of view (512×512 pixels) with 2X binning, giving a final resolution of 256x256 using SPCImage software (Becker & Hickl, GmbH).

To quantify the lifetime for membrane bound chromatin, a region of interest (ROI) was drawn around the nucleus with approximately 1µm of the nuclear boundary and the values were derived using the SPCImage software (Becker & Hickl, GmbH). Similar ROI's were drawn to derive the lifetime values of internal nuclear structures.

2.9 Electron microscopy

Transmission electron microscopy imaging was performed by John James at the electron microscopy facility (University of Dundee) using the following protocol.

The cells after being treated with specific conditions, was fixed in 4% paraformaldehyde, 2.5% glutaraldehyde in 0.2 M Pipes, pH 7.3.

The cells were then scraped and then pelleted in Eppendorf tubes and rinsed in 0.2 M Pipes.

Samples were postfixed in 1% aqueous osmium tetroxide, rinsed in water, dehydrated in graded alcohol-propylene oxide, and then embedded in Durapan resin (Sigma-Aldrich).

Serial sections (60–70 nm) were cut on an ultramicrotome (Ultracut UCT; Leica) and collected on 100 mesh copper grids coated with 1% Pioloform (Agar) in chloroform. Sections were stained with uranyl acetate and lead citrate and examined with a transmission electron microscope (Tecnai 12; FEI) at 6,000 magnification.

Images were collected on digital imaging plates, which were read out with a micrometer imaging plate scanner (Ditabis; Digital Biomedical Imaging Systems AG).

2.10 Chromatin isolation

For FLIM experiment showing chromatin compaction upon increasing Mg^{2+} concentration, chromatin was isolated from HeLa H2b-2FP and HeLa H2b-EGFP cell lines using the following protocol, which is modified from Owen-Huges et al., (Owen-Hughes, Utley et al. 1999). The first part of the protocol describes the isolation of nuclei described in Andersen et al., 2002 (Andersen, Lyon et al. 2002) which is the starting material for the chromatin isolation described by Owen-Huges et al., (Owen-Hughes, Utley et al. 1999).

2.10.1 Nuclear isolation

HeLa cells are grown on 5 X 14 cm Petri dishes and culture until >90% confluence (approx. 10^7 cells per dish).

The cells were harvested by trypsinisation using 2ml trypsin-EDTA solution (Invitrogen ♯25300-054) per dish with incubation for about 4 minutes.

The cells are then harvested using 2ml of ice cold PBS per plate and are pooled together in two 15ml falcon tubes.

The cells are washed three times using ice cold PBS at 218g (1000 rpm, Beckman GS-6 centrifuge, GH-3.8 rotor) at 4°C.

After the final PBS wash, the cells are resuspended in 5ml of Buffer A and incubated on ice for 5 min. The buffer being hypotonic, causes the cells to swell up.

The cell suspension was transferred to a pre-cooled 7 ml Dounce tissue homogenizer (Wheaton Scientific ♯357542).

The cells were homogenised using 10 strokes of a tight pestle (“A” specification: 0.0010" - 0.0030" clearance), while keeping the homogenizer on ice.

The homogenised cells were centrifuged at 218g (1000 rpm, Beckman GS-6 centrifuge, GH-3.8 rotor) for 5 min at 4°C. The pellet contains enriched, but not highly pure, nuclei.

The pellet was resuspended with 3ml S1 solution by pipetting up and down.

The resuspended pellet was layered over 3ml of S2 solution in a 15ml falcon tube.

The tube was centrifuged at 1430g (2500 rpm, Beckman GS-6 centrifuge, GH-3.8 rotor) for 5 min at 4°C. This step results in a cleaner nuclear pellet

Buffer A

0.5ml 1M HEPES (Formedium) pH 7.9

10mM (Final concentration)

0.5ml 1M KCl (Sigma –Aldrich ♯P9541)

10mM (Final concentration)

75µl 1M MgCl2 (Sigma –Aldrich ♯M8266)

1.5mM (Final concentration)

25µl 1M DTT

1mM (Final concentration)

Made up to 50ml using distilled water.

S1 solution

250mM (Final concentration)

0.5ml 1M MgCl2 (Sigma –Aldrich ♯M8266)

10mM (Final concentration)

Made up to 50ml using distilled water.

S2 solution

7ml 2.5M Sucrose (Sigma-Aldrich ♯S7903)

350mM (Final concentration)

25µl 1M $MgCl_2$ (Sigma –Aldrich ♯M8266)

0.5mM (Final concentration)

Made up to 50ml using distilled water.

2.10.2 Isolation of chromatin from isolated nuclei

The isolated nuclei were re-suspended in 5ml extraction buffer.

The suspension was pelleted by centrifugation at 4500g (4750rpm, Beckman GS-6 centrifuge, GH-3.8 rotor) for 5 min at 4°C

The pellet was the re-suspended in fresh extraction buffer and re-centrifuged. This was repeated 3 more times.

The pellet was then re-suspended in 2ml extraction buffer with 0.2% NP-40 and transferred into two 1.5ml eppendorf tubes.

The suspension was centrifuged at 16,000g (13,000 rpm, Thermo Hireus Fresco17 centrifuge) and each pellet was re-suspended in 1ml fresh extraction buffer with 0.2% NP-40. The same was repeated once more.

The pellet was then washed once with extraction buffer.

0.5 ml of permeabilisation buffer was added to each of the two pellets and re-suspended.

The suspension was then sonicated with a Misonix XL 2020 sonicator fitted with a microtip probe and set at power setting 5 for three cycles of 15 s with incubation on ice in between cycles.

To ascertain the size of the obtained chromatin fragments, 2µl of the sample was incubated with proteinase K at a final concentration of 100 µg/ml in a total volume of 10µl at 37°C for 30 minutes.

Gel loading dye was then added to the sample and was run on a 1% (w/v) agarose gel, made from high grade low melting agarose (BDH (VWR) ♯436552V) in 1X Tris Acetate EDTA (TAE) buffer. The gel was run at 100 V in 1 XTAE buffer.

The gel was stained with Ethidium Bromide, imaged with UV light and the size of the isolated chromatin was ascertained.

Extraction buffer

4ml 5M NaCl (Sigma –Aldrich ♯S7653)

400mM (Final concentration)

1ml 1M HEPES (Formedium) (pH 7.4)

20mM (Final concentration)

3.5µl 2-mercaptoethanol (Sigma-Aldrich ♯M7154)

1mM (Final concentration)

5ml glycerol (Sigma-Aldrich ♯G5516)

1 Complete ULTRA protease inhibitor (Roche ♯05892970001)

Made up to 50ml using distilled water.

Permeabilisation buffer

1ml 1M HEPES (Formedium) (pH-7.4)

20mM (final concentration)

5.3ml 1M potassium acetate (Sigma-Aldrich ♯P1190)

110mM (final concentration)

Made up to 50ml using distilled water.

10X Tris Acetate EDTA (TAE) buffer

48.4 g of Tris-HCl (Sigma –Aldrich ♯T5941)

11.4 mL of glacial acetic acid (VWR ♯20104.334)

3.7 g of EDTA (Sigma-Aldrich ♯E6758)

made up to 1 liter using deionised water

2.11 Chromatin isolation from Fixed cells for SILAC experiments

Permeabilisation of cells leads to changes in the ionic environment within the nucleus, which causes the chromatin to lose its original structure. This could also be attributed to the changes in the association of proteins with the chromatin. To prevent the loss of components bound to chromatin upon permeabilisation and chromatin isolation, we isolated chromatin after the cells were fixed. For the SILAC experiments where the changes in proteins was to be quantified, chromatin was isolated using the SimpleChIP® Enzymatic Chromatin IP Kit (Cell Signalling ♯9002)

using the manufacturers protocol. The two differentially labeled and treated cells were mixed together after having been fixed and scraped out of the plates to minimise differences arising due to handling. The isolated chromatin following manufacturers instructions was then quantified using the BCA protein assay (Thermo ♯23225) as per manufacturers instructions.

The samples were then stored in the -80°C freezer before further processing.

2.12 Chloroform methanol protein precipitation

A known amount of isolated chromatin was chloroform methanol precipitated before further processing.

To the protein sample, SDS, TCEP (Sigma ♯93284) and NEM (Sigma ♯ E3876) were added to a final concentrations of 2%, 10mM and 20mM, respectively, to a final volume of 100µl.

The sample was incubated at 90°C for 20 minutes to help reverse fixation and denature the sample.

To the sample in an 2ml eppendorf tube, 400µl of 100% methanol was added and vortexed for 5 seconds.

100µl of 100% chloroform was added and vortexed again for 5 seconds.

300µl of MilliQ water was added and vortexed for 1minute.

The sample was centrifuged at 9000g (9700rpm, Thermo Hireus Fresco17 centrifuge) for 5 minutes at room temperature.

Approximately 80%of the upper phase was removed being careful to not remove the precipitated protein at the interphase between the two liquid phases.

300µl of 100% methanol was added and vortexed briefly followed by centrifuging the tube at 9000g (9700rpm, Thermo Hireus Fresco17 centrifuge) at room temperature for 5 minutes.

The supernatant was discarded and the pellet was allowed to air dry at room temperature under a laminar airflow chamber.

The pellet was the resuspended in 4% SDS, 100 mM NaCl, 25 mM TCEP, 50 mM N-ethylmaleimide, 10 mM Na PO4 pH 6.0 and fractionated using Denaturing Gel Filtration Chromatography.

2.13 Denaturing Gel Filtration Chromatography, Trypsin Digestion and Peptide Clean-up

Using a Dionex Ultimate 3000 HPLC system, protein fractions from isolated chromatin, resuspended in 4% SDS, 100 mM NaCl, 25 mM TCEP, 50 mM N-ethylmaleimide, 10 mM $NaPO_4$ pH 6.0 were heated to 65°C for 10 min, then filtered through a 0.45 mm filter.

Samples were injected (50µl per injection – 200 µg protein) onto a mAbPacSEC column (Dionex) equilibrated with 0.2% SDS, 100 mM NaCl, 10 mM Na PO4 pH 6.0. The flow rate was 0.2 ml min-1 and 8 X 200µl fractions were collected using a low protein binding 96-deep well plate (Eppendorf).

Triethylamine bicarbonate (TEAB, 1 M pH 8.0) (Sigma ♯T7408) was added to each fraction to adjust the pH to 8.0, and trypsin diluted in 0.1 M TEAB was added at a ratio of 1:50 of the protein mass, with incubation for 18 h at 37°C.

SDS was removed from each fraction using Pierce detergent removal spin plates (Pierce ♯88304).

For peptide desalting trifluoroacetic acid was added to 1% (v/v) final concentration and peptides were purified using a Sep-Pak tC18 96-well m-elution plate (Waters ♯186002318).

Peptides were eluted in 200µl of 50% (v/v) acetonitrile and sample was evaprorated to dryness prior to resuspension in 5 % (v/v) formic acid.

Peptide concentrations were determined using the CBQCA assay (Invitrogen ♯C-6667) after 25-fold dilution of peptide samples in 0.1 M borate buffer pH 9.3 using manufacturers instructions.

2.14 LC-MS/MS and Maxquant Analysis

Using a Dionex Ultimate 3000 nanoHPLC system, 1mg of peptides in 5% (v/v) formic acid were injected onto an Acclaim PepMap C18 nano-trap column (Thermo Scientific).

After washing with 2% (v/v) acetonitrile 0.1 % (v/v) formic acid peptides were resolved on a 150mm X 75µm Acclaim PepMap C18 reverse phase analytical column over a 100min organic gradient with a flow rate of 300ml/min.

Peptides were ionised by nano-electrospray ionization at 1.2kV using a fused silica emitter with an internal diameter of 5µm (New Objective).

Tandem mass spectrometry analysis was carried out on an LTQ-Velos Orbitrap mass spectrometer Thermo Scientific. The data dependent acquisition method used was the FT10 protocol as described previously (Haas, Faherty et al. 2006).

Data were processed, searched and quantified using the Maxquant software package version 1.2.2.5 as described previously (Cox and Mann 2008)using the default settings and employing the Human Uniprot database (06/07/11) containing 109824 entries.

The settings used for the Maxquant analysis were: 2 failed cleavages were allowed; fixed modification was N-ethylmaleimide on cysteine; enzymes were Trypsin (K/R not before P); Variable modifications included in the analysis were methionine oxidation, deamidation of glutamine or asparagine, N-terminal pyro-glutamic acid formation, protein N-terminal acetylation and lysine acetylation.

A mass tolerance of 7ppm was used for precursor ions and a tolerance of 0.5Da was used for fragment ions.

Using the default Maxquant settings a maximum false positive rate of 1% was allowed for both peptide and protein identification. This cut-off was used for accepting individual spectra as well as whole proteins in the Maxquant output. This threshold has previously been shown to be a rigorous method for identifying true positive matches (Cox and Mann 2008).

2.15 Protein selection criteria for SILAC experiment

The data generated from Maxquant gives a list of all the identified proteins in the mass spectometry analysis with the corresponding normalised Heavy/Light SILAC ratios. The protein SILAC ratios are calculated as the median of all SILAC pair ratios that belong to peptides contained in this protein. The ratio corresponds to the fold change of the quantified protein in the TSA treated condition.

From the protein list, contaminants and those identified from reverse sequences were removed. Contaminants were identified by MaxQuant, from their database of commonly occurring contaminants. Contaminants include bovine proteins and keratins that come from handling. From the remaining proteins, those with a minimum of two unique peptides and having been identified in at least two of the three biological replicates were chosen.

The $\log_2$ of the ratios was calculated. From these values, a distribution was obtained by plotting the number of proteins against the $\log_2$ of the SILAC ratios. The standard deviation (σ) was calculated. Proteins with $\log_2$ normailsed SILAC ratios greater or less than 2σ from the median of the distribution were considered to be significantly changed, upon treatment with TSA.

Using the 2σ criteria, a set of minimally changing proteins was identified. A students t-test was performed using the normalised H/L SILAC ratios from the three biological replicates for each individual protein against the set of minimally changing proteins and p-values were obtained. A lower p-value will indicate the reproducibility of the fold change in each of the three biological replicates being significantly different form those of the minimally changing proteins. A 0.05 p value cutoff was used in

combination with a 2 standard deviation fold change in the normalised SILAC H/L ratio (calculated from all three biological replicates), to identify reliably changing proteins.

Chapter 3

Charge based chromatin compaction

3.1 Abstract

The basic unit of chromatin is the nucleosome, which contains DNA wound around a histone octamer. DNA is negatively charged with the presence of the poly-phosphate backbone, with ~60% of the negative charge being neutralised by the presence of positively charged lysine and arginine residues in the histones (Strick, Strissel et al. 2001). The remaining ~40% of the negative charge remaining in DNA results in repulsion, causing decompaction. In vitro, nucleosome arrays adopt the decompacted 'beads on a string' structure in the absence of polyvalent cations. Polyvalent cations have been shown to increase compaction of nucleosome arrays, presumably by neutralising the charge on DNA (Korolev, Allahverdi et al. 2010). Most studies on chromatin compaction have been performed on well defined nucleosome arrays (Simpson, Thoma et al. 1985). These studies, however valuable, do not represent the native environment of chromatin within cells.

The work in this chapter studies charge-based chromatin compaction in more native environments. The induced compaction of chromatin in permeabilised cells, upon addition of polyvalent cations, is shown to be similar to the compaction in nucleosome arrays. The chromatin also compacts when treated with RNAse, which will decrease the net negative charge of chromatin. Finally, I also show that the increase in compaction of chromatin with increasing polyvalent cation concentration is also true for intact, live cells.

3.2 Results

3.2.1 Chromatin compaction in isolated chromatin increases with increasing Mg^{2+} concentration

Increasing Mg^{2+}concentration is known to increase the compaction of nucleosome arrays (Korolev, Allahverdi et al. 2010). The increase in the cation concentration neutralises the charge of the phosphate backbone of DNA, thereby facilitating chromatin compaction.

Two sets of chromatin were extracted from $HeLa^{H2B\text{-}EGFP}$ and $HeLa^{H2B\text{-}2FP}$ cells. The chromatin was sonicated in a buffer containing 110mM potassium acetate buffered with 10mM HEPES (pH-7.4). The size range of the resulting chromatin was ascertained by gel electrophoresis after Proteinase K treatment. The size of the resulting chromatin was predominantly between 0.6 to 1.5kb (Fig 9).

Chromatin compaction was studied by acquiring FLIM measurements of the isolated chromatin. The FLIM measurements of the two sets of isolated chromatin were acquired with increasing amounts of Mg^{2+} concentration. With increasing concentration of Mg^{2+} ions, there was a decrease in the measured lifetime of the imaged chromatin (Fig 10). The same trend was seen for both forms of chromatin, indicating compaction. There was an increase in chromatin compaction with increasing Mg^{2+} concentration, saturating at 6-8mM of Mg^{2+} (Fig 10).

The decrease in EGFP fluorescence lifetime of the chromatin from $HeLa^{H2B\text{-}2FP}$, which expresses the histone H2B tagged with EGFP, as well as m-Cherry, was found to be

greater than the decrease in lifetime from chromatin containing EGFP alone ($HeLa^{H2B\text{-}EGFP}$). The decrease in lifetime in the latter can be explained by collisional quenching (Vishwanath, Zhong et al. 2006) as compaction brings the fluorophore (EGFP) in closer proximity to other chromatin components with increasing cation concentration. Chromatin extracted from $HeLa^{H2B\text{-}2FP}$ cells contains m-Cherry in addition to EGFP. The two fluorophores are a known FRET pair (Shaner, Campbell et al. 2004), where m-Cherry can accept energy from EGFP when in close proximity and lower the fluorescence lifetime of EGFP. Hence in cells containing both the fluorophores, a decrease in fluorescence lifetime of EGFP can be brought about by FRET as well as by collisional quenching, thereby making the latter a better tool for the study of chromatin compaction using FLIM measurements.

To show that the decrease in lifetime was not a direct effect of increasing Mg^{2+} concentration on the lifetime of EGFP, FLIM measurements of free EGFP in solution were acquired with increasing Mg^{2+} concentrations. The increase in Mg^{2+} has little or no effect on the fluorescence lifetime of free EGFP (Fig 11).

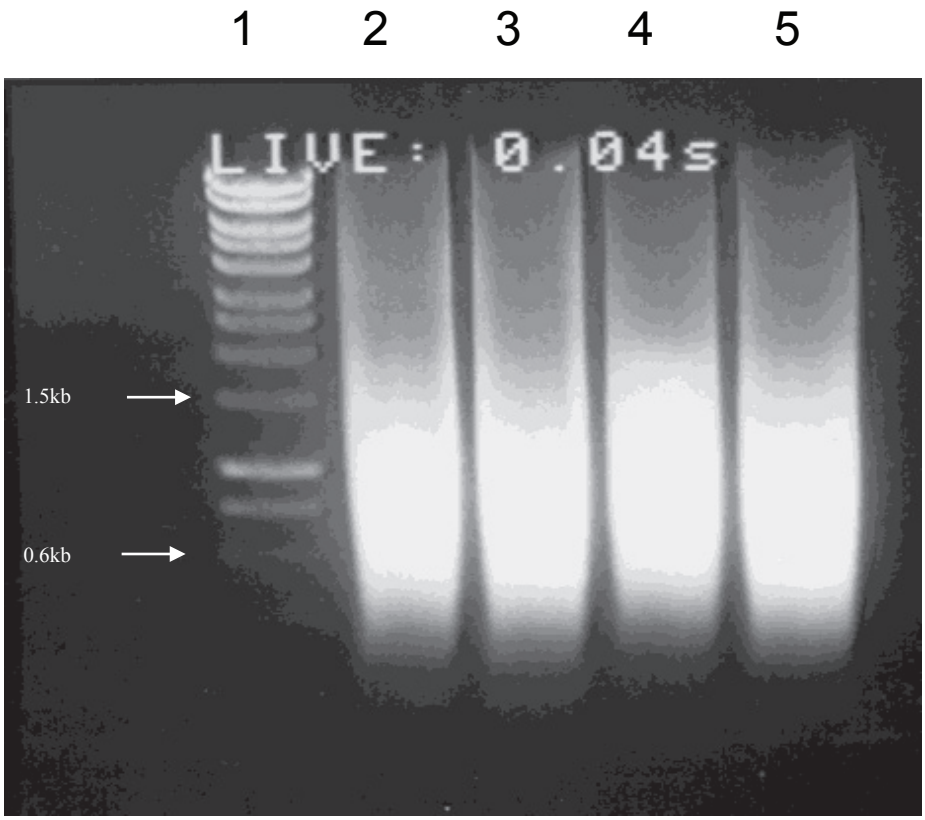

Fig 10 – Lane 1- DNA molecular marker
Lane 2, 3 – chromatin from HeLa^{H2b_EGFP} cells
Lane 4, 5 – chromatin from HeLa$^{H2B\text{-}2FP}$ cells.
Chromatin isolated from cells, was digested with Proteinase K, run on a 1% Agarose gel and stained with EtBr to ascertain the size of the isolated chromatin.

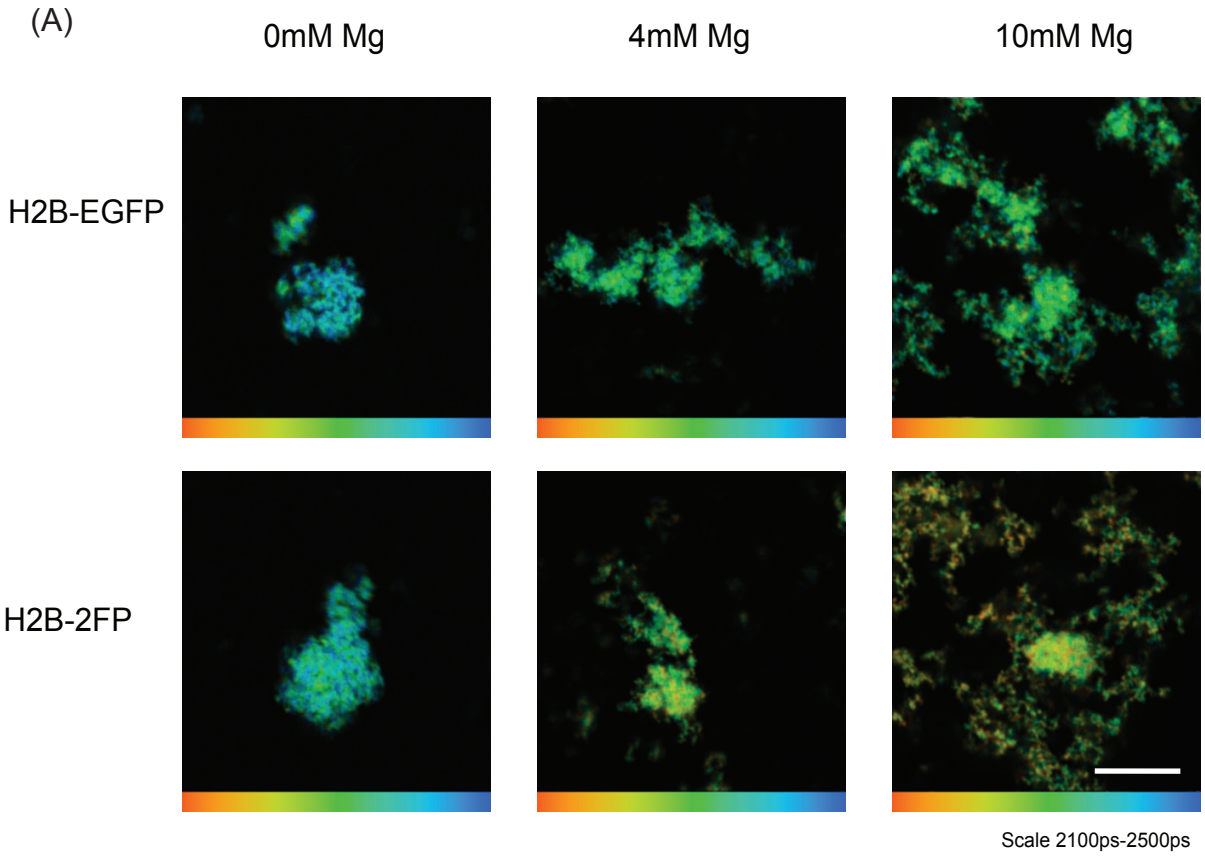

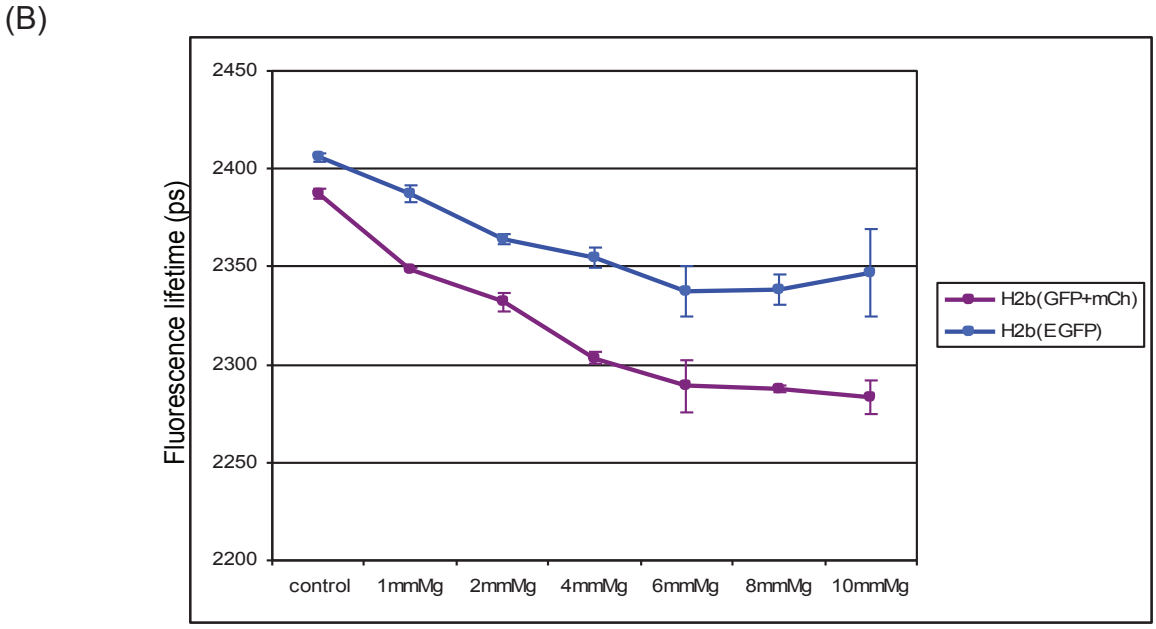

Fig 11 – FLIM measurements of chromatin isolated from HeLa^{H2B_2FP} and HeLa^{H2B_EGFP} with varying Mg^{2+} concentrations. (A) FLIM images show a decrease in fluorescence lifetime with increasing concentrations of Mg^{2+} (Scale bar - 10µm). (B)There is a decrease in the fluorescence lifetime with saturation seen at 6mM of Mg^{2+} for both forms of chromatin. The decrease in lifetime for chromatin form HeLa^{H2b_2FP} is greater than that of HeLa^{H2b_EGFP}.

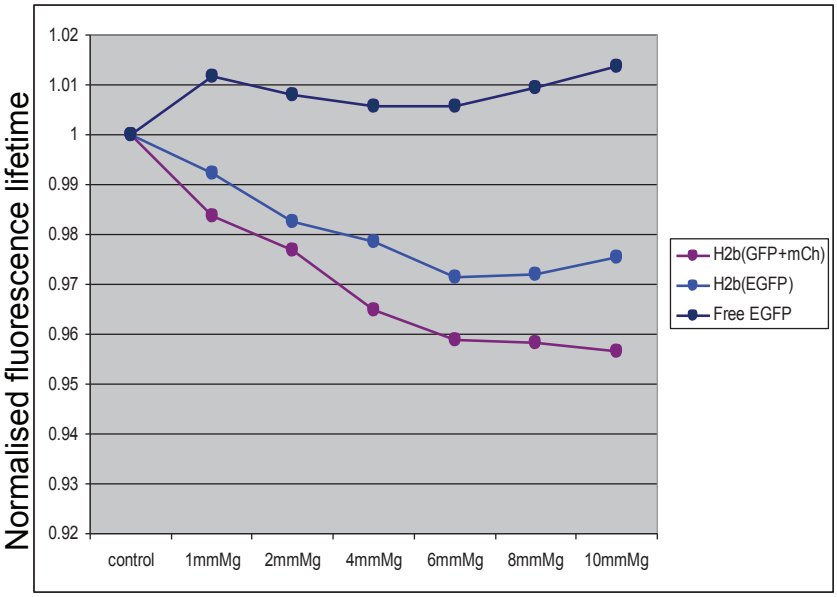

Fig 11 (C) – Normalised fluorescence lifetime measurements of free GFP and chromatin isolated from HeLa$^{H2b\text{-}2FP}$ and HeLa$^{H2b\text{-}EGFP}$ with varying Mg2+ concentrations. There is a decrease in the fluorescence lifetime for both forms of chromatin, but there is no change of lifetime for free EGFP.

3.2.2 Chromatin of permeabilised cells increases in compaction with increasing Mg^{2+} ion concentration

Most studies on chromatin compaction have been done with well defined nucleosome arrays (Simpson, Thoma et al. 1985). However, the nuclear chromatin environment differs from in vitro systems, due to the presence of additional factors including histone modifications and other chromatin associated proteins. Increasing Mg^{2+} concentration has been shown to increase compaction of nucleosome arrays (Korolev, Allahverdi et al. 2010). Inter and intra nucleosome array association increases with increasing Mg^{2+} concentration (Schwarz and Hansen 1994).

To better our understanding of chromatin compaction with increasing cation concentrations in a more native environment, $HeLa^{H2B\text{-}2FP}$ cells were permeabilised with 0.00125% digitonin for 7 minutes in a buffer containing 110mM potassium acetate with 20mM HEPES(pH 7.4). The cells were then washed in the same buffer lacking digitonin. Fluorescence lifetime measurements were acquired from cells in the presence of increasing concentration of Mg^{2+}(Fig 12). The increase of Mg^{2+} concentration leads to a decrease in the measured fluorescence lifetime of EGFP in the individual cells, indicating an increase in compaction. There was a saturation of compaction at 6-8mM of Mg^{2+}(Fig 12). Upon addition of an excess of EDTA the fluorescence lifetime of EGFP in the cells increased again, indicating decompaction when the Mg^{2+} ions are chelated. However, the decompaction was not complete and EGFP fluorescence lifetime values correlated with those observed at a concentration

of 2mM of Mg^{2+}. The increase in compaction can also be visualised in the corresponding intensity images (Fig 12).

Analysis was also carried out on separate regions within the imaged nuclei. The nuclei were analysed in three regions, membrane associated chromatin, clusters of heterochromatin which correspond to the perinucleolar heterochromatin and internal chromatin which excluded the membrane associated and internal heterochromatin structures. The membrane associated chromatin is known to have higher concentration of compact heterochromatin in un-permeabilised HeLa cells. Separate analysis of these structures showed no changes in the compaction dynamics when analysed separately and compared with each other and the whole nuclei. This indicates that in permeabilised cells chromatin compaction upon increase in Mg^{2+} concentration was uniform among the chromatin within the nucleus irrespective of its location (Fig 12C).

This increase in compaction was also confirmed by electron microscopy of permeabilised cells treated with varying concentrations of Mg^{2+} (Fig 13). Upon permeabilisation, the cells lost the distinct heterochromatic and euchromatic regions and assume a diffuse arrangement. At 2mM of Mg^{2+} the chromatin loses its diffused pattern as seen in Fig-0. At 8mM Mg^{2+} the chromatin is observed as highly condensed and stained regions predominantly along the nuclear envelope and nucleoli.

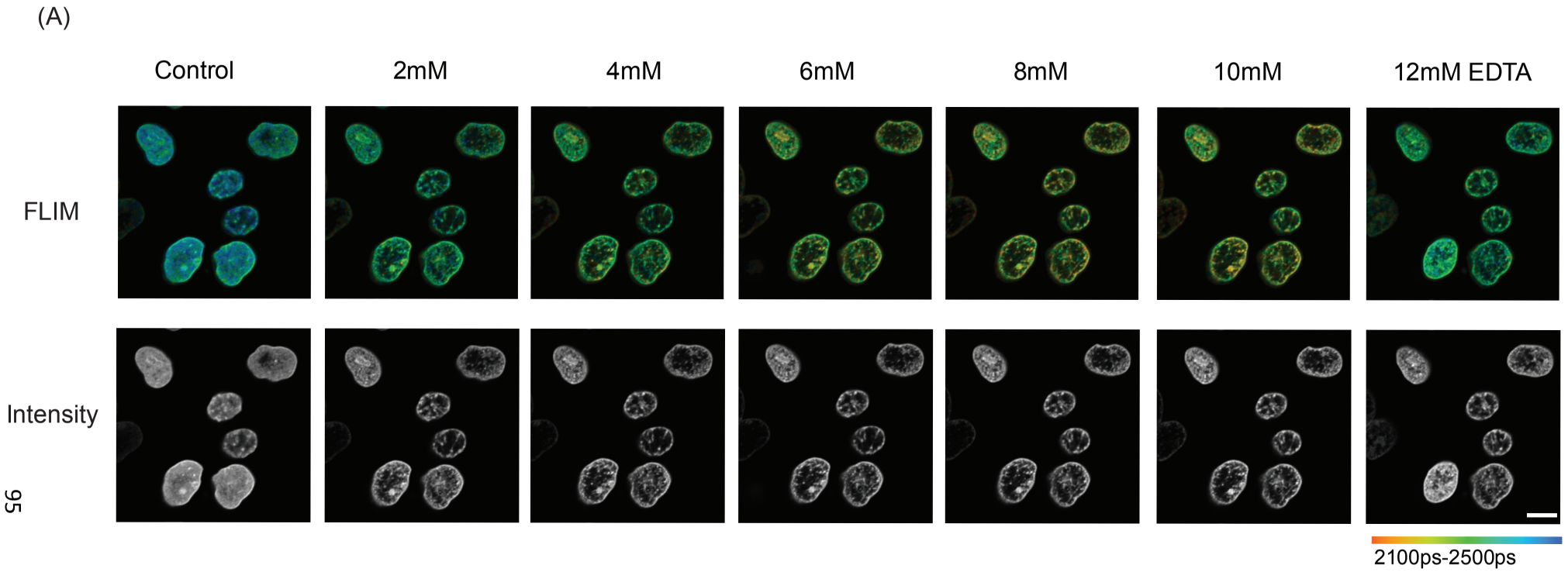

Fig 12 - (A) FLIM images of permeabilised cells with increasing Mg2+ concentation. there is a decrease in lifetime with increasing Mg2+ concentrations and an increase with the addition of 12mM of EDTA. The increase in compaction is also seen with the fluorescence intensity image.
(Scale bar - 10µm).
(B) the normalised fluorescence lifetime of the cells are plotted against the Mg2+ concentration.

(C)

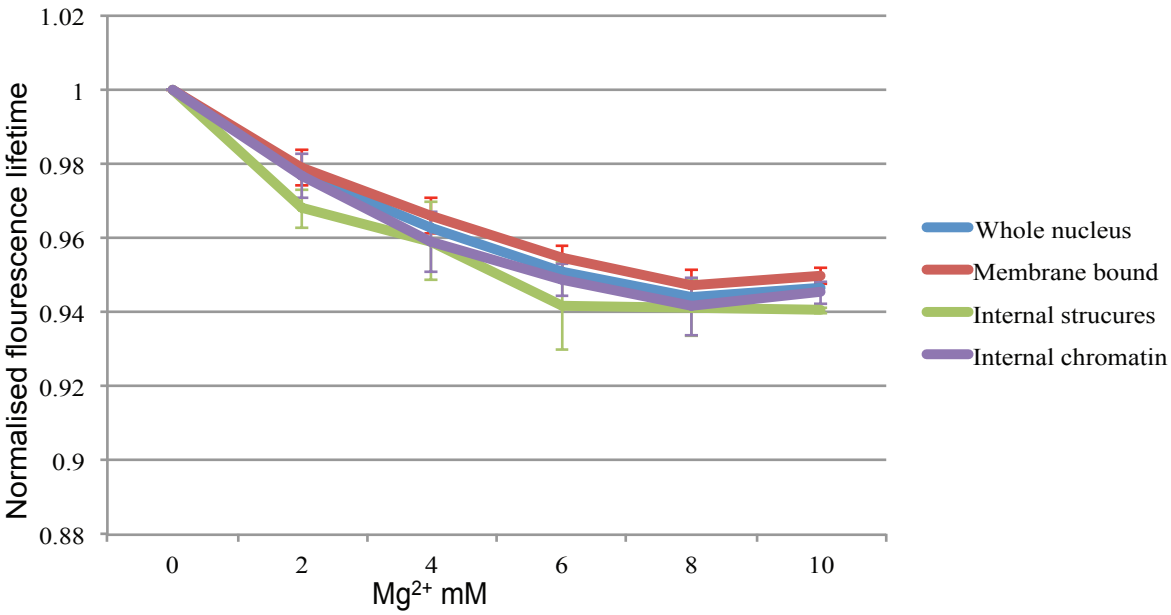

Fig 12 - (C) Normalised fluorescence lifetime of the different forms of chromatin are plotted against concentration of Magnesium.

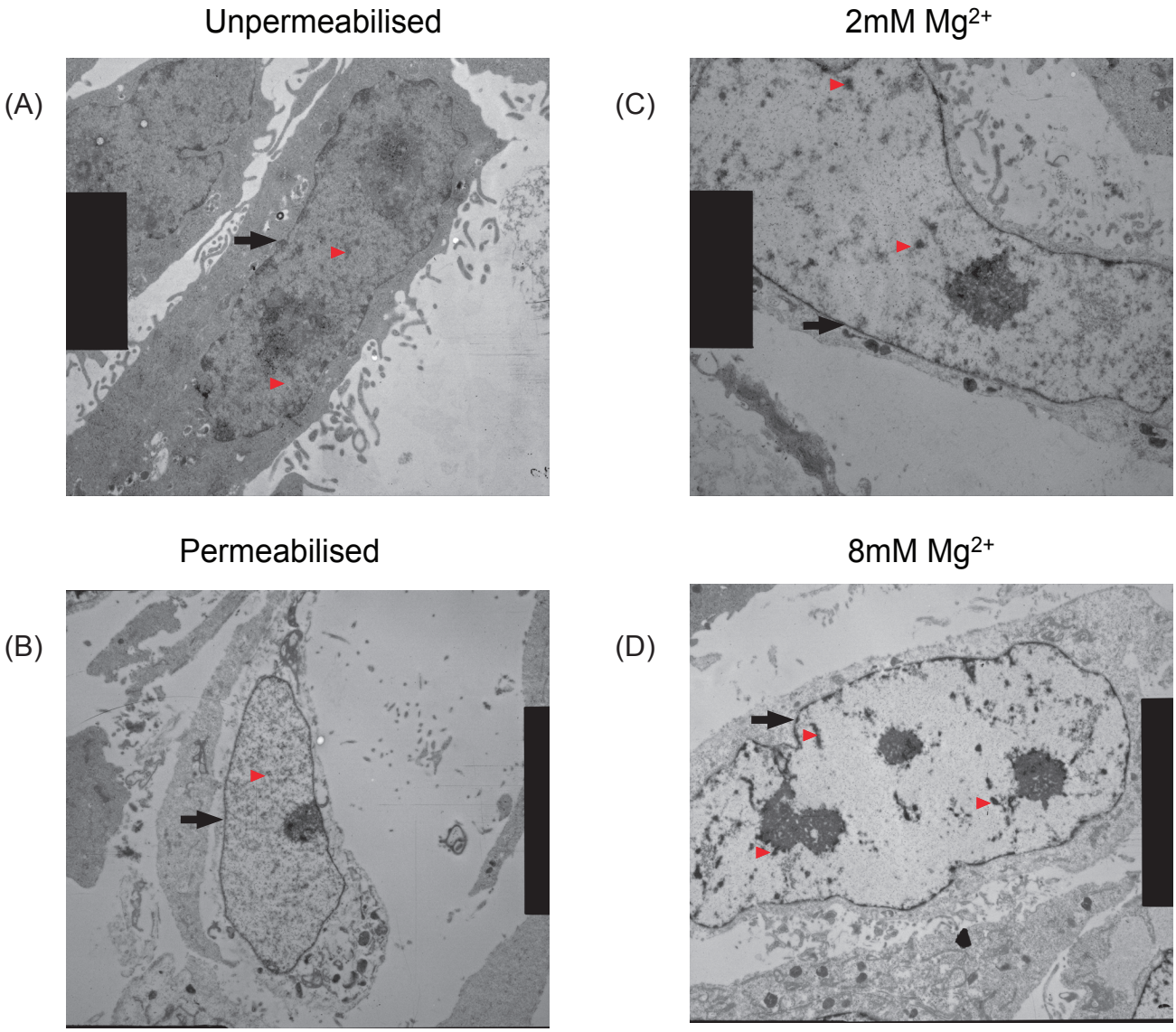

Fig 13 - Electron microscopy images show the changes to chromatin structure (red arrow heads) upon permeabilistion and changes in Mg^{2+} concentration. Permeabilisation (B) results in the loss of distinct heterochromatin and euchromatin regions found in unpermeabilised control cells (A), leading to a diffused structure. At 2mM of Mg^{2+} (C) the chromatin forms aggregates, with formation of dense structures at 8mM of Mg^{2+} (D). The nuclear membrane is indicated with arrows. (Scale bars - A,C- 3920nm ; B,D-7233nm)

3.2.3 Chromatin of permeabilised cells increases in compaction with increasing Ca^{2+} ion concentration

Calcium ions are similar to magnesium in being bivalently charged. To test if calcium could cause compaction of chromatin in a manner similar to that of Mg^{2+}, experiments on permeabilised cells were performed as described above. The increase in Ca^{2+} led to an increase in compaction of the chromatin in permeabilised $HeLa^{H2B\text{-}2FP}$ cells and compaction was similar to what was observed with increasing Mg^{2+} ions. The increase in compaction saturates at 6-8mM of Ca^{2+} (Fig 14). The chelation of Ca^{2+} with excess of EDTA also led to a decrease in compaction. Similar to the result observed with the chelation of Mg^{2+}, the de-compaction was not complete and lifetime values correlated with those observed at the concentration of 2mM of Ca^{2+}.

The results indicate that Mg^{2+} and Ca^{2+} ions have similar effects on the compaction of chromatin in permeabilised cells. The incomplete reversal of compaction upon the addition of a chelater possibly indicates the formation of two or more compaction states not all of which are reversible.

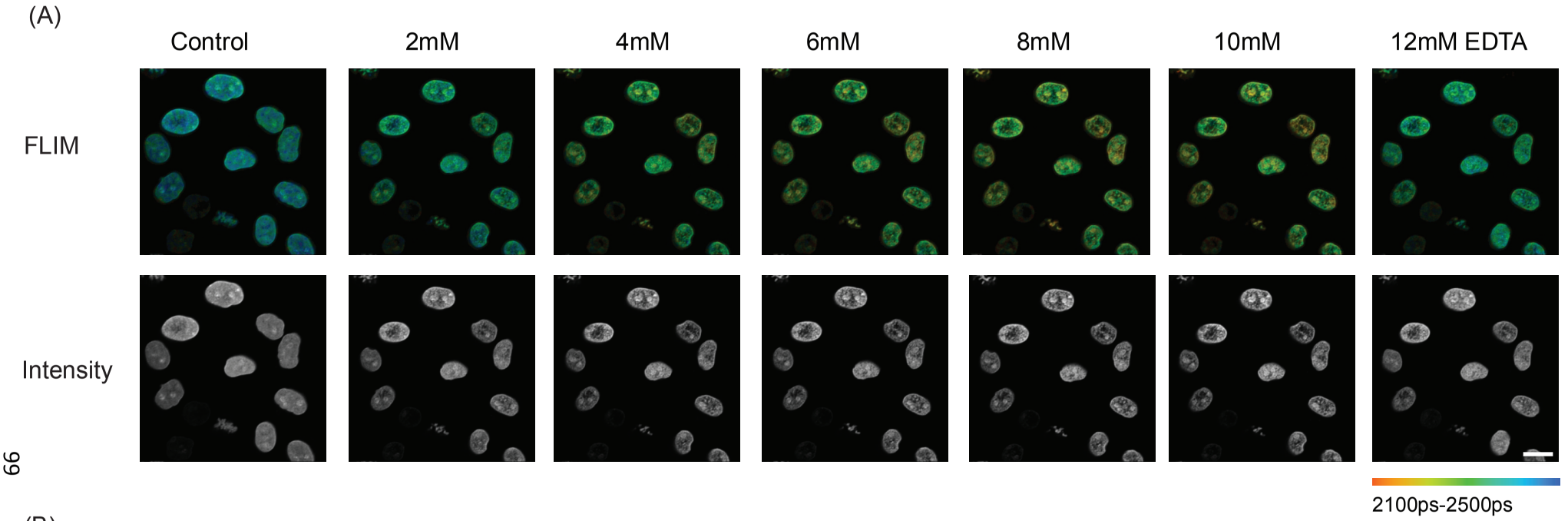

Fig 14- (A) FLIM images of permeabilised cells with increasing Ca2+ concentation. there is a decrease in lifetime with increasing Ca2+ concentrations and an increase with the addition of 12mM of EDTA. The increase in compaction is also seen with the fluorescence intensity image. (Scale bar - 10µm).
(B) the normalised fluorescence lifetime of the cells are plotted against the Ca2+ concentration. Error bars indicate standard deviation.

3.2.4 Chromatin of permeabilised cells increases in compaction with increasing polyamine concentration

Polyamines are small molecules found within cells that have been implicated in functions such as regulation of gene expression, the stabilization of chromatin and the inhibition of DNA damage (Ha, Sirisoma et al. 1998). A decrease in cellular polyamine concentrations often results in a reduction of nucleic acid and protein syntheses, eventually giving rise to cell growth inhibition (Persson 2009). They are positively charged at physiological pH by virtue of their amine groups and bind negatively charged cellular components. They have the highest affinity towards ATP followed by RNA, DNA and phospholipids (Watnabe et al., 1991). Spermidine and spermine are polyamines with charges of +3 and +4. They have been shown to compact nucleosome arrays (Korolev, Allahverdi et al. 2010).

If the compaction of chromatin in permeabilised cells with the addition of bivalent cations results from charge neutralization, the same effect should also be observed by the addition of polyamines. Experiments were done on permeabilised HeLa$^{H2B\text{-}2FP}$ cells, wherein the concentration of the polyamines was gradually increased and FLIM measurements were acquired. Increasing the concentration of polyamines led to an increase in chromatin compaction of permeabilised cells. There was also an inverse correlation between the charge of the polyamine and the concentration required for a given compaction state. Maximum compaction was seen at 1.5mM of spermidine (Fig 15) and at 0.21mM of spermine (Fig 16).

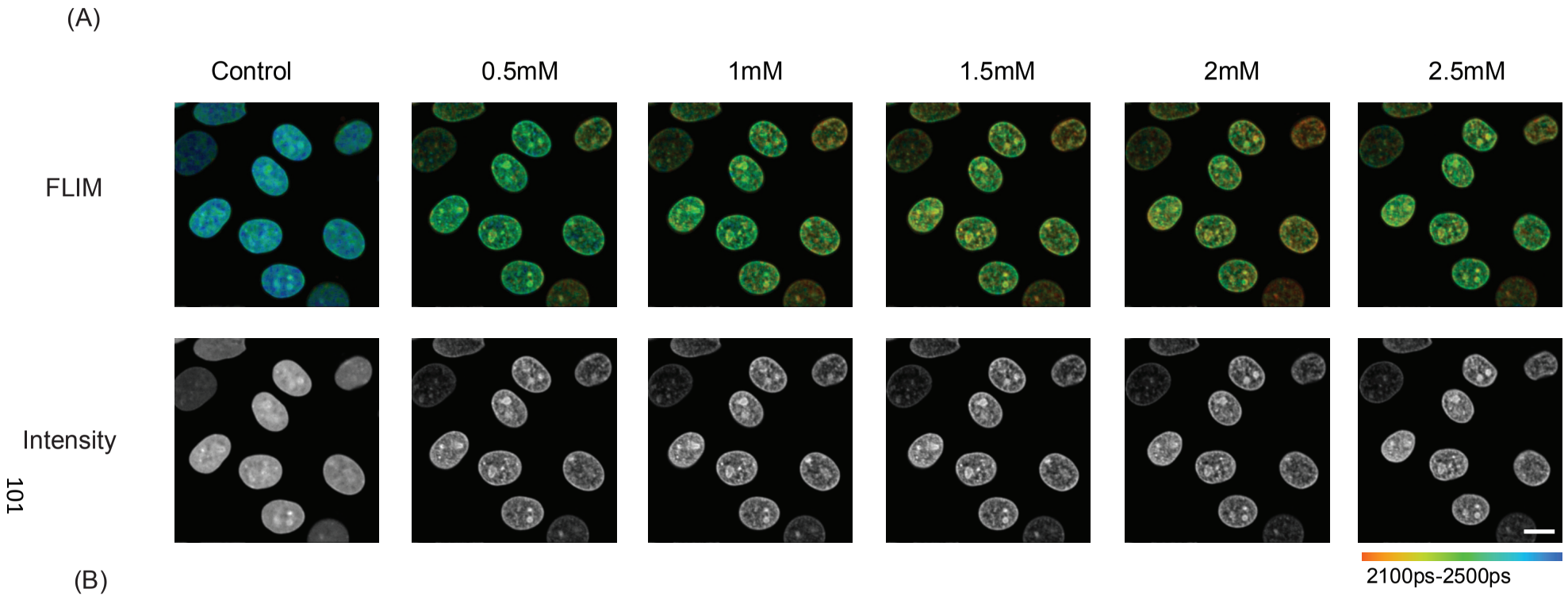

Fig 15 - (A) FLIM images of permeabilised cells with increasing Spermidine concentation. The increase in compaction is also seen with the fluorescence intensity image.
(Scale bar - 10µm)
(B) the normalised fluorescence lifetime of the cells are plotted against the Spermidine concentration. Error bars indicate snadard deviation.

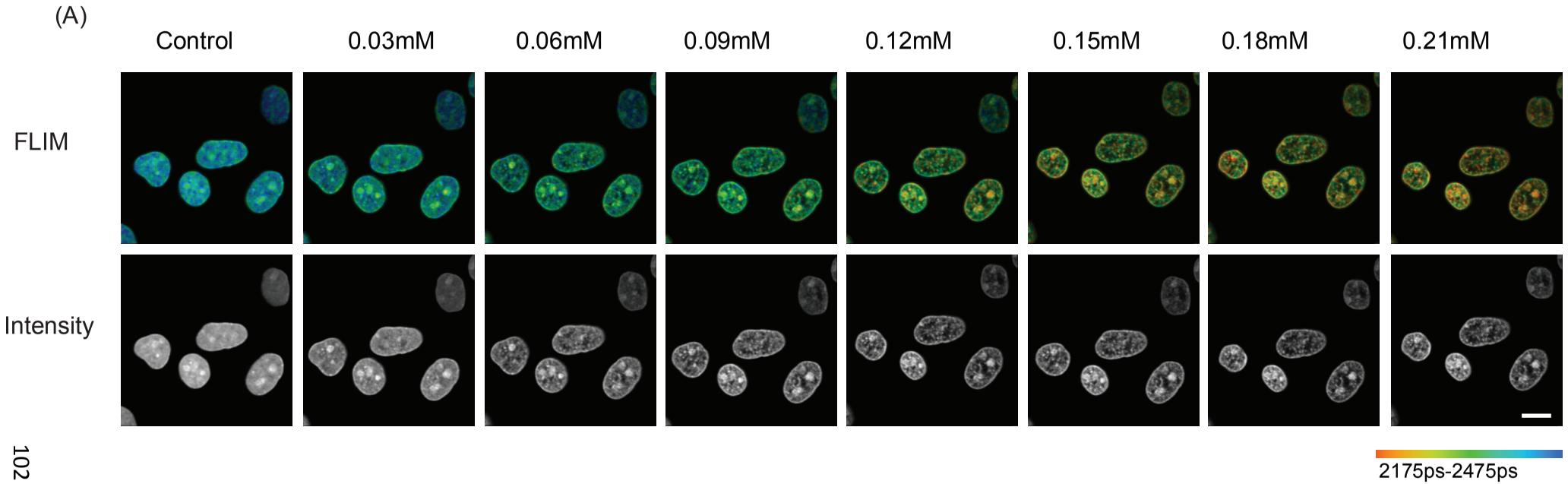

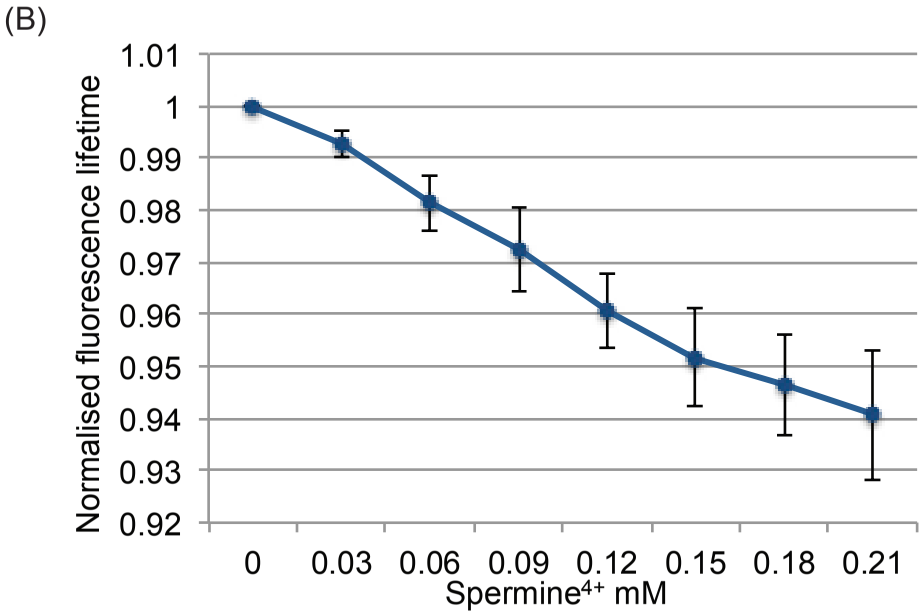

Fig 16 - (A) FLIM images of permeabilised cells with increasing Spermidine concentation. The increase in compaction is also seen with the fluorescence intensity image.
(Scale bar - 10µm)
(B) the normalised fluorescence lifetime of the cells are plotted against the Spermidine concentration. Error bars indicate standard deviation.

3.2.5 Chromatin compacts in permeabilised cells upon RNAse treatment

RNA, like DNA, is also made of nucleotides and has a negatively charged sugar-phosphate backbone. RNA is a known component of chromatin in cells. The presence of RNA thus increases the overall negative charge of chromatin within the nucleus. RNA can possibly compete with DNA to complex with positively charged molecules within the nucleus and thus increase the net negative charge of the nucleosomes. Treating the permeabilised nuclei with RNAse will cleave the RNA into its constituent nucleotides and enable it to go into solution. This will result in lowering the net negative charge of chromatin. I therefore tested whether this alters compaction.

Treating permeabilised HeLa$^{H2B\text{-}2FP}$ cells with RNAse led to the increase in compaction of chromatin as observed from the resulting decrease in EGFP fluorescence lifetime. The increase in compaction is also seen from the EGFP intensity images, which marks chromatin (Fig 17).

The chromatin compaction of regions within the nuclei was also separately analysed. The nuclei were analysed in three regions, membrane associated chromatin, clusters of heterochromatin which correspond to the perinucleolar heterochromatin and internal chromatin which excluded the membrane associated and internal heterochromatin structures. The compaction dynamics on the addition of RNAse was not significantly changed between the membrane associated and internal chromatin when compared to the compaction dynamics of the whole nuclei. However, clusters

of heterochromatin which correspond to the perinucleolar heterochromatin showed higher compaction when compared to the whole nuclei (Fig 17B).

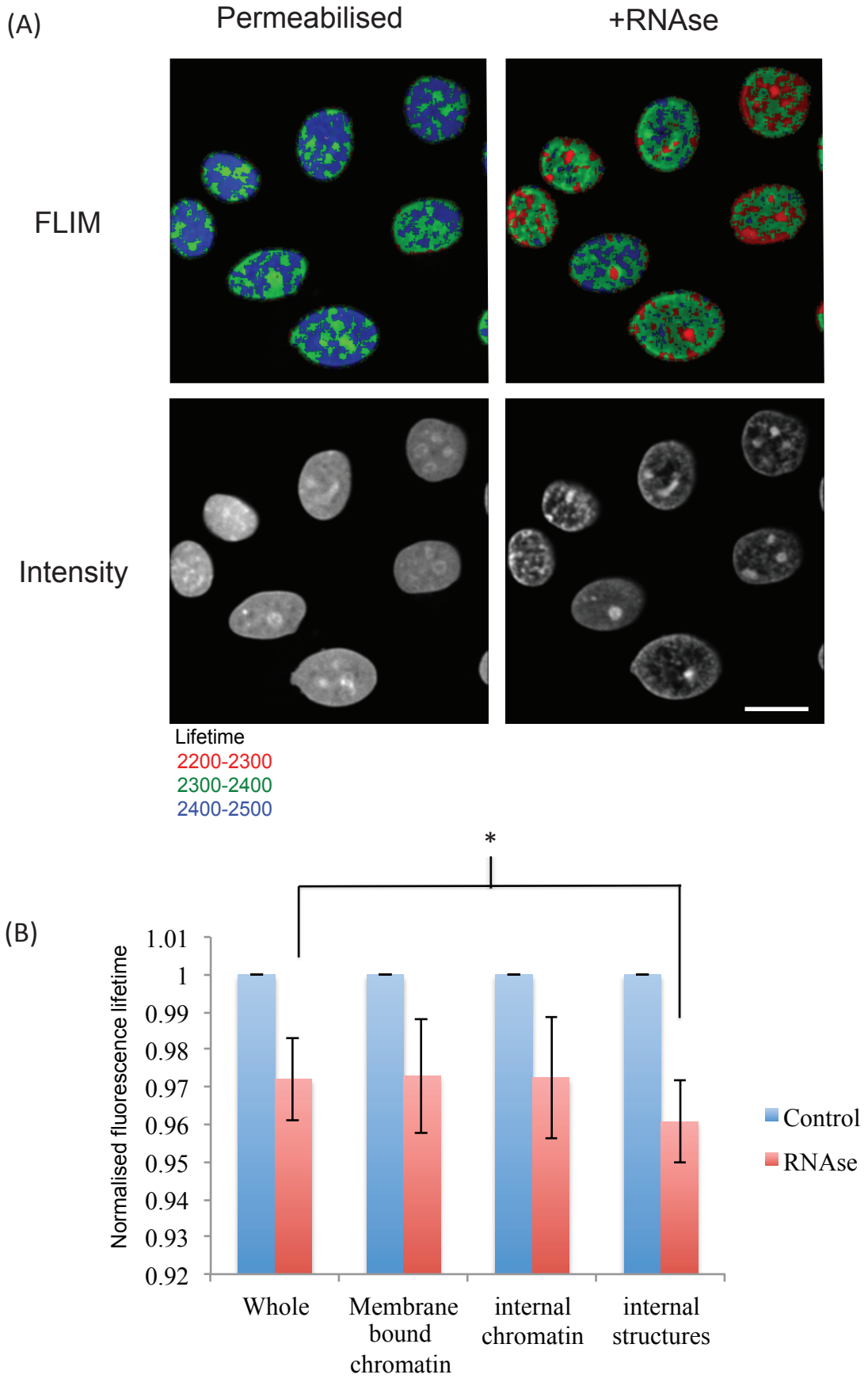

Fig 17 - chromatin of permeabilised cells compacts with the addition of RNAse. (A) FLIM images show the decrease in lifetime in cells that have been treated with RNAse. the increase in compaction is also seen in the intensity images, which show fluorescence from H2b-GFP. (Scale bar - 10µm) (B) The chart shows the average decrease in normalised fluorescence lifetime values for the whole nucleus, membrane bund chromatin, internal chromatin and internal structures representing nucleoli. Error bars indicate standard deviation.
* $p < 0.02$

3.2.6 Increase in intracellular Ca^{2+} causes increase in chromatin compaction

The above experiments show that an increase in calcium causes an increase in chromatin compaction in permeabilised cells. However, the chromatin in permeabilised cells, although it more closely resembles native chromatin than defined nucleosome arrays, is not identical to the chromatin of live cells. To test if chromatin condenses in live cells upon the increase in calcium, I used a Ca^{2+} ionophore (A23187) to increase the intracellular concentration of calcium. Ionophores are lipid soluble molecules that are able to transport ions across a lipid bilayer. A23187 can transport bivalent cations across cell membranes. Addition of 10µM of A3187 to cells leads to an increase in intracellular calcium levels. To show that the addition of A23187 leads to an increase in intracellular calcium levels, HeLa cells were loaded with the dye fluo4-AM and imaged prior and after the addition of A23187. Fluo4-AM is a calcium specific fluorescence indicator (Gee, Brown et al. 2000). Upon addition of the A23187 there was an increase in fluorescence of fluo4, confirming the increase in intracellular Ca^{2+} (Fig 18A).

To ascertain if this increase in calcium causes an increase in chromatin compaction, FLIM measurements of $HeLa^{H2B\text{-}2FP}$ cells were acquired before and after addition of A23187. There was a decrease in the measured EGFP fluorescence lifetime of cells after the addition of the ionophore indicating compaction of chromatin (Fig 18B, 18C). To asses if the compaction was global or increased only in region specific, fluorescence lifetime was calculated separately for the regions adjoining the nuclear

membrane, and the internal chromatin separately. The nuclear membrane is known to have higher concentratins od more compact heterochromatin. When analysed separately, there was no change in the levels of compaction of the two regions indicating that compaction induced with increasing calcium concentration was global.

Electron microscopy of HeLa cells after treatment with A23187 shows the presence of more dense chromatin regions indicating that the increase in Ca^{2+} in live cells leads to an increase in chromatin compaction (Fig 19).

Fig 18- (A)

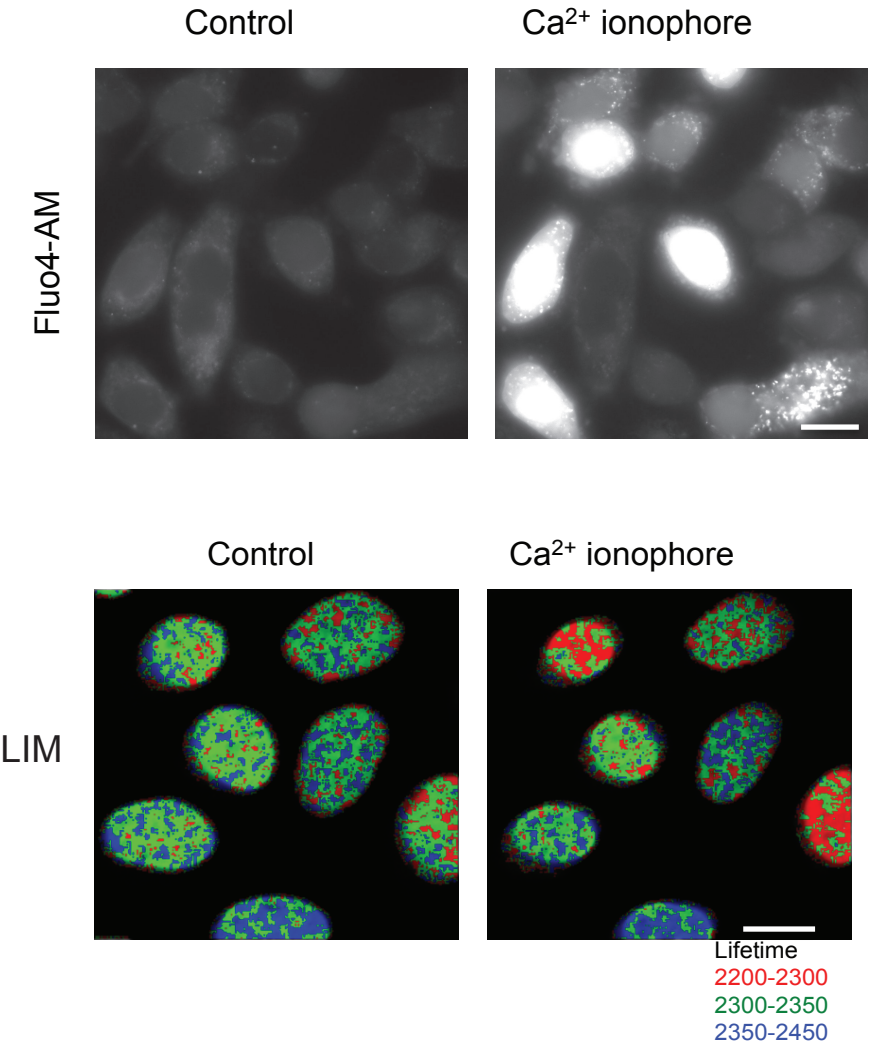

Fig 18 - (A) Fluo4-AM fluorescence images showing an increase in free intracelllar calcium levels on treating the cells with Ca^{2+} ionophore. (B) FLIM images showing a decrease in fluorescence lifetime of cells that have been treated with Ca^{2+} ionophore. (C) chart showing the mean normalised lifetime values of cells before and after treating with Ca^{2+} ionophore. (Scale bar - 10µm)

Control

Ca^{2+} ionophore

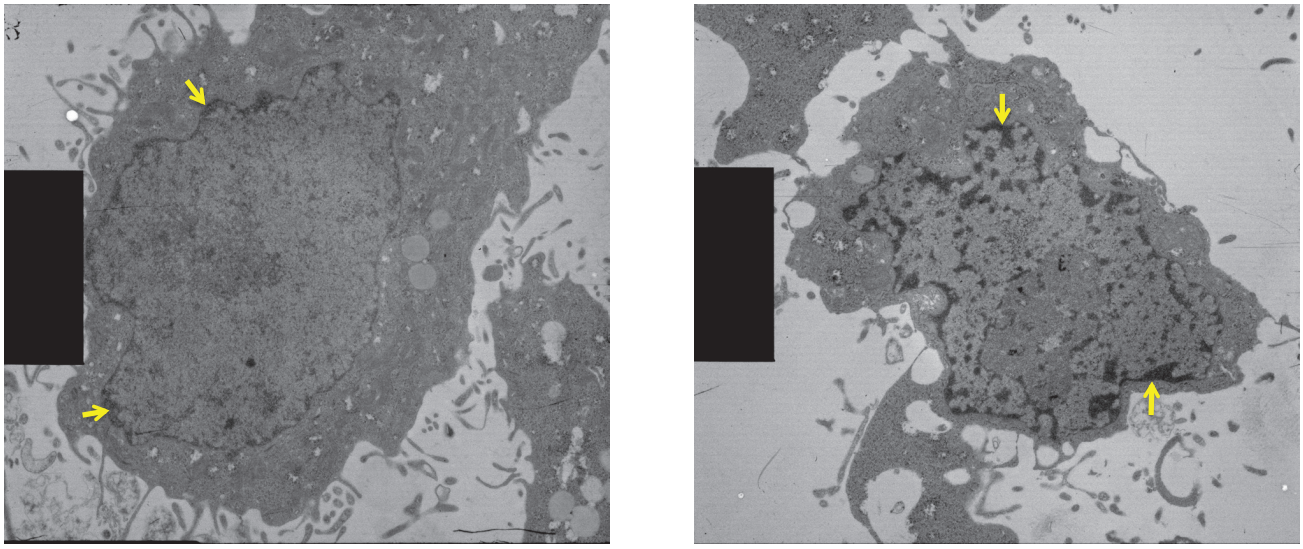

Fig 19 - Electron micrograps showing an increase in chromatin compaction of HeLa cells upon treatment with Ca^{2+} ionophore. The nuclear membrane is indicated with arrows. (Scale bar - 3920nm)

3.3 Discussion

The principle constituents of chromatin in eukaryotic cells are DNA and histones. DNA is highly negatively charged due to the presence of a negatively charged sugar phosphate backbone. Two copies of each of the four core histones form a single histone octamer, which complexes with DNA to form the nucleosome, which is the basic unit of chromatin. The histones are positively charged, due to the presence of positively charged lysine and arginine residues, which can neutralise ~60% of the DNA's phosphate backbone (Muthuswami, Mesner et al. 2000; Strick, Strissel et al. 2001). This still leaves the remaining 40% of the negative charge which can create internal repulsion. This repulsion, if not otherwise counteracted, will tend to cause the chromatin to adopt a de-compacted conformation.

Addition of polyvalent cations to nucleosome arrays has been shown to increase compaction (Korolev, Allahverdi et al. 2010). Most studies involving charge based compaction have been performed in well defined nucleosome arrays (Simpson, Thoma et al. 1985), prepared using vitro by assembly of their DNA and histone components.

The compaction state of nucleosome arrays can be quantified using a differential centrifugation assay and also by calculation of sedimentation velocity. The differential centrifugation assay involves the nucleosome array being suspended in the buffer of choice, incubated at room temperature and then centrifuged at

13,000g in a micro centrifuge and the percentage of the sample present in the supernatant being calculated (Schwarz and Hansen 1994). Upon complete intra-array nucleosome association brought out by increasing buffer polyvalent cation concentration, 100% of the arrays get pelleted. Sedimentation velocity also gives another measure of compaction of the nucleosome array. In saturated 12 nucleosome arrays, it was observed that sedimentation coefficient increases upon increasing the ionic concentration of the buffer. The increase in sedimentation coefficient correlates directly with the degree of compaction of the chromatin (Schwarz and Hansen 1994).

The above techniques however can only be used to quantify compaction of either assembled nucleosome arrays or isolated and fragmented native chromatin. The native chromatin in cells differs from isolated or reconstituted chromatin arrays due to the presence of a number of other factors, which can influence chromatin structure. The composition of the basic unit of the nucleosome varies with the presence of a number of different histone variants (Talbert and Henikoff 2010). The next level of complexity is brought about by the myriad of different histone post translational modifications, most of which are known to regulate the suitability of the modified chromatin for various processes (Kouzarides 2007). Chromatin binding proteins associate with chromatin and alter the local environment of chromatin, with some known to alter chromatin structure (Reeves 2010; Kwon and Workman 2011). Hence, the data obtained from the studies of nucleosome arrays, however valuable, does not necessarily represent chromatin dynamics in vivo in the nuclear environment.

Work from the Lamond laboratory has previously described a FLIM-FRET based technique for the quantification of chromatin compaction in live cells (Lleres, James et al. 2009). Using this technique, chromatin compaction changes in cells were described after ATP depletion, increased histone acetylation and during mitotis (Lleres, James et al. 2009). The technique is quantitative, making it possible to compare the obtained data with previously published quantitative data, derived using other techniques.

Nucleosome arrays compact following an increase in Mg^{2+} ions. This has been shown in studies using the differential centrifugation and sedimentation velocity assays (Schwarz and Hansen 1994). I first tested if this compaction can be quantified using the FLIM-FRET based technique. For the compaction assay, chromatin from $HeLa^{H2B-2FP}$ and $HeLa^{H2B-EGFP}$ cell lines was isolated. The chromatin from the $HeLa^{H2B-2FP}$ cells had histone H2B tagged separately with both EGFP or mCherry fluorescent proteins. The chromatin isolated from the $HeLa^{H2B-GFP}$ however, only had histone H2B tagged with EGFP alone.

The isolated chromatin from $HeLa^{H2B-2FP}$ was suspended in a buffer system devoid of any polyvalent cations. FLIM measurements of the chromatin was made with increasing concentrations of Mg^{2+}. As the concentration of Mg^{2+} are increased, the EGFP fluorescence lifetime values that gradually decreased. The decrease in EGFP lifetime values indicates that there is an increase in compaction (Lleres, James et al. 2009). When the chromatin isolated from $HeLa^{H2B-EGFP}$ was treated with the same conditions and imaged, there was also a decrease in the fluorescence lifetime values

with increasing Mg^{2+} ion concentration. However, it was seen that the decrease in normalised lifetime values of the chromatin from $HeLa^{H2B\text{-}2FP}$ was greater than the decrease in normalised lifetime values of chromatin from $HeLa^{H2B\text{-}EGFP}$ (Fig 11).

As chromatin compacts, the proximity between the histones, and thereby the fluorophores, will decrease. In cells expressing EGFP tagged histone H2B alone, compaction will result in crowding of the molecules due to the decreased proximity. This molecular crowding will result in an increased number of interactions/collisions between EGFP and the surrounding molecules, resulting in collisional quenching. Collisional quenching is know to decrease fluorescence lifetime (Vishwanath, Zhong et al. 2006). In $HeLa^{H2B\text{-}2FP}$ cells, in addition to EGFP, mCherry is also present. mCherry can act as an acceptor in a FRET reaction with EGFP. Thus the compaction results in bringing the two fluorophores in close proximity. FRET between molecules results in a decrease in fluorescence lifetime of the donor fluorophore and has been previously used to study protein-protein interactions (Lleres, Swift et al. 2007). Thus, chromatin from cells expressing both H2B-EGFP as well as mCherry-H2B, shows a greater decrease in the EGFP lifetime values, resulting from FRET and collisional quenching.

To show that the reduction in lifetime was not a consequence of Mg^{2+} interacting directly with EGFP, purified free EGFP was imaged using FLIM with increasing concentrations of Mg^{2+}. There was no decrease in the lifetime of EGFP with increasing concentrations of Mg^{2+} (Fig 11). This confirms that the decrease in lifetime

of H2B-GFP when comparing imaging of chromatin with increasing Mg^{2+} is due to chromatin compaction.

This experiment proved that the FLIM-FRET technique could quantify the increase in compaction of chromatin with increasing concentrations of Mg^{2+}, corroborating the studies from previous work (Schwarz and Hansen 1994). Chromatin from $HeLa^{H2B\text{-}2FP}$ cells with EGFP and mCherry labeled histones showed a greater decrease in the lifetime in FLIM measurements when compared with chromatin from $HeLa^{H2B\text{-}EGFP}$ and consequently provided better resolution.

To test if the increase in compaction was also observed for chromatin within nuclei, cells were first permeabilised so that the ionic concentrations could be manipulated. Permeabilisation was done in a buffer system containing HEPES and potassium acetate and digitonin. The concentration of digitonin to cause permeabilisation of the outer cellular membrane without permeabilising the nuclear membrane was empirically determined. After permeabilisation, $HeLa^{H2B\text{-}2FP}$ cells were imaged and fluorescence lifetime values were calculated with increasing concentrations of Mg^{2+}. Increasing the Mg^{2+} concentration led to a decrease in the calculated fluorescence lifetime values of EGFP, indicating an increase in chromatin compaction (Fig 12). The results were also corroborated by electron microscopy, where I observe an increase in chromatin compaction with increasing Mg^{2+} concentration (Fig 13).

The results showed that the chromatin compaction gradually increased with increase in Mg^{2+} ion concentration and saturated at about 6-8mM of Mg^{2+}. Mg^{2+} ion concentration was increased to 10mM and then 12mM of EDTA was added to the

cells. EDTA being a strong chelating agent will bind the divalent ion and thereby prevent its association with chromatin. Addition of EDTA resulted in decompaction of the chromatin. However, the reversal of the compaction was not complete and the lifetime values of EGFP fell back to the same level of compaction as observed with 2mM of Mg^{2+}, although an excess of EDTA was present. This indicates the possibility of an intermediate structure of greater stability being formed at 2mM of Mg^{2+} and/or the chromatin having different modes/sites of binding with different binding affinities. If binding of Mg^{2+} to certain sites in chromatin has higher affinity than to EDTA, the Mg^{2+} ions would not have been displaced.

Previous experiments conducted with defined nucleosome arrays, show that the compaction results from of two types of interactions- intra-array and inter-array. Intra-array interactions occur between nucleosomes in the same nucleosome array and lead to the formation of the 30nm fiber (Zheng, Lu et al. 2005). Inter-array interactions are the interactions between nucleosomes in different nucleosome arrays. Intra-array interactions that result in the formation of the 30nm fiber from an extended 'beads on a string' structure has been shown to happen at 2mM of Mg^{2+} with intermediate structures formed at lower concentrations (Zheng, Lu et al. 2005). Further increasing the Mg^{2+} concentration has been shown to cause inter-array nucleosome interactions. Experiments studying the interaction of histone tails of H3 and H4 (Kan, Lu et al. 2007; Kan, Caterino et al. 2009) associating with histones of other arrays (inter-array) has shown that at 2mM of Mg^{2+} there are no inter-array nucleosome interactions, but this gradually increases at higher Mg^{2+} concentrations, saturating at 6-8mM of Mg^{2+}. This indicates that intra-array interactions precede

inter-array nucleosome interactions. Their data suggest that at a concentration 2mM of Mg^{2+} only intra-array interactions occur, with the absence of inter-array interactions. At higher concentrations of Mg^{2+}, these nucleosome arrays that have formed intra-array interactions associate with each other saturating at 6-8mM of Mg^{2+}.

The data obtained form FLIM based experiments in permeabilised cells also show maximal compaction at 6-8mM of Mg^{2+}. Addition of EDTA did not cause complete reversal of compaction, with the lifetime values falling back to what was observed at 2mM of Mg^{2+}. This could suggest that chromatin of permeabilised cells forms the 30nm structure at 2mM of Mg^{2+}, which is more stable and inter array associations of chromatin fibers occur at higher concentrations of Mg^{2+}, which is reversible upon the addition of EDTA.

To test if the observed effects with increasing Mg^{2+} is either specific to Mg^{2+}, or is a charge based effect, similar experiments were done with Ca^{2+}. Increasing Ca^{2+} concentration also showed the same compaction dynamics in $HeLa^{H2B\text{-}2FP}$ cells. There was a gradual increase in compaction of chromatin, as observed by the reduction of EGFP fluorescence lifetime values. The compaction saturated at 6-8mM of Ca^{2+}. Chelation of Ca^{2+} by addition of excess of EDTA resulted in de-compaction of chromatin, however the reversal again was not complete. The fluorescence lifetime values after addition of EDTA were similar to those observed with 2mM of Ca^{2+}. The effect of increasing Ca^{2+} concentration on chromatin compaction was almost

identical to that of increasing Mg^{2+} (Fig 14). This shows that the compaction was possibly an effect of charge neutralization and not specific to Mg^{2+}.

Calcium and magnesium ions in solution have a charge of +2. All living cells, from bacteria to eukaryotes, have polyamines that have been shown to be essential for growth (Wallace, Fraser et al. 2003). The levels of these polyamines have been shown to be regulated, with their reduction leading to a reduction of nucleic acid and protein synthesis, eventually giving rise to cell growth inhibition (Persson 2009). These polyamines are charged in solution, ranging from +2 to +4. If the observed chromatin compaction with Mg^{2+} and Ca^{2+} was a charge-based effect, the addition of the polyamines to permeabilised cells should also result in the compaction of chromatin.

It has been previously shown that the addition of polyamines to nucleosome arrays leads to their compaction as observed with an increase in their sedimentation coefficient (Korolev, Allahverdi et al. 2010). To test this $HeLa^{H2B\text{-}2FP}$ cells were permeabilised and the polyamines spermidine and spermine, with charges of +3 and +4, respectively, were gradually added to the cells. As the concentration of the polyamines was increased, there was an increase in the compaction of chromatin, as observed by the reduction of the calculated EGFP fluorescence lifetime values (Fig 15-16). The EGFP fluorescence lifetime values gradually decreased, with a minimum reached at about 1.5mM of spermidine and 0.21mM of spermine. Thus the charge of the cation increased, there was a corresponding reduction in the concentration

needed to cause a similar compaction state. The above experiments show a direct correlation between charge neutralisation and chromatin compaction.

Another important constituent of chromatin in cells is RNA. RNA, similar to DNA, is also made of nucleotides and has a highly negatively charged poly phosphate backbone. If the addition of cations to permeabilised cells can cause compaction of chromatin, the removal of RNA, which would also influence the net charge, should also show an effect on the compaction state of chromatin. To test if this was true, $HeLa^{H2B\text{-}2FP}$ cells were permeabilised and imaged by FLIM before and after the addition of RNAse A to the cells. Treating the permeabilised nuclei with RNAse A will cleave single stranded RNA into its constituent nucleotides, allowing these small molecules to diffuse from the nucleus. This will result in lowering the net negative charge of chromatin.

As expected, there was an increase in the compaction of chromatin after treating the cells with RNAse, as observed with a decrease in the calculated fluorescence lifetime of EGFP (Fig 17). The compaction of chromatin in cells that have been treated with RNAse has also been shown recently by Caudron-Herger et al., (Caudron-Herger, Muller-Ott et al. 2011). In their experiments, RNAse was micro-injected into living cells and this led to an increase in the compaction of chromatin. RNAse treatment of live cells could also lead to the loss of RNA that is not transported out of the nucleus, but which might have a role to play in modulating chromatin compaction. The effect observed in live cells could also be due to the change in the charged state of chromatin and thus is not specific to permeabilised cells.

The nucleoli of a cell account for all the rRNA production within a cell. rRNA transcription accounts for 50% of the RNA produced within the cell (Raska, Koberna et al. 2004). Considering that the nucleolus accounts for all the rRNA production, with a much smaller nuclear volume, one can expect a higher proportion of RNA in the nucleolus when compared to other regions of the nucleus. If the increase in compaction is a result of loss of charge, the chromatin associated with nucleolar regions should compact more than other regions of chromatin. The results showed that perinucleolar heterochromatin did compact to a higher extent with RNAse treatment when compared to the rest of the chromatin.

The experiments described above were all done with permeabilised cells. Although they represent a more native environment when compared with defined nucleosome arrays, they still differ from intact live cells. The 30nm fibre although extensively studied in an in vitro system, has not been identified in live cells (Tremethick 2007; Eltsov, Maclellan et al. 2008; Joti, Hikima et al. 2012). However, the data from increasing bivalent cation concentrations correlates with data from nucleosome arrays, where the 30nm fibre has been observed. If the structure formed at either 2mM Mg^{2+}, or 2mM Ca^{2+}, in the chromatin of permeabilised cells is the 30nm fibre, it could be an artifact created by the permeabilisation of cells.

To study the effect of changing cation concentration within live cells, I used the calcium ionophore – A23187. Addition of the calcium ionophore to cells causes an increase in the intracellular concentration of calcium. The effect is quick and drastic.

To visualise the increase in calcium, I used the cell permeable calcium binding dye Fluo4-AM. Fluo4-AM is a cell permeable compound, which, on entering the cells is cleaved to its active form and becomes impermeable to the cell membrane. This dye only fluoresces when bound to calcium, hence its fluorescence is an indication of the concentration of free calcium within the cell.

When calcium ionophore was added to cells loaded with the calcium sensing dye, there was an increase in fluorescence, indicating an increase in the free calcium concentration (Fig18A). This increase in fluorescence varied between cells, with some cells showing much higher fluorescence than other cells. To check if this increase in intracellular calcium concentration had an effect of chromatin compaction, HeLa$^{H2B\text{-}2FP}$ cells were imaged both before and after addition of the calcium ionophore and the EGFP fluorescence lifetime values were calculated. The results showed that after the addition of the calcium ionophore, there was an increase in chromatin compaction observed as the decrease in the EGFP fluorescence lifetime values of the cells (Fig 18). The increase in compaction was seen through out the nucleus and not localised to the membrane bound or internal chromatin regions.

The difference in EGFP fluorescence lifetime values varied between cells. This could possibly be attributed to the fact that the increase in calcium was not identical between cells after calcium ionophore treatment, as observed with the differences in the increase of Fluo4 fluorescence. To corroborate the observed result, the HeLa cells treated with calcium ionophore were fixed and imaged using electron

microscopy. Electron micrographs also showed an increase in chromatin compaction after the cells were treated with calcium ionophore (Fig19). This shows that increasing intracellular calcium concentration leads to an increase in chromatin compaction.

These results show a strong correlation between charge and chromatin compaction. The intracellular concentration of free magnesium was measured to be around 1.5mM in Mouse Skeletal Muscle Fibers using a fluorescent indicator (Csernoch, Bernengo et al. 1998). Ion microscopy experiments by Strick et al., (Strick, Strissel et al. 2001) have shown that the concentration of calcium and magnesium bound to the interphase and mitotic chromosomes varies, with a four fold increase during mitosis. That study suggests that the increase in divalent cation concentration could facilitate the increase in chromatin compaction seen during mitosis. Other known mechanisms of influencing the charge of chromatin include varying histone modifications, like acetylation and phosphorylation, leading to changes in chromatin structure (Kouzarides 2007). These previous results, along with the data in this thesis, show that there is a direct effect of the internal ionic environment on the maintenance of chromatin structure.

Chapter 4

ATP dependent chromatin compaction

4.1 Abstract

ATP is called the energy currency of the cell and is consequently required for most energy-dependent cellular processes. ATP is highly negatively charged with a charge of -4 in solution, which causes it to bind cations. It has been reported that the depletion of ATP leads to the formation of compacted chromatin in vivo, indicating a role for ATP in the maintenance of decompacted chromatin (Lleres, James et al. 2009). However, the mechanism responsible for this effect was unclear. ATP depletion leads to the inactivation of a number of processes, one or more of which could lead to the observed increase in chromatin compaction.

In this chapter I have investigated the mechanism of ATP-dependent chromatin decompaction. Cells were treated in various ways to replicate the separate effects of ATP depletion, independent of each other and their effect on chromatin compaction was studied. ATP depletion-induced compaction was observed in cells that were pretreated with a kinase inhibitor or after transcription inhibition. An increase in compaction was also seen in mitotic chromosomes, in the absence of processes like transcription and DNA synthesis. I finally show the mechanism leading to compaction might involve polyvalent cations, which have been shown to compact chromatin in the first chapter of this thesis.

4.2 Results

4.2.1 ATP depletion leads to an increase in chromatin compaction

ATP is required for many processes within living cells where it acts as an energy donor to drive a wide range of reactions that are coupled to ATP hydrolysis. Depletion of ATP in vivo can be accomplished with the addition of drugs that inhibit both oxidative phosphorylation as well as glycolytic pathways (Endale, Kim et al. 2010). It has been previously shown that depletion of ATP causes major changes in the nucleus, including the formation of electron-dense barriers inside the nucleoplasm (Shav- Tal et al., 2004; Lleres et al 2010), which correspond to compacted chromatin.

$HeLa^{H2B\text{-}2FP}$ cells stably expressing H2B-EGFP and mCherry-H2B can be depleted of ATP by treating with 10mM sodium azide and 50mM 2-deoxy glucose (Lleres, James et al. 2009). $HeLa^{H2B\text{-}2FP}$ cells were imaged and FLIM measurements were acquired. The cells were then treated with the above-mentioned drugs to deplete the cells of ATP and FLIM measurements were acquired after 10 minutes of treatment. The drug was then washed away and another set of FLIM measurements were acquired after 10 minutes of having washed the cells (Fig 20).

There was a drastic increase in the compaction of chromatin upon addition of the drugs. The effect can be seen within 10 minutes of adding the drug. On removal of the drugs, decompaction was observed after 10 minutes with the fluorescence lifetime reverting to the control levels. The results were consistent with the

previously observed results shown by Lleres et al,. (Lleres, James et al. 2009) confirming that the chromatin compacts reversibly with the depletion of ATP.

I further analysed if the changes in compaction were in specific regions. To test this the lifetime of the chromatin surrounding the nuclear membrane and the internal regions were analysed separately. The chromatin adjacent the nuclear membrane is known to contain higher concentrations of condensed heterochromatin. Analysis showed that there was no difference in the compaction dynamics between the two regions indicating global compaction of chromatin (Fig 20B).

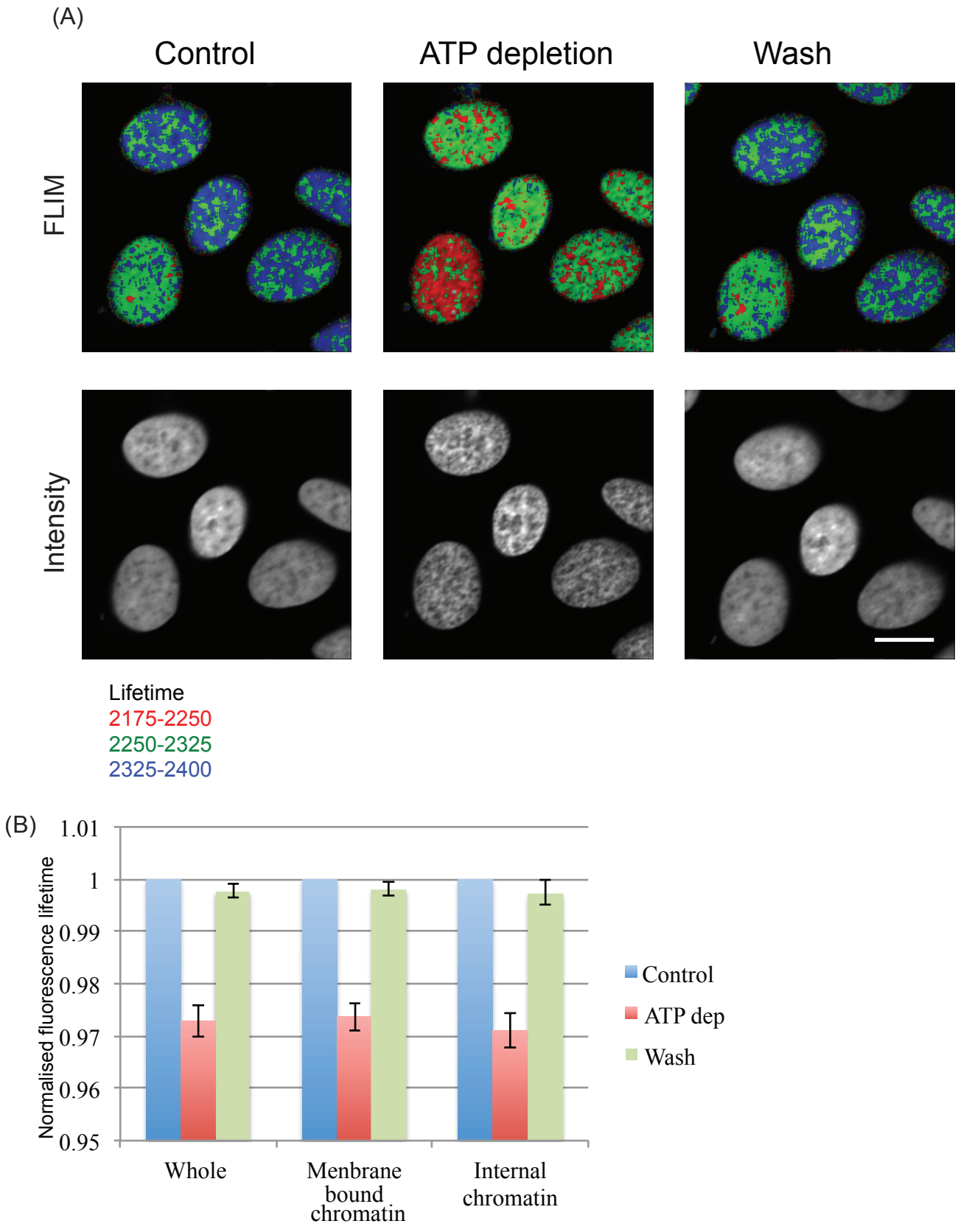

Fig 20 - (A) Flim images show the reduction of fluorescence lifetime in HelaH²b²FP cells upon ATP depletion and an increase when the drugs are washed away. The increase in compaction is also seen in the intensity images (Scale bar - 10µm). (B) The chart shows the average decrease and subsequent increase in normalised fluorescence lifetime values. Error bars indicate standard deviation.

4.2.2 ATP depletion after treatment with staurosporine

Staurosporine is a broad spectrum kinase inhibitor (Ruegg and Burgess 1989). Phosphorylation plays a major role in signaling pathways that are activated upon energy depletion. Staurosporine has been shown to inhibit AMPK, which is activated during reduced energy levels (Anderson, Cool et al. 2004). To check if protein phosphorylation had a role to play in the compaction dynamics caused by the depletion of energy, $HeLa^{H2B\text{-}2FP}$ were first treated with 0.5µM staurosporine for two hours. FLIM measurements were then acquired before and after 10 minutes of ATP depletion as explained in the previous result. The treatment of the cells with drugs that deplete ATP led to increased compaction of chromatin as observed by a decrease of EGFP fluorescence lifetime after ATP depletion showing that the compaction caused due to ATP depletion was not prevented by staurosporine treatment (Fig 21). The ATP depleting drugs were then washed away but the presence of staurosporine was maintained. Washing away the ATP depleting drugs led to de-compaction of the chromatin in the presence of 0.5µM staurosporine (Fig 21). The activity of Staurosporine was confirmed by blotting for Histone 3 serine 10 phosphorylation which is reduced upon treatment (Fig 21 C).

This result showed that the compaction of chromatin caused by the depletion of ATP is independent of kinases that are inhibited by staurosporine.

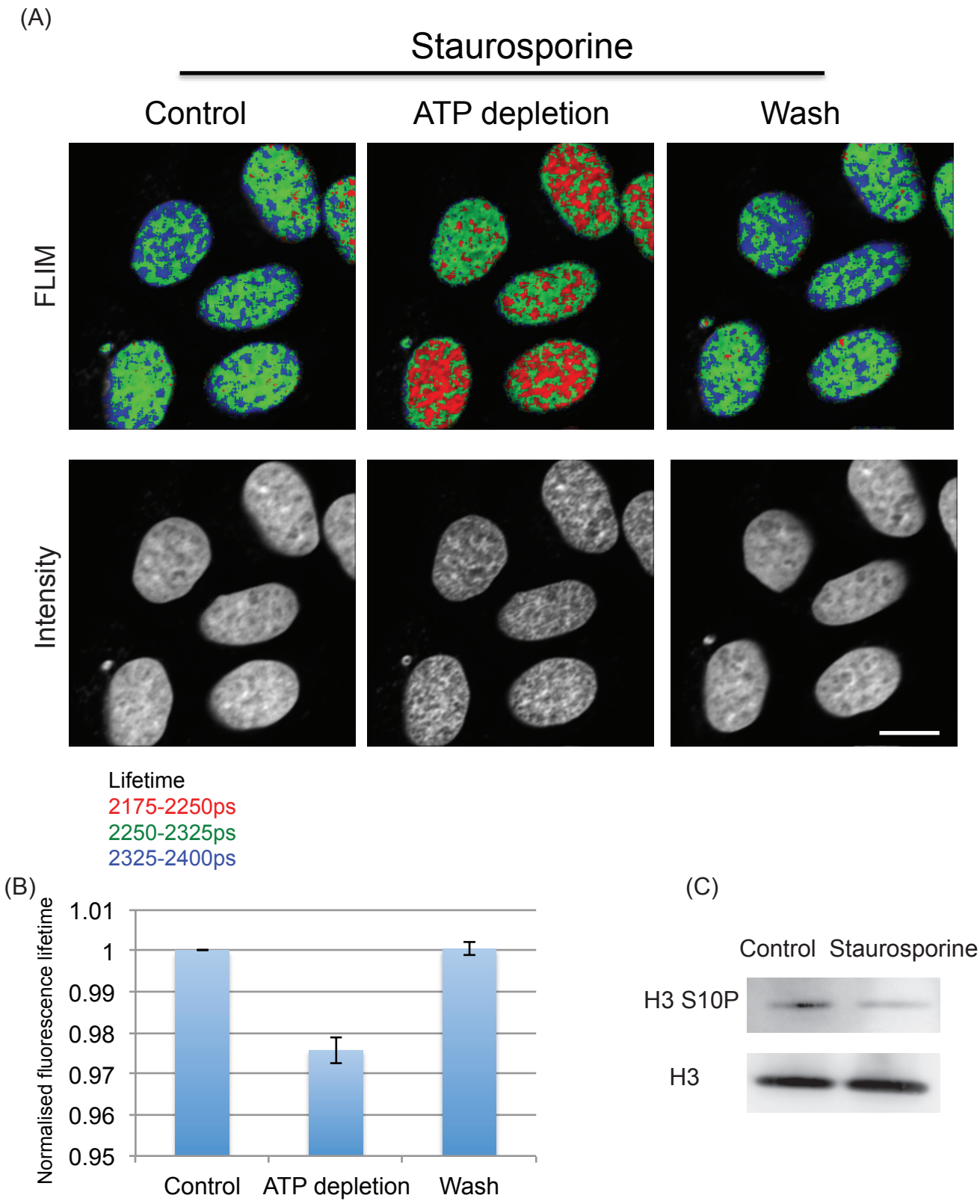

Fig 21 - (A) Flim images show the reduction of fluorescence lifetime in Hela^{H2b2FP} cells upon ATP depletion and an increase when the drugs are washed away in the presence of Staurosporine. The cells were incubated in the presence of Staurosporine for 2 hours at a concentration of 0.5µM, prior to ATP depletion. The increase in compaction is also seen in the intensity images. (Scale bar - 10µm)
(B) The chart shows the average decrease and subsequent increase in normalised fluorescence lifetime values. Error bars indicate standard deviation. (C) Western blotting showing the decrease of H3 serine 10 phosphorylation after staurosporine treatment for 2 hours at a concentration of 0.5µM.

4.2.3 Chromatin compaction arising from ATP depletion does not result from transcription inhibition

Actively transcribed regions have been shown to be associated with decompacted regions of chromatin in interphase cells (Schneider and Grosschedl 2007). Depletion of ATP leads to the inhibition of transcription. To test if the compaction of chromatin associated with depletion of ATP is brought about primarily by the inhibition of transcription, transcription was inhibited in cells directly and the resulting effect of chromatin compaction was studied.

Inhibition of transcription was caused by the addition of DRB at a concentration of 25µg/ml (Sehgal, Darnell et al. 1976). DRB is an inhibitor of Cdk-activating kinase, and consequently prevents elongation by RNA polymerase II (Yankulov, Yamashita et al. 1995). The cells were pulse labeled with 5-ethynyl uridine for 30 minutes prior to fixation. The newly synthesised RNA incorporates 5-ethynyl uridine, which can then be visualised by conjugating it with Alexa fluor-488 fluorophore. At 60 minutes after addition of DRB, transcription in the nucleoplasm was inhibited, as seen from Alexa fluor-488 fluorescence (Fig 22A).

To test if the inhibition of transcription led to changes in chromatin compaction, FLIM measurements were acquired form HeLa$^{H2B\text{-}2FP}$ cells before and after treatment with 25µg/ml DRB for 60 minutes. The measured fluorescence lifetime values showed a small decrease of about 10ps on average after treatment with DRB to inhibit transcription. Subsequently treating the cells with ATP depleting drugs led to a much higher increase in compaction with a decrease in the fluorescence lifetime by

about 56ps on average (Fig 22). The compaction is also seen from the intensity images, which correspond to H2B-EGFP fluorescence (Fig 22B).

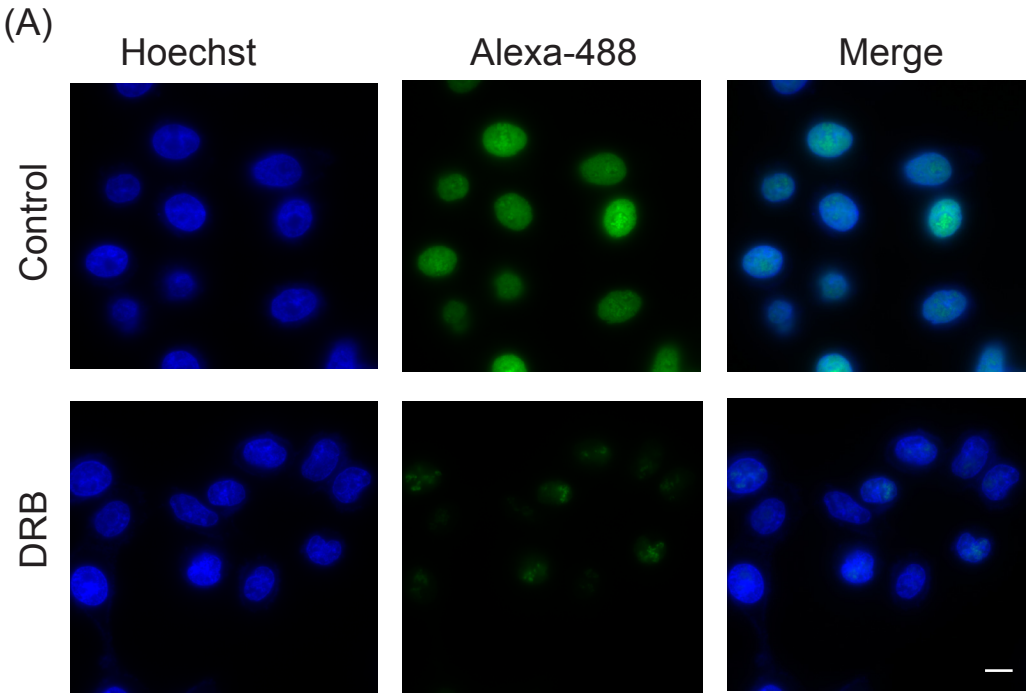

Fig 22 - (A) the panel shows HeLa cells with nuclear (Hoechst) and nascent RNA (Alexa-488) staining (pulse labelled with EU for 30m). The upper panel shows control cells and the lower panel shows cells treated with DRB at a concentration of 25µg/ml for 60 minutes. (Scale bar-10µm)

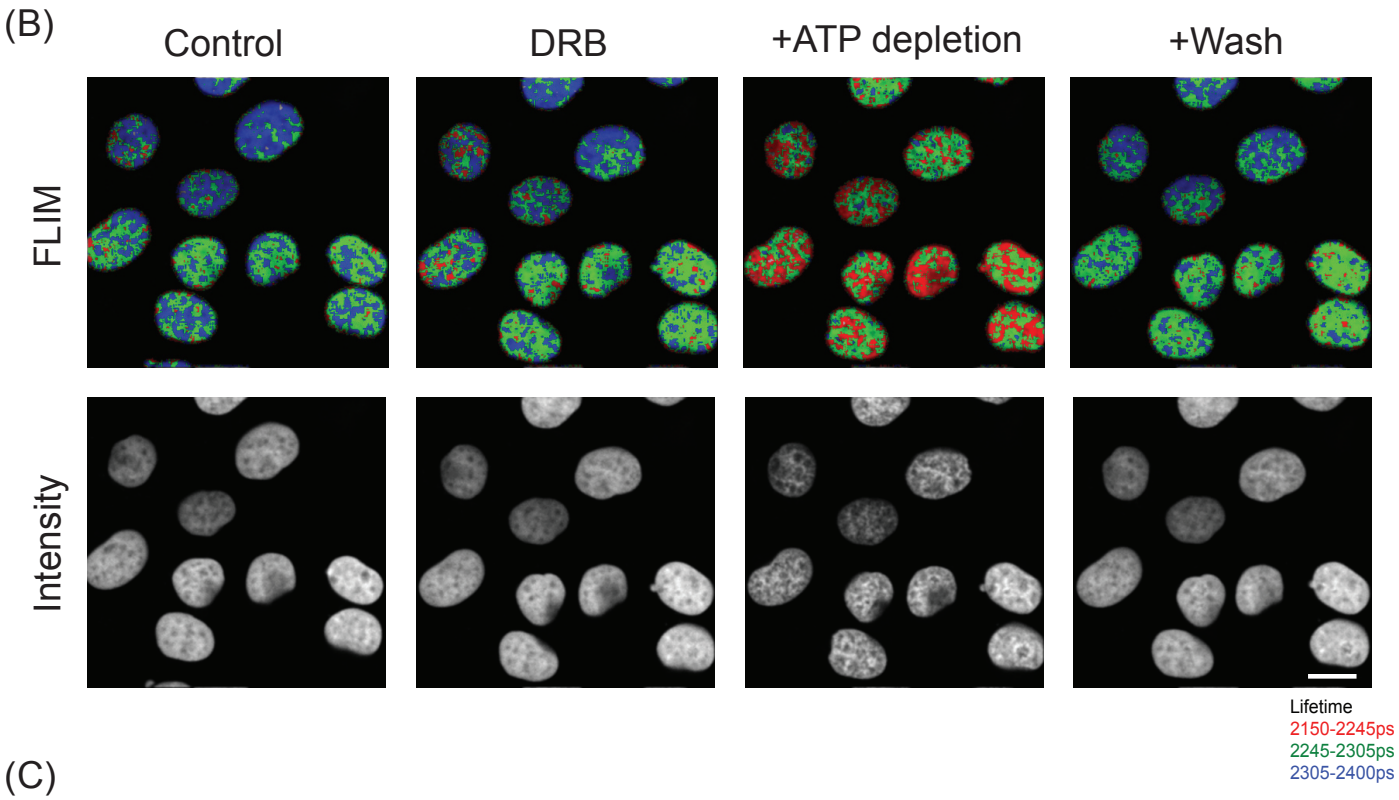

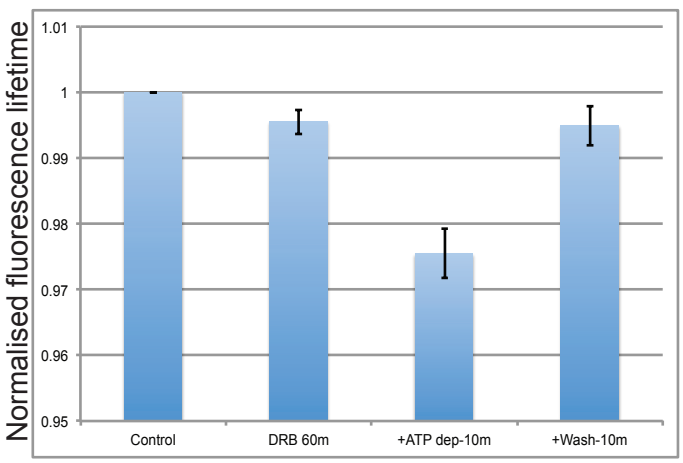

Fig 22 - (B) FLIM images showing a decrease in fluorescence lifetime upon ATP depletion for 10 minutes in cells treated with DRB at a concentration of 25µg/ml for 60 minutes, which is reversed upon washing away of the drugs. The resulting chromatin compaction is evident from the Intensity images of H2B-GFP fluorescence. (Scale bar-10µm)
(C) The chart shows the averaged normalised fluorescence lifetime values of each of the cells upon treatement. Error bars indicate standard deviation.

4.2.4 ATP depletion increases compaction of mitotic chromosomes

Mitotic chromosomes are formed by condensation of the interphase chromosomes, but also lack a number of associated proteins and are not active in transcription or replication. To check if the compaction of chromatin upon ATP depletion is either specific for interphase chromatin, or if the effect can also be seen in mitotic chromosomes, FLIM measurements of mitotic chromosomes before and after ATP depletion were acquired as described in previous experiments. ATP depletion using the drugs sodium azide and 2-deoxy glucose of $HeLa^{H2B\text{-}2FP}$ mitotic cells led to a decrease in the measured fluorescence lifetime, indicating further compaction of the mitotic chromosomes (Fig 23). This compaction could be reversed upon washing away the drugs, similar to that observed in interphase cells.

(A)

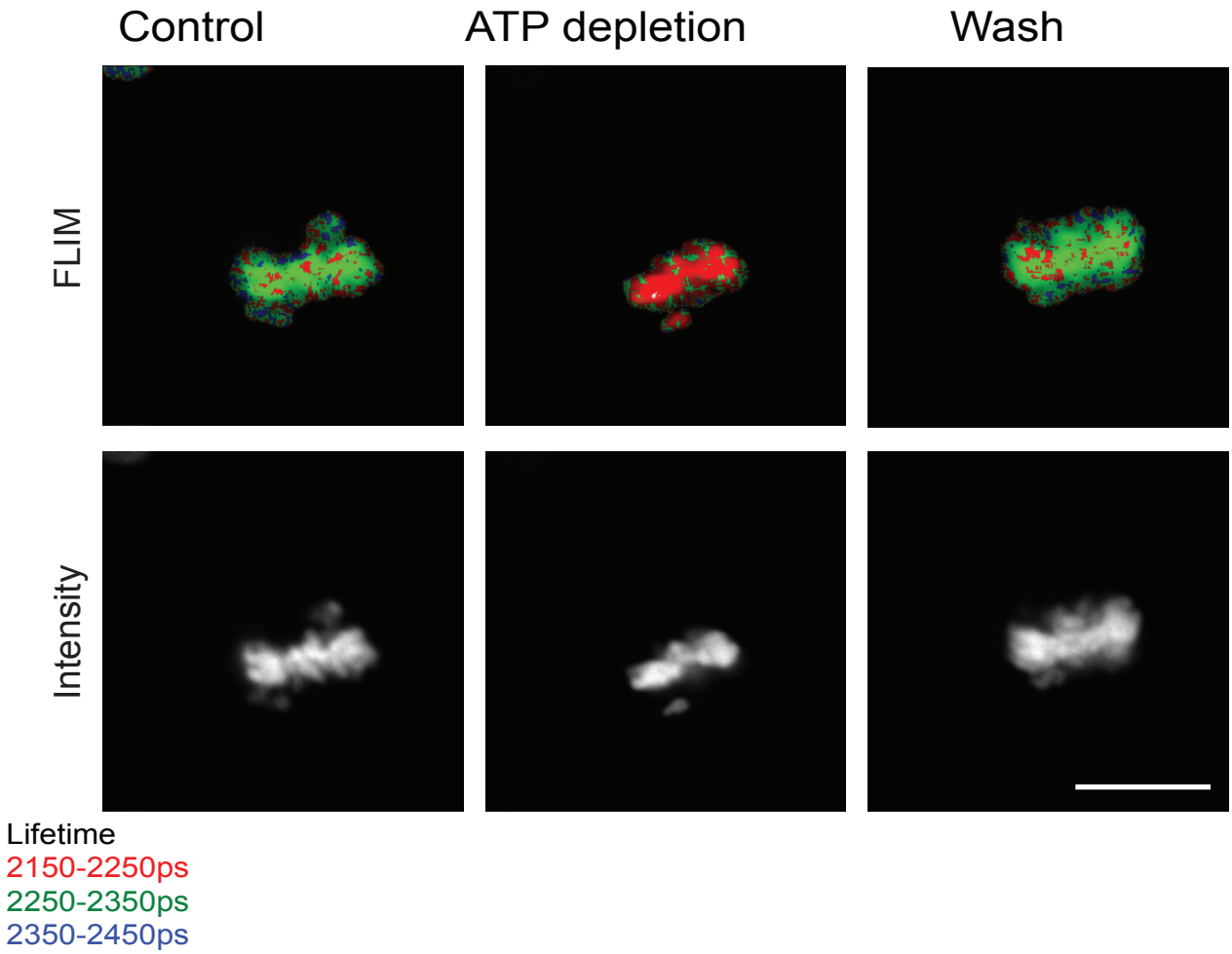

(B)

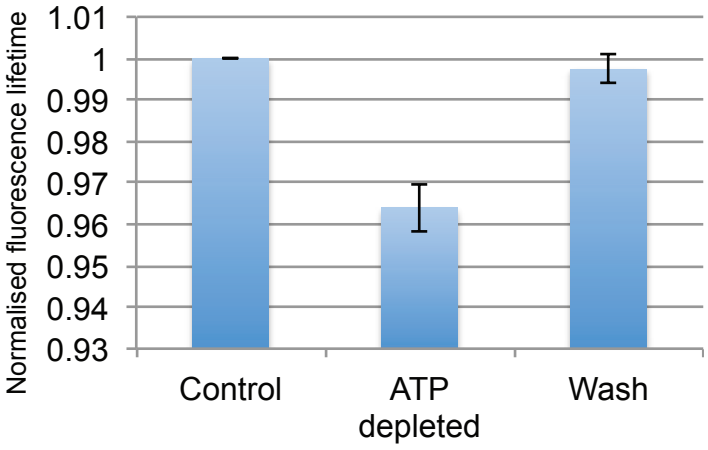

Fig 23 - Mitotic chromatin compacts with ATP depletion. (A) FLIM images showing a decrease in fluorescence lifetime on ATP depletion and its subsequent increase to control levels when the drugs are washed away in Hela^{H2b2FP} cells (Scale bar - 10µm). (B) Chart showing the average normalised fluorescence intensity from three mitotic cells showning changes upon ATP depletion and repletion. Error bars indicate standard deviation.

4.2.5 Compaction caused by ATP is lost upon permeabilisation of treated cells

To check if the mechanism leading to chromatin compaction in cells upon ATP depletion is mediated either by a stable modification of chromatin, or by a soluble factor, cells were permeabilised after ATP depletion, which results in the loss of soluble factors by dilution. HeLa$^{H2B\text{-}2FP}$ were treated with sodium azide and 2-deoxy glucose to cause depletion of ATP. FLIM measurements were acquired, both before and 10 minutes after the addition of the drugs. The observed decrease in fluorescence lifetime showed the compaction of chromatin upon ATP depletion. These cells were then incubated in a buffer containing 110mM potassium acetate, 20mM HEPES (pH- 7.4) and 0.00125% digitonin for 5 minutes at 37°C to permeabilise them. The buffer was then washed away and replaced with the same buffer lacking digitonin. FLIM measurements acquired after permeabilisation showed an increase in the measured lifetime indicating decompaction (Fig 24). The lifetime values of the cells upon permeabilisation were higher that the control values by an average of about 33ps, indicating lower levels of compaction when compared to unpermeabilised control cells. This shows the possibility that one or more factors leading to chromatin compaction after ATP depletion are lost upon permeabilisation.

(A)

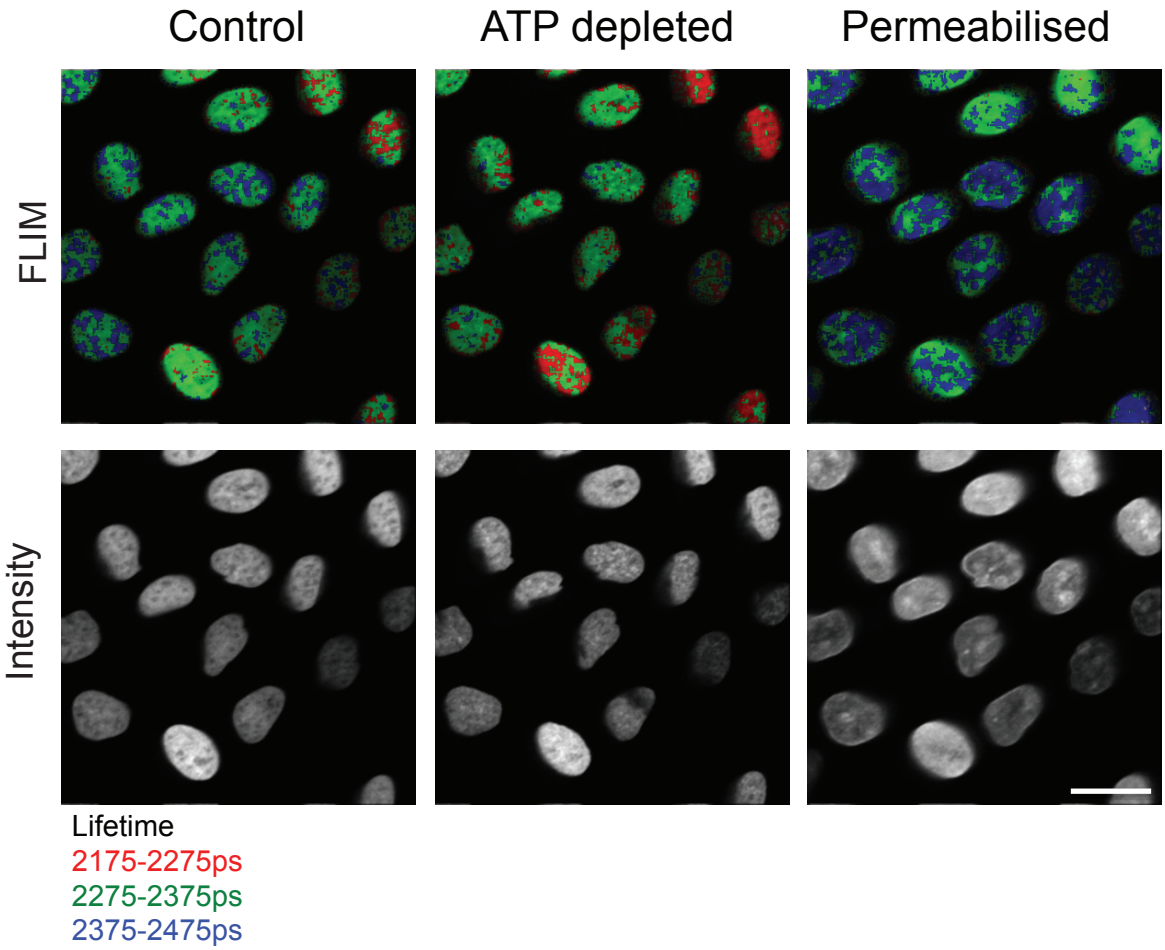

(B)

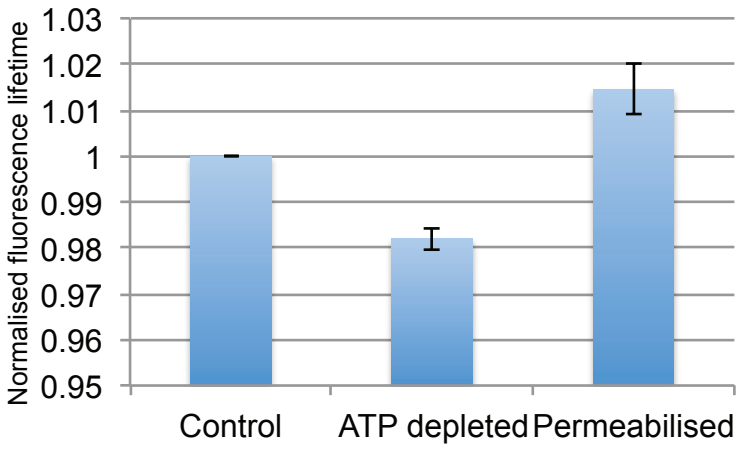

Fig 24 - (A) Flim images show the incresae in compaction observed as the decrease in lifetime, upon ATP depletion is lost when the cells are permeabilised. The permeabilised cells have lifetimes that are higher than the control cells (Scale bar - 10µm). (B) The chart below shows the decrease and increase of the normalised lifetime values of the cells. Error bars indicate standard deviation.

4.2.6 Addition of ATP to permeabilised cells

ATP is impermeable to cell membranes. To check if the presence of ATP could lead to de-compaction, HeLa$^{H2B\text{-}2FPs}$ cells were permeabilised by incubating in a buffer containing 110mM potassium acetate, 20mM HEPES (pH- 7.4), 2mM Mg acetate and 0.00125% digitonin for 7 minutes at room temperature. The cells were then washed with the same buffer lacking digitonin. FLIM measurements of the permeabilised cells were acquired before and after the addition of 2mM magnesium salt of ATP. There was no significant change in the measured FLIM values after the addition of ATP (Fig 25).

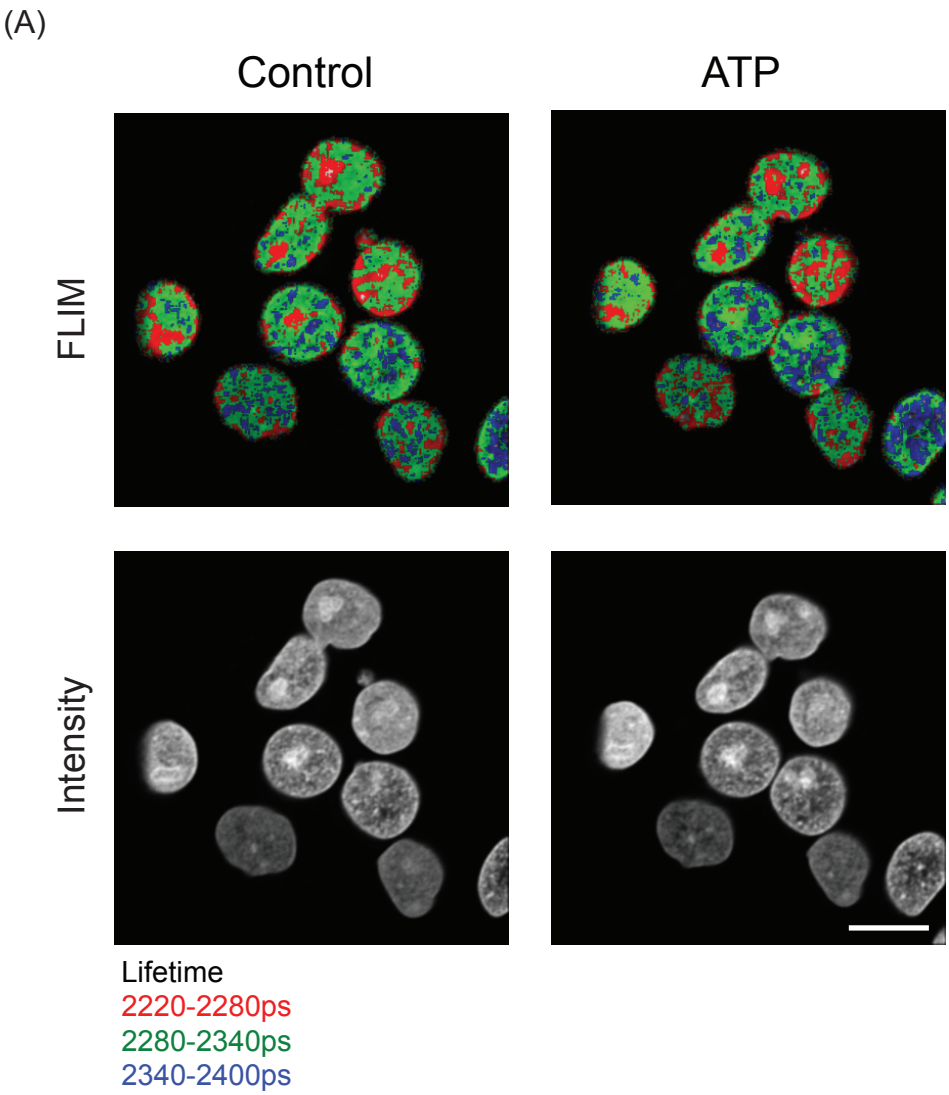

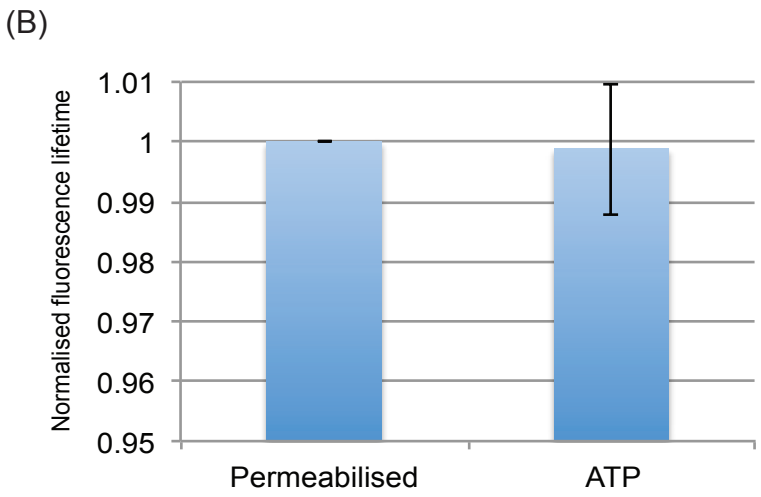

Fig 25 - (A) FLIM images showing no changes in the flourescence lifetime in permeabilised Hela^{H2b2FP} cells with the addition of ATP (Scale bar - 10µm). (B) Chart showing the average normalised lifetime for permeabilised cells with addition of ATP. Error bars indicate standard deviation.

4.2.7 ATP depletion leads to an increase in the intracellular Ca^{2+} concentration

Increasing Ca^{2+} in cells leads to increased chromatin compaction in permeabilised as well as live cells, as shown in previous results (Fig - 14, 19). Ca^{2+} has also been implicated in compaction of mitotic chromosomes as shown by ion microscopy, wherein there is an increased concentration of Ca^{2+} on mitotic chromosomes when compared with interphase chromatin (Reiner Strick et al., 2001). It has also been shown by the same technique that cytoplasmic Ca^{2+} is higher than the nuclear Ca^{2+} concentration using the same technique (Reiner Strick et al., 2001). However there have been conflicting reports on the differential regulation of Ca^{2+} concentrations between the nucleus and cytoplasm (Enrico Zampese and Paola Pizzo 2012) in interphase cells.

Calcium was imaged in HeLa cells using the Fluo4-AM dye. Fluo4-AM is a cell permeable compound, which, on entering the cell, is cleaved into the active form by cellular esterases, rendering it impermeable to cellular membranes. When active, the dye fluoresces only when bound to calcium (Gee, Brown et al. 2000). The dye has an excitation maxima and minima at 488nm and 506nm, respectively.

HeLa cells loaded with Fluo4-AM were imaged before and after ATP depletion with sodium azide and 2-deoxy glucose. Control cells showed lower fluorescence in the nuclear regions, identified by nuclear staining with Hoechst 33342, when compared to cytoplasmic regions. This indicates lower calcium levels within the nucleus than in the cytoplasm in interphase cells. Upon ATP depletion, there was an increase in

fluorescence showing an increase in Ca^{2+} concentration, which was homogenous throughout the cell (Fig 26). The compaction of chromatin can be seen with the Hoechst 33342 staining (Fig 26- indicated by yellow arrowheads).

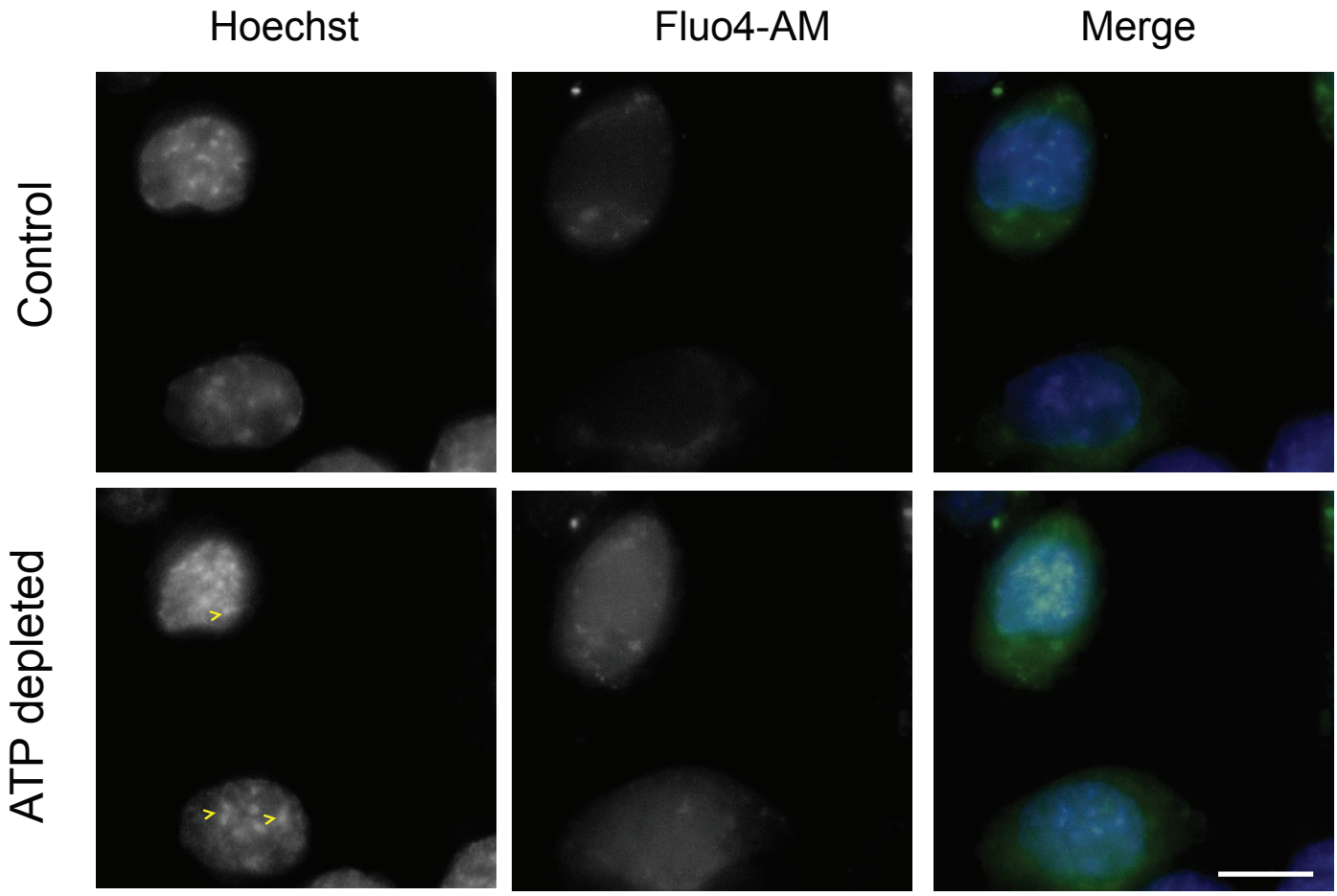

Fig 26 - ATP depletion leads to an increase in intrecellular free calcium levels. Fluo4-AM loaded HeLa cells were imaged before and after ATP depletion. The increase in fluorescence indicates an increase in free intracellular calcium levels. The increase in chromatin compaction (yellow arrow head) can be seen from Hoechst staining after ATP depletion. (Scale bar - 10µm)

4.2.8 Preventing the increase in unbound intracellular Ca^{2+} upon ATP depletion using BAPTA-AM does not prevent chromatin compaction

ATP depletion causes an increase in intracellular calcium concentration. This increase in free calcium can be inhibited using the cell permeable chelater of calcium BAPTA-AM. BAPTA-AM is a cell permeable chelater of calcium, which when inside the cell is cleaved by esterases to form the active form – BAPTA, and loses its ability to traverse cellular membranes.

Cells were loaded with BATA-AM along with Fluo4-AM to image the changes in Ca^{2+}. Cells were imaged before and after ATP depletion. In the presence of BAPTA, there was no increase in the fluorescence of Fluo4-AM showing that there was no increase in the free intracellular Ca^{2+} (Fig 27). However, there was an increase in compaction of chromatin as seen with Hoechst 33342 staining (Fig 27 - indicated by yellow arrowheads). Preventing the increase in free intracellular calcium, therefore, did not inhibit chromatin compaction caused by ATP depletion.

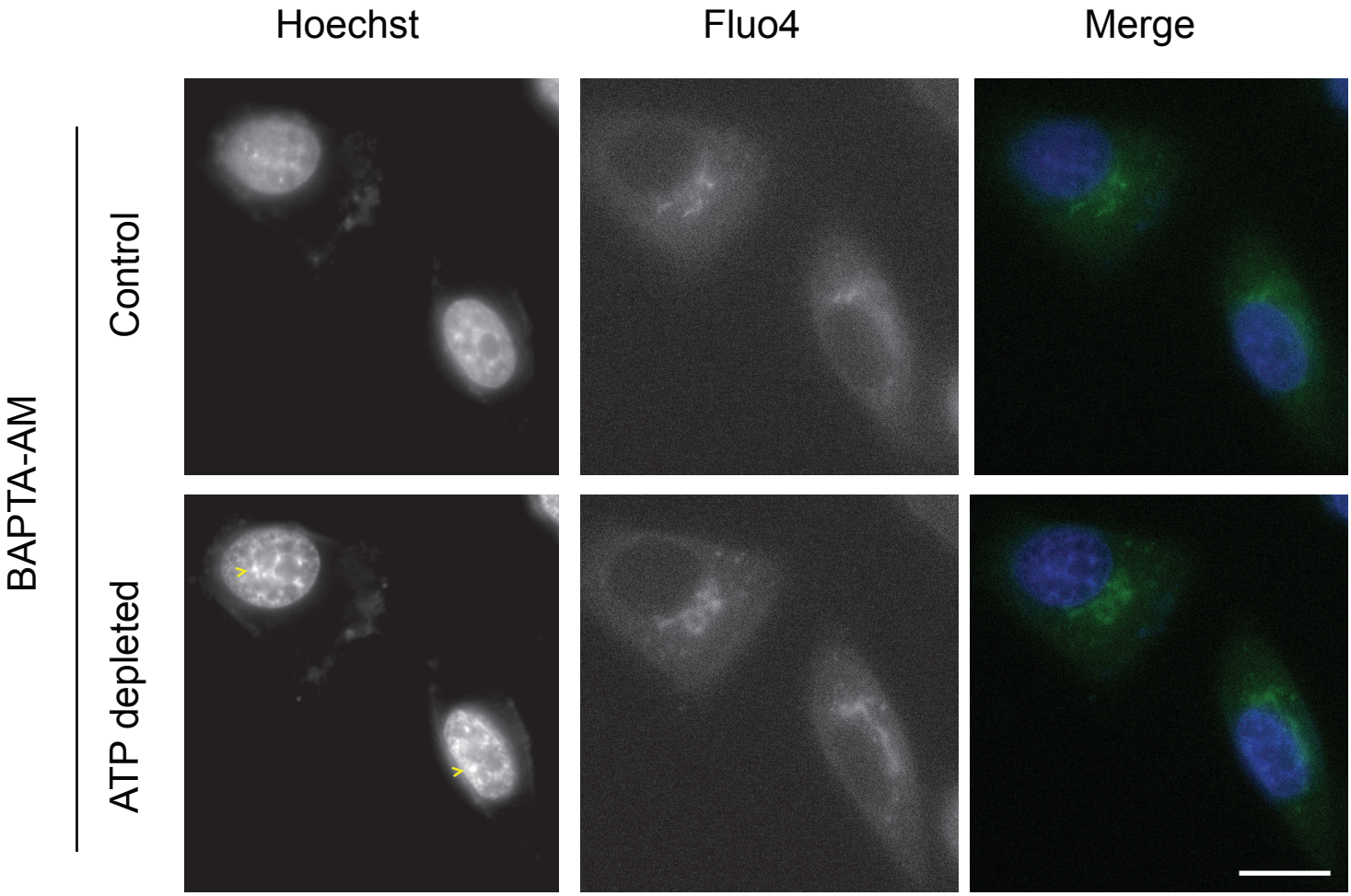

Fig 27 - Increase in free intracellular calcium can upon ATP depletion can be prevented by preloading the cells with BAPTA-AM, an intracellular Ca^{2+} chelater. Fluo4 fluorescence in cells preloaded with BAPTA-AM does not change with ATP depletion, indicating no changes in the intracellular calcium concentration. Increase in compaction of chromatin (yellow arrow head) is seen from Hoechst staining after ATP depletion. (Scale bar 10µm)

4.2.9 Depletion of ATP leads to changes in the localisation of the polyamine -Spermine

Polyamines are positively charged molecules found in cells. They have been shown to complex with DNA, RNA, Phospholipids and ATP. They have the highest affinity towards ATP, followed by RNA, DNA and phospholipids (Watanabe *et al.,*1991). Spermine is a polyamine with a charge of +4 in physiological conditions. Spermine causes compaction of chromatin in permeabilised cells and compaction of reconstituted nucleosomes (Korolev, Allahverdi et al. 2010). There is a possibility that Spermine bound to ATP under normal conditions translocates to chromatin after ATP hydrolysis, wherein it can cause compaction.

Control and ATP depleted cells were fixed with PFA and were stained for spermine using an anti-spermine antibody. Prior to staining, the cells were treated to denature chromatin. In control cells, staining was more concentrated in the euchromatic regions with a clear staining of nucleolar regions (Fig 28). Upon ATP depletion, the distribution pattern within nuclei was more diffuse with absence of staining in the nucleolar regions (Fig 28).

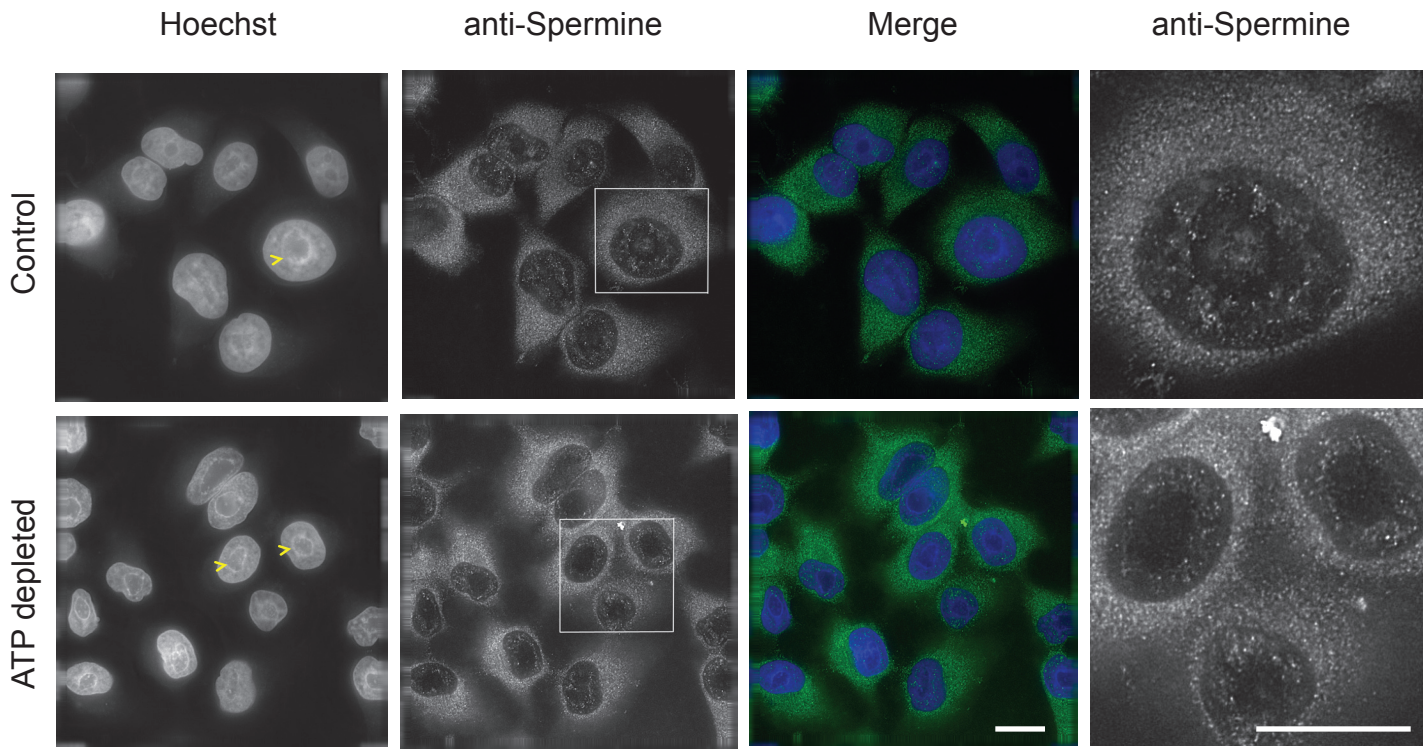

Fig 28 - Immuno-staining with anti-spermine antibody shows changes in spermine localisation within the nucleus after ATP depletion in HeLa cells. There is a distinct loss of nucleolar staining of spermine after ATP depletion. Arrow heads indicate nucleoli. (Scale bar - 10µm)

4.2.10 Depletion of the Adenomatous polyposis coli protein leads to an increase in compaction of mitotic chromosomes

Adenomatous polyposis coli (APC) protein is encoded by the APC gene. APC is a large multifunctional multi-domain protein that regulates beta-catenin turnover and also organizes the microtubule cytoskeleton (McCartney and Nathke 2008). Mutations in APC have been seen in many colorectal cancers. Lower level of APC have been shown to lead to increased polyamine levels (Rial, Meyskens et al. 2009).

$HeLa^{H2B\text{-}2FP}$ cells were treated with siRNA against APC. There was a decrease in APC protein levels after siRNA treatment for 72 hours (Fig 29E). FLIM measurements on $HeLa^{H2B\text{-}2FP}$ mitotic cells showed a decrease in the measured fluorescence lifetime in APC depleted cells when compared to control cells, indicating further compaction of the mitotic chromosomes (Fig 29). However, Interphase chromatin did not show a corresponding increase in chromatin compaction after APC depletion (Dikovskaya, Khoudoli et al. 2012). This could suggest a role for APC in modulating the polyamine concentrations in mitotic cells but not interphase cells, which is consequently lost with its depletion.

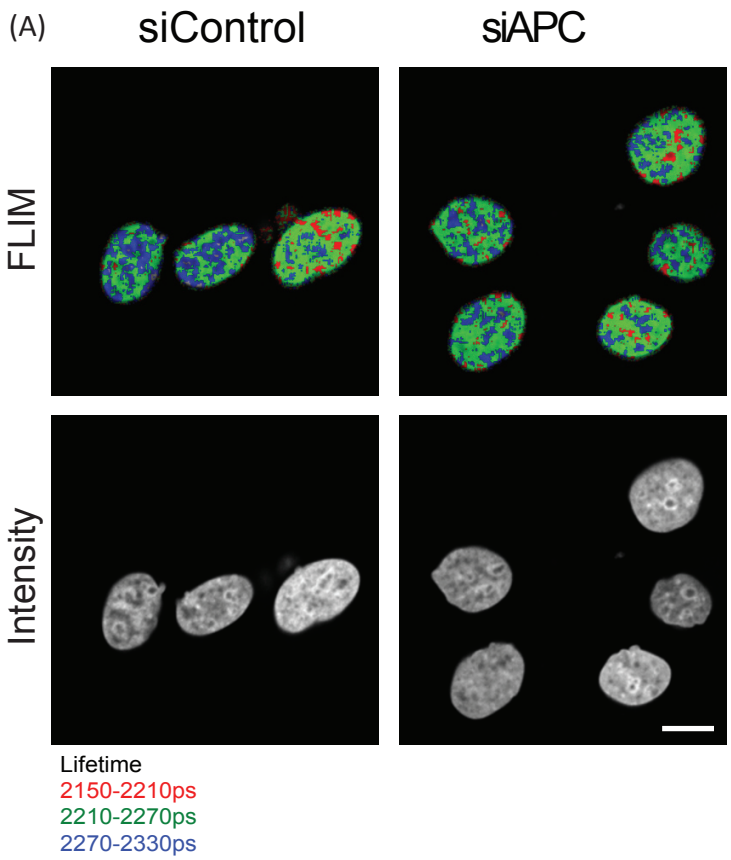

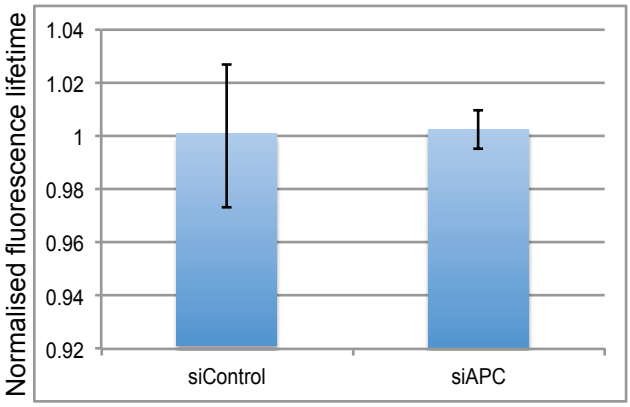

Fig 29 (A) FLIM images show no change in EGFP fluorescence lifetime in Hela^{H2b2FP} cells with knock down od APC using siRNA when compared to control cells (Scale bar - 10µm). (B) The chart shows the average EGFP fluorescence lifetime from 10 cells, normailsed to the average control value. Error bars indicate standard deviation. p value = 0.37

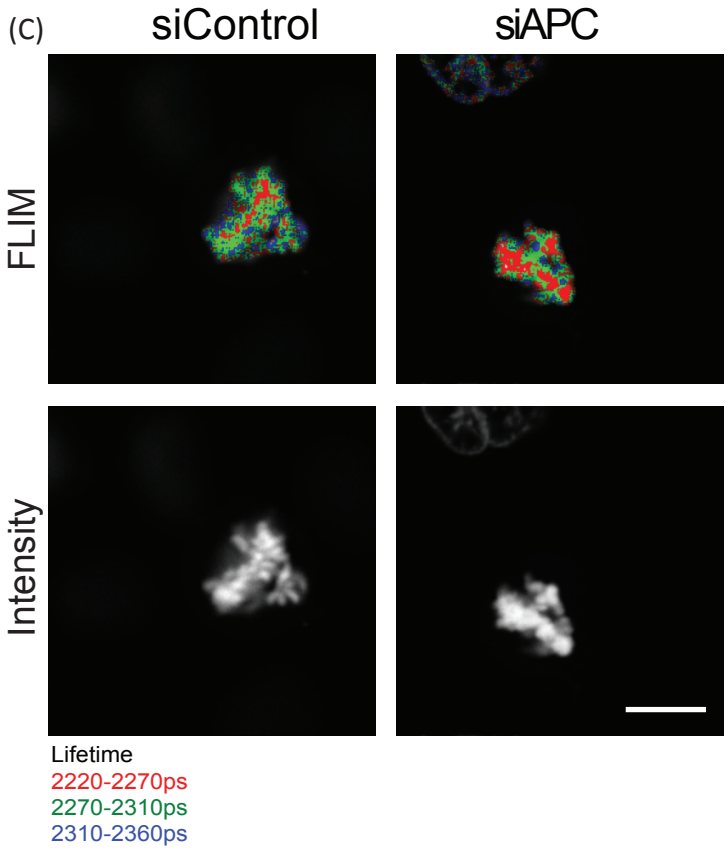

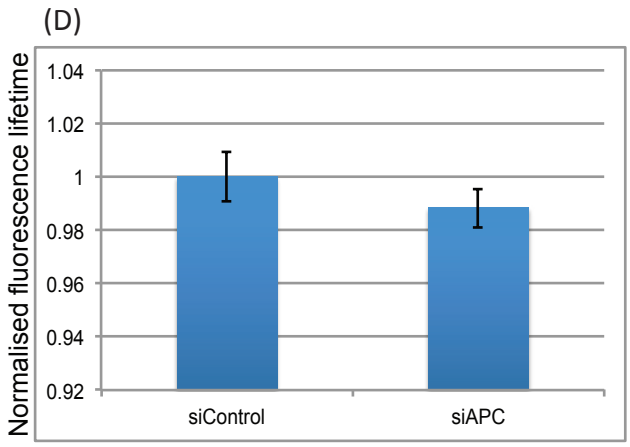

Fig 29 (C) FLIM images show a decrease in EGFP fluorescence lifetime in mitotic Hela^{H2b2FP} cells with knock down od APC using siRNA when compared to control cells (Scale bar - 10µm). (D) The chart shows the average EGFP fluorescence lifetime from 10 cells, normailsed to the average control value. Error bars indicate standard deviation. p value < 0.002

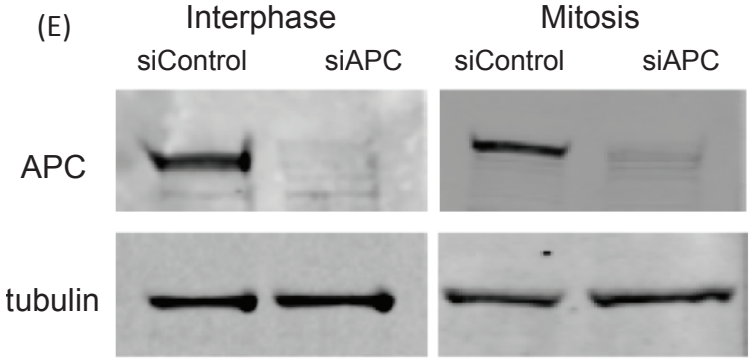

Fig 29 (E) Level of APC depletion of cells used in A and C is visualised by immunobloting the corresponding lysates with anti-APC antibodies. Tubulin level was measured to confirm equal loading.

4.3 Discussion

ATP is the main energy transfer molecule in cells and is consequently required to drive most energy-dependent cellular processes. ATP production in eukaryotes occurs predominantly in the mitochondria by oxidative phosphorylation. ATP can be depleted by treating cells with 2-deoxyglucose (2-DG) and sodium azide, which inhibits the glycolysis and oxidative phosphorylation pathways (Endale, Kim et al. 2010). Depletion of ATP has been shown to result in the compaction of chromatin in interphase cells (Shav-Tal, Darzacq et al. 2004; Lleres, James et al. 2009). This effect is occurs within 10 minutes and is reversible upon washing away of the drugs. ATP depletion leads to a number of effects in the cell, including the inactivation of numerous proteins like kinases, ATPases, inhibition of transcription, increase in the intracellular calcium levels (Carafoli 1991) and activation of signalling pathways. Inhibition of one or more of these processes could lead to the compaction of chromatin. Martin el, al., have implicated the increase in calcium as a possible factor in facilitating the increase in compaction in interphase cells upon ATP depletion (Martin, Gorisch et al. 2007). However none of the other effects brought about by ATP depletion have been studied, nor have there been any studies on mitotic chromosomes upon ATP depletion.

The increase in compaction after ATP depletion was observed using the FLIM-FRET system in HeLa$^{H2B\text{-}2FP}$ cells, as previously published by the Lamond lab (Lleres, James et al. 2009). The experiment was repeated, using the addition of the drugs 2-deoxyglucose (2-DG) and sodium azide to deplete ATP. In agreement with previous

findings, an increase in chromatin compaction with corresponding decrease in the calculated EGFP fluorescence lifetime values was observed.

ATP depletion will no doubt inhibit kinases, as the gamma phosphate from ATP is required for the phosphorylation reaction. Phosphorylation has directly been implicated in the regulation of chromatin structure. For example histone H3 is known to be phosphorylated at serine10 and serine28 in condensed mitotic chromosomes (Kouzarides 2007). However, the same modifications have also been shown to displace HP1 and PRC1 bound to tri-methyl lysine in interphase cells and thereby cause chromatin to attain a more active and open conformation (Hirota, Lipp et al. 2005).

If kinases were involved in modulating the chromatin compaction state in an ATP dependent manner, the inhibition of kinases should lead to changes in the pattern of chromatin compaction and de-compaction when ATP is depleted and repleted. To test this, we treated cells with Staurosporine at a concentration of 0.5µM for two hours. Staurosporine is a known broad spectrum serine/threonine kinase inhibitor (Ruegg and Burgess 1989). The inhibition of phosphorylation was tested by western blotting for the phosphorylation of Histone H3 at serine10. After the treatement of cells with staurosporine, there was a reduction in the phosphorylation of Histone H3 at serine10 (Fig 21C).

$HeLa^{H2B\text{-}2FP}$ cells were treated with staurosporine for 2 hours at a concentration of 0.5µM. The cells were then imaged and the fluorescence lifetime values of EGFP in

the cells were calculated. ATP depletion was carried out with the addition of 2-deoxyglucose (2-DG) and sodium azide, which caused an increase in compaction, which was then lost when the drugs were washed away (Fig 21). This result showed that the compaction of chromatin by the depletion of ATP is independent of kinases that are inhibited by staurosporine. This also indicates that signaling pathways, which will be inhibited by the broad spectrum kinase inhibitor are also not involved in the mediation of compaction caused by ATP depletion.

Transcription has been implicated in keeping chromatin in an open 'active' conformation. A number of studies show that genes that are active are found in euchromatic regions (Schneider and Grosschedl 2007). Experiments from the Bickmore lab have shown that the HoxB locus decondenses upon the activation of these genes during development (Chambeyron, Da Silva et al. 2005). Similar results have also been seen in plants, in genes that have been activated during development or in a cell specific manner (Wegel, Vallejos et al. 2005; Costa and Shaw 2006; Wegel, Koumproglou et al. 2009). This strongly suggests that transcription keeps the chromatin in an open, more de-condensed conformation. ATP depletion will lead to the inhibition of transcription. To study if inhibition of transcription can by itself lead to the observed level of compaction of chromatin seen after ATP depletion, cells were treated with DRB to inhibit transcription (Sehgal, Darnell et al. 1976). Labeling of nascent RNA by pulsed incorporation of modified uridine showed that transcription in the nucleoplasm was inhibited at 60 minutes after treating with the drug (Fig 22A). However after treating HeLa$^{H2B\text{-}2FP}$ cells with DRB for 60 minutes and quantifying chromatin compaction using FLIM-FRET showed only a small increase in

compaction upon inhibition of transcription. When these cells were then treated with sodium azide and 2-deoxy-glucose to deplete ATP, a much higher increase in chromatin compaction was observed. The increase in compaction was observed with a decrease in the fluorescence lifetime of EGFP as well as in the intensity images, corresponding to H2B-EGFP fluorescence (Fig 22B). Thus, although a small increase in chromatin compaction was brought about by the inhibition of transcription, the major effector of increased chromatin compaction upon ATP depletion cannot be the inhibition of transcription alone.

Mitotic cells do not have a nuclear membrane and a number of associated proteins and processes associated with chromatin in interphase cells. Mitotic chromosomes are however show higher compaction when compared with interphase chromatin. When mitotic HeLa$^{H2B\text{-}2FP}$ cells were depleted of ATP, there was an increase in the compaction of the already condensed mitotic chromosomes as seen with the reduction of calculated EGFP fluorescence lifetime values. This effect, like that seen with interphase chromatin is reversible upon washing away the drugs (Fig 23). This hyper compaction of mitotic chromatin and its consequent reversal indicate that the mechanism of compaction induced in mitotic and interphase cells is possibly the same. This provides further evidence that the compaction brought about by ATP depletion is not simply a consequence of inhibition of transcription. It further indicates that the more highly condensed state of mitotic chromosomes does not represent a maximally compacted state and may represent a different structural change to that induced by ATP depletion.

The effect of ATP depletion leading to chromatin compaction could be possibly caused either by post-translational modification of chromatin proteins, or by a soluble factor acting on the chromatin. To address this question, cells were depleted of ATP and then permeabilised. The permeabilisation was accomplished by the use of digitonin. Digitonin permeabilised cells have provided a powerful system for studying the nuclear import of proteins through the nuclear pore complex as the nuclear membrane is kept intact, with permeabilisation of the outer cellular membrane (Adam and Gerace 1991). When the cells were permeabilised after ATP depletion in a buffer containing 20mM of HEPES and 110mM of potassium acetate, but containing no polyvalent cations, there was a decrease in chromatin compaction (Fig 24). The chromatin in permeabilised cells was found to be more decompacted than the control, untreated cells. This shows that the compacting factor is either of a soluble nature, or becomes inactive when the cell is permeabilised. The decompaction can also be attributed to the loss of polyvalent cations, which would have been washed away during permeabilisation, as the buffer used to permeabilise and image only have the monovalent cation, potassium.

Addition of Mg^{2+} to the buffer in which the cells are permeabilised results in chromatin that is more compacted compared with that seen in the previous results. If the presence of ATP by itself was sufficient to cause the maintenance of decompacted chromatin, addition of ATP to permeabilised cells should be able to reverse the compaction. The addition of a magnesium salt of ATP, however did not lead to decompaction in the permeabilised system (Fig 25). However, this effect is

not necessarily representative of what happens in intact cells as a number of other factors would have been lost or become inactive upon permeabilisation.

Increasing Ca^{2+} concentration leads to increased chromatin compaction in nucleosome arrays (Korolev, Allahverdi et al. 2010). Permeabilised and live cells also show an increase in chromatin compaction when the concentration of free calcium in increased. It has been previously shown that there is an increase in free cellular calcium when cells are depleted of ATP (Martin, Gorisch et al. 2007). Free intracellular calcium can be visualised by loading the cells with the cell permeable calcium specific fluorescence indicator, Fluo4-AM. Fluo4 is the active form that is formed by the cleavage of Fluo4-AM by esterases found within the cell. When calcium concentration increases within the cells, there is an increase in fluorescence (Gee, Brown et al. 2000). When cells loaded with Fluo4 are subjected to ATP depletion, there is an increase in the fluorescence of Fluo4, indicating an increase in the intracellular calcium concentration (Fig 26). This increase in fluorescence is distinctly visible in the nuclear region of the cells. The resulting chromatin compaction after ATP depletion can also be visualised by Hoechst fluorescence, which stains the DNA. There has been one other report that suggests a link between an increase in calcium and compaction caused by ATP depletion (Martin, Gorisch et al. 2007), where they show the increase in calcium concentration with the depletion of ATP brought about by the addition of sodium azide.

This increase in free intracellular calcium can be prevented by the presence of an intracellular chelater of calcium, such as BAPTA. BAPTA-AM is a cell permeable

chelater of calcium, which upon entering the cells is cleaved by cellular esterases to an impermeable active form- BAPTA. HeLa cells were preloaded with BAPTA along with Fluo4 before ATP depletion. ATP depletion did not lead to an increase in the fluorescence of Fluo4 in the presence of BAPTA. However, an increase in compaction of the chromatin was seen by Hoechst fluorescence (Fig 27). The increase in free intracellular calcium can be prevented by BAPTA, which chelates calcium. Thus, while calcium is known to induce chromatin compaction and could contribute to the compaction observed, I conclude that calcium alone is not the sole factor that affects chromatin upon ATP depletion.

Another set of molecules present within cells that can contribute to compaction due to their inherent charged state, are polyamines. The major polyamines present in cells are putrescene, spermidine and spermine. They have charges of +2, +3 and +4, respectively. Spermidine and spermine are required in much lower concentrations to cause compaction when compared with the divalent cation Ca^{2+}. In the previous experiments with permeabilised cells, maximal, saturating levels of chromatin compaction brought about by 8mM of Ca^{2+} only required 1.5mM of spermidine and 0.21mM of spermine.

Polyamines have been shown to be essential for growth from bacteria to human cells. Studies have shown that Spermine has the highest affinity towards RNA, followed by ATP and DNA, while Spermidine has the highest affinity towards ATP, followed by RNA and DNA (Watanabe, Kusama-Eguchi et al. 1991). Phospholipids, the other cellular macromolecule with a negative charge, had the least affinity for

polyamines (Watanabe, Kusama-Eguchi et al. 1991). In the absence of ATP there is the possibility that the polyamines now bind to DNA and RNA. An antibody against spermine was used to check for changes in localisation after ATP depletion. Immunostaining revealed the loss of nucleolar staining after ATP depletion (Fig 28). This change in localisation of spermine and possibly spermidine to the chromatin could possibly contribute to the increase in chromatin compaction observed after ATP depletion.

The results show that the inhibition of processes like transcription, which are known to affect the compaction of chromatin locally within the nucleus, is not the major cause of compaction after ATP depletion. This is corroborated by the result that ATP depletion also leads to an increase in compaction of mitotic chromosomes that are transcriptionally silent. ATP depletion also leads to an increase in calcium and causes a change in the localisation of the polyamine spermine. This will result in a charge in the charge distribution within the cell. Previous results have shown that increasing polyvalent cations in permeabilised cells causes an increase in the compaction state of chromatin. Thus the change in charge distribution within the cell after ATP depletion can cause changes in chromatin compaction states. Further experiments to quantify the concentration of free and bound polyamines after ATP depletion would help in understanding if the changes in concentration are sufficient to cause the observed compaction.

Further evidence for polyamines playing a role in chromatin compaction comes from cells that have lower levels of Adenomatous polyposis coli protein (APC). Lower

levels of APC have been shown to lead to higher levels of polyamines (Rial, Meyskens et al. 2009). We have recently shown using the FLIM-FRET technique that mitotic HeLa$^{H2B\text{-}2FP}$ cells with lower levels of the APC protein show higher compaction when compared to control cells, however no effect was seen in interphase cells (Fig 29) (Dikovskaya, Khoudoli et al. 2012). This results indicates a possible role of APC in modulating the concentration of polyamines in mitotic cells, but not in interphase cells. A possible explanation for differential regulation of polyamines in interphase and mitotic cells, could be in assisting compaction of chromatin during mitosis, where an increase in polyamine levels is possibly required for increased chromatin compaction. Polyamine depletion in cells has also been shown to affect chromatin by increasing its sensitivity to DNAse, which is increased in decompacted chromatin (Snyder 1989).

Other factors that utilise ATP, like chromatin remodelers also play a role in modulating chromatin structure. There are a number ATP dependent remodeling complexes which could play a role in bringing about chromatin compaction after ATP depletion, however there are no tools currently available to inhibit their collective activity. SiRNA knock down studies could be done to study the roles of the ATP dependent remodeling complexes in maintaining decompacted chromatin.

Chapter 5

Identification of changes in chromatin bound protein levels upon TSA treatment

5.1 Abstract

Acetylation of histones has been shown to be associated with processes requiring a more open decompacted structure, like activation of transcription, DNA synthesis and DNA repair (Kouzarides 2007). Trichostatin A (TSA) is a drug that inhibits Class II Histone deacetylase complexes (HDACs) (Yoshida, Horinouchi et al. 1995). Treating cells with TSA shows an increase in histone acetylation and chromatin decompaction (Lleres, James et al. 2009). Acetylation of lysines leads to the neutralisation of its positive charge, which has been shown to make nucleosome arrays more resistant to compaction (Tse, Sera et al. 1998). However, the possible role of other proteins that could be involved in causing chromatin decompaction upon increased acetylation is not known. (Yoshida, Horinouchi et al. 1995)

Experiments in this chapter use a SILAC based mass spectrometry approach to identify chromatin-associated proteins whose levels change with increasing acetylation of histones. I have identified 38 proteins whose levels were significantly down regulated, and 41 proteins whose levels were significantly up regulated, in the chromatin fraction. The changes in protein levels for three proteins from this list were confirmed using western blotting. This list gives a set of candidate proteins that could influence chromatin compaction.

5.2 Results

5.2.1 Trichostatin A (TSA) treatment of HeLa cells leads to increased histone acetylation

Acetlylation of histones is known to be a mark of active transcription and decompacted chromatin (Kouzarides 2007). TSA is a class II histone deacetylase inhibitor (Yoshida, Horinouchi et al. 1995). Treating cells with TSA has been shown to cause an increase in histone acetylation. To confirm the activity of the drug on HeLa cells, HeLa cells were treated with TSA at a concentration of 200ng/ml. The cells were lysed and the increase in acetylation of histone H4 at lysine 5 was ascertained using western blotting. There was an increase in the acetylation of Histone H4, four hours after treatment with TSA when compared to control levels (Fig 30). The increase in acetylation is also seen at 6 hours, 12 hours and 24 hour time points (Fig 30).

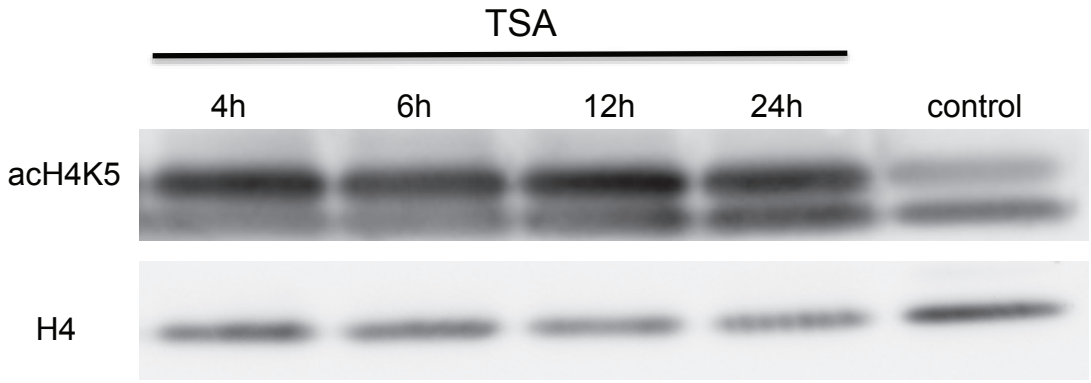

Fig 30 - histone acetylation increases with TSA treatment. HeLa cells were treated wth 200ng/ml TSA over different time points and blotted for Histone H4 lysine 5 acetylation. There was an increase in the acetylation of the histone although total H4 levels remained approximately constant.

5.2.2 Trichostatin A (TSA) treatment of HeLa cells leads to chromatin decompaction

Treating HeLa cells with TSA increases acetylation as shown from the western blotting experiments. Acetylation of lysine residues leads to the loss of positive charge. Acetylation is known to be associated with decompacted chromatin and TSA treatment has been shown to cause chromatin decompaction (Toth, Knoch et al. 2004; Lleres, James et al. 2009). HeLa$^{H2B\text{-}2FP}$ cells were imaged using FLIM before and after treating with 200ng/ml TSA for 12 hours. Treating the cells with TSA showed an increase in the measured lifetime of EGFP fluorescence, indicating chromatin decompaction (Fig 31). The decompaction of chromatin along the nuclear periphery was not significantly different to the decompaction observed in the interior of the nucleus, indicating that the chromatin decompaction was global (Fig 31 B).

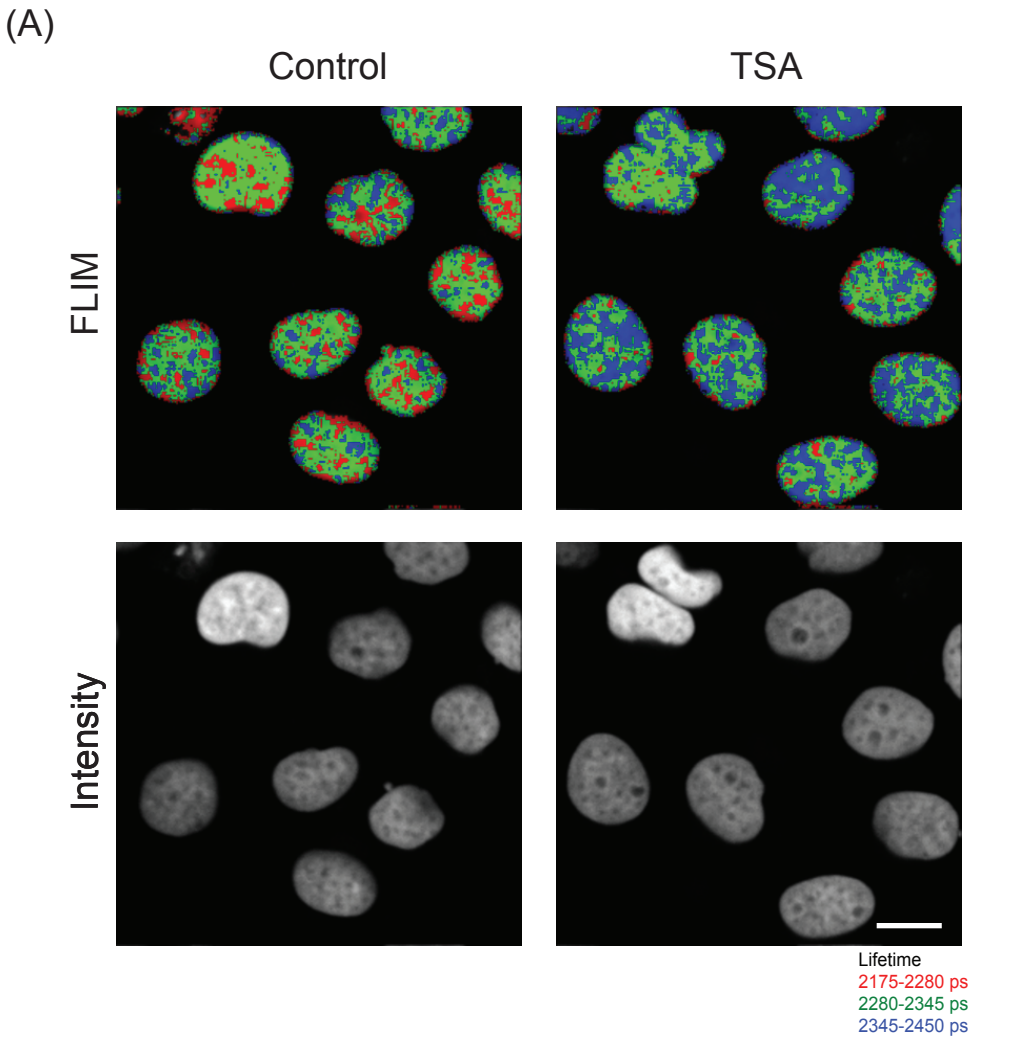

Fig 31 - (A) FLIM images show the increase in fluorescence lifetime in cells after having been treated with TSA at a concentration of 200ng/ml for 12 hours. The increase in fluorescence lifetime corresponds to a decrease in the chromatin compaction after TSA treatment. (Scale bar -10µm) (B) the graph shows the average normalised fluorescence lifetime of the imaged cells. Error bars indicate standard deviation.

5.2.3 Analysis of TSA treated - PFA fixed chromatin and whole cell lysates using SILAC

TSA treatment of HeLa cells leads to the decompaction of chromatin. Acetylation of lysine residues has been shown to inhibit cation dependent chromatin compaction of nucleosome arrays (Tse, Sera et al. 1998). The mechanism by which chromatin is decondensed in cells is not known. Charge neutralisation brought about by acetylation of lysine is possibly a mechanism of causing decompaction. However, the possible roles of other proteins that might be involved is not known.

SILAC based proteomics have been used to identify changes in protein levels and to compare cellular proteomes under different conditions (Andersen, Lyon et al. 2002; Boisvert, Ahmad et al. 2012). To characterise changes in the chromatin associated proteome in TSA treated cells, a SILAC based approach was used.

HeLa cells were grown in media containing arginine and lysine either with the normal 'light' isotopes of carbon and nitrogen (i.e. ^{12}C ^{14}N) (light), or 'heavy' isotopes of carbon and nitrogen L-[$^{13}C_6$,$^{15}N_4$] arginine and L-[$^{13}C_6$,$^{15}N_2$]lysine. Cells grown with the light media were the control cells. Cells grown with heavy media were treated with 200ng/ml TSA for 12 hours.

For the quantification of proteins associated with chromatin, equal numbers of TSA treated and control cells were then fixed with PFA, mixed and chromatin was isolated using the SimpleChIP® Enzymatic Chromatin IP Kit (Cell Signalling ♯9002) as per manufacturers instructions. For total cell lysate analysis, equal numbers of

control and TSA treated cells were harvested by scraping in denaturing lysis buffer and mixed.

The isolated chromatin and whole cell lysates were then fractionated using denaturing gel filtration chromatography, trypsin-digested, and analyzed by LC-MS/MS using an LTQ Orbitrap (Cox and Mann 2008; Olsen, Schwartz et al. 2009). The resulting ratios between light and heavy isotopic forms for each peptide, identified using Andromeda, were quantified using MaxQuant (Cox and Mann 2008). The separate ratio values for each peptide in a given protein gives a measure of the relative concentration of the protein in the treated and untreated conditions. The values from peptides mapped to a given protein, are combined to give a final ratio of protein abundance. Three independent experiments of TSA treatments were performed using separate preparations of isotope-labeled HeLa cells. In the chromatin fraction, a total of 175,975 peptides were identified, which correspond to 3,219 proteins and a total of 170,534 peptides corresponding to 3147 proteins were identified from analysis of the whole cell lysate proteome.

A total of 4,330 and 3,075 peptides mapped to histones were identified from the isolated chromatin and total cell lysate experiments, respectively. Acetylated peptides from the histones H3 and H2B were identified from both sets of experiments and acetylated peptides of histone H2A were identified from the whole cell lysate (Table -1, 2). There was an increase in histone acetylation in both samples after TSA treatment. The increase in acetylation ranged from two to eleven fold depending on the individual peptides (Table – 1, 2). Highest fold increase in acetylated peptides was observed for histone H2A. There were, however, no

significant changes in the averaged peptide ion intensities for the corresponding histones between the untreated and TSA treated cells, indicating that the histone abundance was not changing upon treatment with TSA (Table – 1, 2). Acetylated peptides form the protein Small Nuclear Ribonucleoprotein F (SNRPF) were also identified and quantified from both sets of experiments, showing there was no change in the abundance of acetylated peptides (Table – 1, 2). This indicated that the increase in acetylation was not global.

From the list of identified proteins, only those with a minimum of two unique peptides and identified in at least two of the three biological replicates were chosen for further analysis. Commonly occurring contaminants that were identified form the MaxQuant contaminants database were excluded from analysis (Cox, Matic et al. 2009). The contaminants include bovine proteins and keratins that come from sample handling. The median fold change (normalised H/L ratio) was calculated to be 1.0012 and 1.0311 for chromatin associated proteins, and lysate proteins, respectively (Fig 32). Protein concentrations were considered to be significantly changed if the fold change of the proteins was two standard deviations away from the median. The following cutoffs were used for the chromatin fraction, and total cell lysate, respectively : $X > 1.90$ or $X < 0.52$ and

$X > 1.92$ or $X < 0.54$.

Table 1 - TSA treatement leads to the increase in Acetylated peptides of histones from isolated chromatin with no significant change in the total protein levels.

Protein ID	Protein	Acetylated peptide	Fold change of acetylated peptide	Fold change of total protein
H32_HUMAN	Histone H3	RKQIATKAARKSA	6.22	1.12
B2R4S9_HUMAN	Histone H2B	SKKAVTKAQKKDG	4.28	0.96
B2R4S9_HUMAN	Histone H2B	PKKGSKKAVTKAQ	6.19	0.96
H32_HUMAN	Histone H3.1	ATKAARKSAPATG	1.90	0.75
RUXF_HUMAN	Small nuclear ribonucleoprotein F	SIPINPKPFINGI	1.03	1.04

Table 2 - TSA treatement leads to the increase in Acetylated peptides of histones from whole cell lysate with no significant change in the total protein levels.

Protein ID	Protein	Acetylated peptide	Fold change of acetylated peptide	Fold change of total protein
H2AV_HUMAN	Histone H2A	__MAGGKAGKDSG	11.06	0.93
H2AV_HUMAN	Histone H2A	AGGKAGKDSGKAK	11.46	0.93
H32_HUMAN	Histone H3	RKQIATKAARKSA	1.82	0.88
H32_HUMAN	Histone H3	ATKAARKSAPSTG	4.51	0.88
B2R4S9_HUMAN	Histone H2B	SKKAVTKAQKKDG	6.69	0.94
B2R4S9_HUMAN	Histone H2B	SKKAVTKVQKKDG	2.62	0.94
H32_HUMAN	Histone H3.1	ATKAARKSAPATG	1.99	0.75
RUXF_HUMAN	Small nuclear ribonucleoprotein F	SIPINPKPFINGI	1.04	1.04

(A)

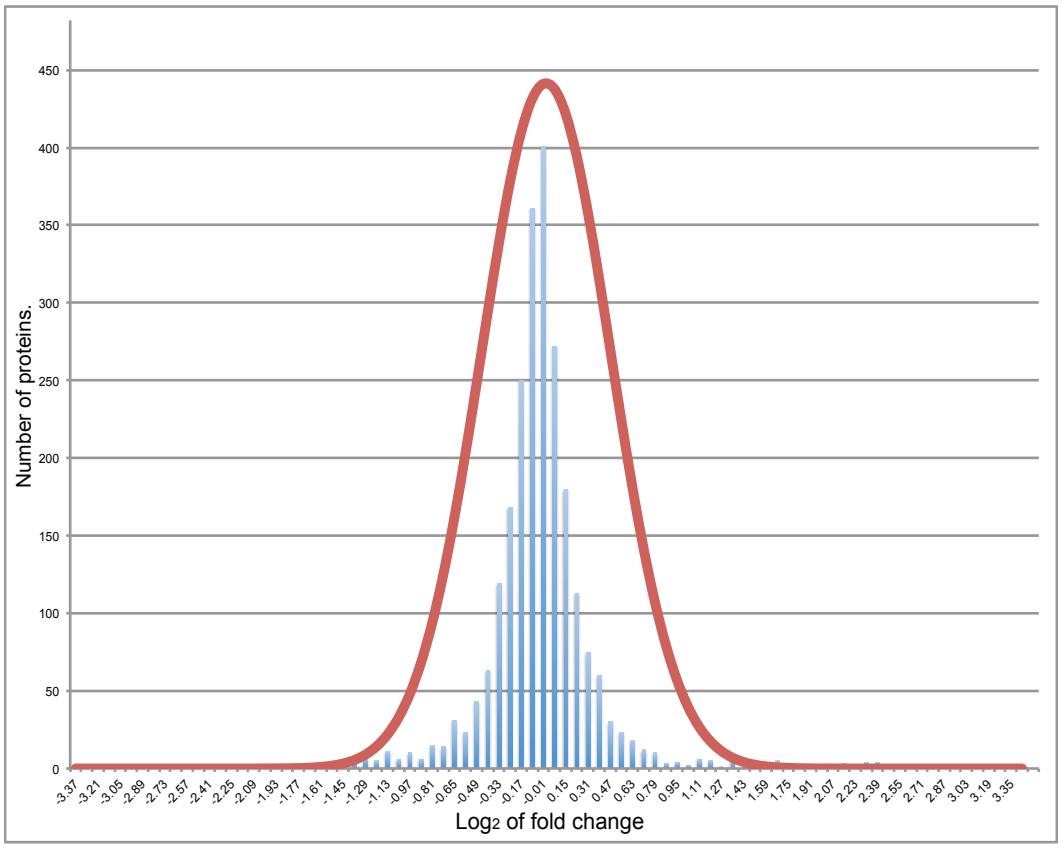

(B)

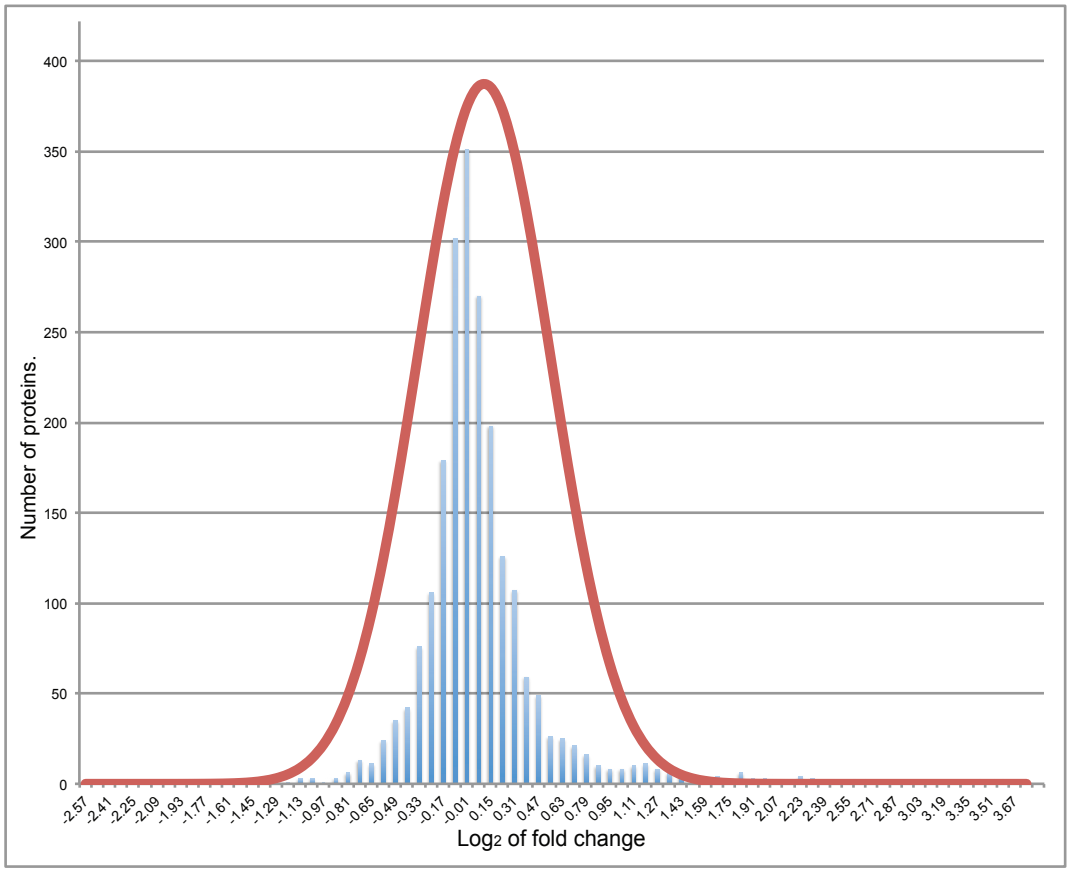

Fig 32 - Graph showing the number of proteins versus fold change for the chromatin fraction (A) and whole cell lysate (B). The median was calculated at 0.00173 and 0.0441 corresponding to 1.0012 and 1.0311 fold changes for chromatin fraction and whole cell lysate respectively. Proteins that were two standard deviations away from the median were considered to be significantly changed.

5.2.4 Confirmation of changes in protein levels of Histone H1.0, PCNA associated factor (PAF) and Epiplakin using western blotting

Mass spectrometry analysis showed that the protein levels of Histone H1.0 and Epiplakin were increased, and PAF was decreased, after TSA treatment in both the chromatin and total cell lysate samples (Table 3).

To confirm the changes seen from mass spectometry analysis using an independent method, cells were treated with TSA and the lysate was subjected to western blotting analysis with commercially available antibodies for these proteins. There was an increase in Epiplakin and Histone H1, while PAF was decreased, when analysed using western blotting. The changes in protein levels observed with mass spectometry were confirmed with western blotting (Fig 33).

Fig 0 - Western blotting showing the changes in expression of Epiplakin, Histone H1.0 and PAF in HeLa cells after having been treated with 200ng/ml TSA for 12hours.

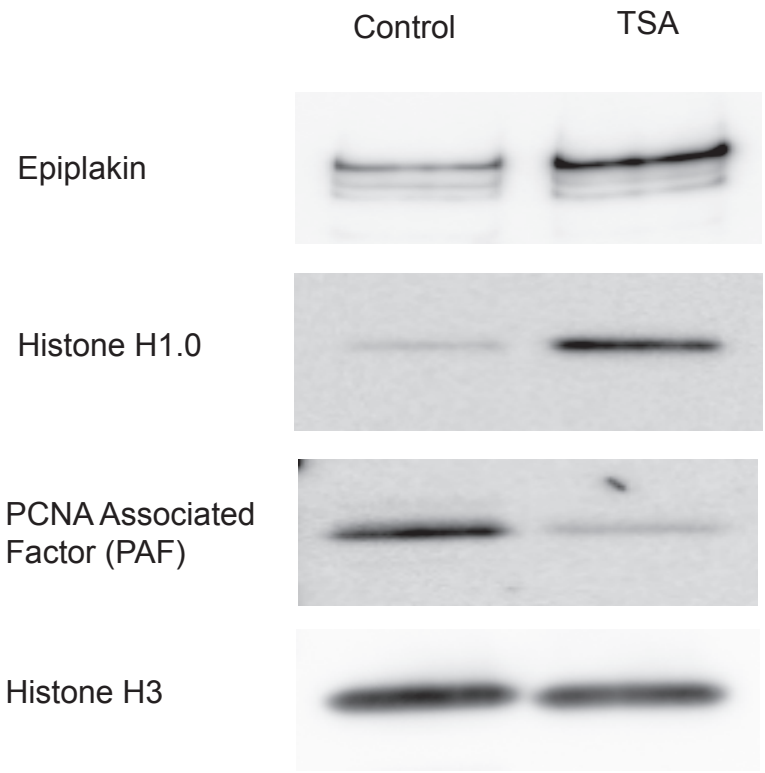

Table 0 - showing the changes in expression of Epiplakin, Histone H1.0 and PAF in HeLa cells after having been treated with 200ng/ml TSA for 12hours obtained from Mass spec analysis. The fold change of the protein in chromatin and whole cell lysate fractions are specified by the corresponding normailsed H/L ratios.

Protein ID	Protein	Normalised H/L Chromatin	Normalised H/L whole cell	Unique peptides-Chromatin	Sequence coverage (%) Chromatin	Unique peptides-whole cell	Sequence coverage (%) whole cell
EPIPL_HUMAN	Epiplakin	2.34	2.40	30	62.6	28	57.3
H10_HUMAN	Histone H1.0	3.21	4.18	9	32	9	32
PAF_HUMAN	PCNA-associated factor (PAF)	0.41	0.35	2	33.3	3	43.2

5.2.5 Chromatin associated proteins HP1 and HMG remained unchanged upon TSA treatment

TSA treatment leads to the de-compaction of chromatin in HeLa cells. HP1 is known to be associated with compacted heterochromatin (Grewal and Jia 2007). The HMG proteins have been shown to be associated with a number of processes, including regulation of transcription and modulation of DNA repair, requiring chromatin remodelling (Reeves 2010). HMGA proteins have been shown to recruit histone acetylases (Merika and Thanos 2001) and HMGNs are also the only non-histone proteins known to specifically bind inside the nucleosome between the gyres of DNA and the histone octamer core (Bustin 2001). To check if the decompaction upon TSA treatment results from changes in the levels of proteins known to be associated with the modulation of chromatin compaction, the relative combined peptide intensities of the different protein isoforms of HP1 and HMG were analysed.

Eight isoforms of HMG were identified from the chromatin fraction and whole cell lysate. There was no significant change in the relative ratios of the combined peptide intensities for the analysed proteins either before, or after, TSA treatment, in both experiments (Table 4). All the three isoforms of HP1 – HP1α, HP1β and HP1γ, were identified with the aforementioned conditions. Similar to the HMG proteins, there were no significant changes in the levels of these proteins in both experiments, indicting an absence in their role, in decompaction caused by TSA treatment (Table 5).

Table 4 - Table showing the protein fold change values of HMG proteins in chromatin fraction and whole cell lysate after TSA treatment

Protein ID	Protein	Normalised H/L Chromatin	Normalised H/L whole cell	Unique peptides-Chromatin	Sequence coverage (%) Chromatin	Unique peptides-whole cell	Sequence coverage (%) whole cell
HM20A_HUMAN	High mobility group protein 20A	0.65	NA	2	9.8	NA	NA
HMGA1_HUMAN	High mobility group protein HMG-I/HMG-Y	0.97	1.01	2	60.7	3	65.4
HMGB1_HUMAN	High mobility group protein B1	0.98	0.98	16	72.6	16	70.7
HMGB2_HUMAN	High mobility group protein B2	0.90	0.87	12	70.8	13	65.6
HMGB3_HUMAN	High mobility group protein B3	0.89	0.89	9	51.5	8	49
HMGN1_HUMAN	Non-histone chromosomal protein HMG-14	1.00	1.08	8	56	9	59
HMGN2_HUMAN	Non-histone chromosomal protein HMG-17	0.97	1.00	2	45.6	2	45.6
HMGN3_HUMAN	High mobility group nucleosome-binding domain-containing protein 3	1.00	0.96	3	27.3	3	27.3
HMGN4_HUMAN	High mobility group nucleosome-binding domain-containing protein 4	NA	0.94	NA	NA	2	33.3

Table 5 - Table showing the protein fold change values of Heterochromatin (HP1) proteins in chromatin fraction and whole cell lysate after TSA treatment

Protein ID	Protein	Normalised H/L Chromatin	Normalised H/L whole cell	Unique peptides-Chromatin	Sequence coverage (%) Chromatin	Unique peptides-whole cell	Sequence coverage (%) whole cell
CBX5_HUMAN	Chromobox protein homolog 5 (HP1α)	1.10	1.01	7	33	10	51.3
CBX1_HUMAN	Chromobox protein homolog 1 (HP1β)	1.13	1.13	6	49.7	8	57.7
CBX3_HUMAN	Chromobox homolog 3 (HP1γ)	0.80	0.81	11	67.2	12	67.2

5.2.6 Identification of chromatin associated proteins that change with TSA treatment and their comparison with changes in whole cell lysate

Proteins were identified with varying fold changes (0.16 to 9.8) (normalised H/L ratio) after TSA treatment in the chromatin fraction. Significant proteins were identified as being two standard deviations away from the mean, i.e. fold change less than 0.52 or greater than 1.90. Using these criteria, a set of minimal changing proteins was identified (fold change between 0.52 and 1.90). A p-value was calculated for the significant proteins using data collected from three biological replicates. The ratios from the three biological replicates for each individual protein were compared with the set of non-significant proteins, using the students t-test. A 0.05 p value cutoff was used in combination with a 2 standard deviation fold change to identify reliably changing proteins. 37 proteins were found to be downregulated and 41 proteins were found to be upregulated using the above-mentioned criteria (Fig 34).

A total of 41 proteins were found to be up regulated in the chromatin fraction upon TSA treatment, of which 22 proteins were identified in the whole cell lysate. 11 of the proteins that were identified from the whole cell lysate were also found to be significantly upregulated, while eleven were not significantly changed upon TSA treatment (Table 7).

Of the 37 proteins found to be significantly down regulated in the chromatin fraction, 20 were also identified in the whole cell lysate, of which 8 proteins were

significantly down regulated, 1 significantly upregulated and 11 were not significantly changed upon TSA treatment (Table 6).

There was a single protein, ASH1L, that contained an acetyl lysine binding, bromodomain, in the list of upregulated proteins. A histone chaperone, ASF1A, was found to be downregulated and there was an increase in a single isoform the histone H1, H1.0. A number of proteins that were a part of the mitochondrial ribosome were also detected with significant changes in their abundance after treatement with TSA.

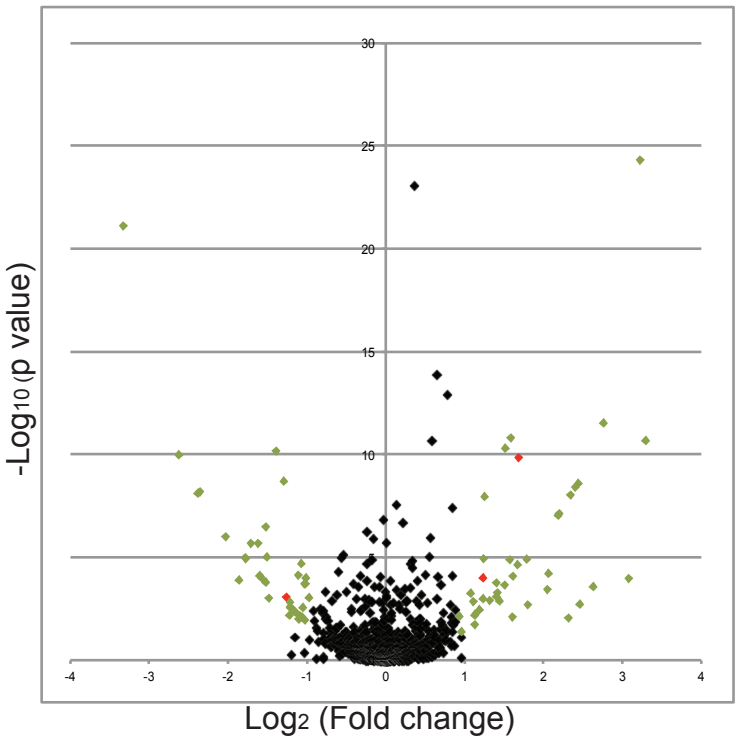

Fig 34 - Scatter plot with Log_2 of the normalised average peptide fold change of proteins between the control and TSA treated chromatin fraction plotted against the $-Log_{10}$ of the p-value for the corresponding proteins. Proteins indicated in green and red were considered to be significantly changed in abundance over the three biological replicates. The points indicated in red are Histone H1.0 (right), Epiplakin (middle) and PAF (left) whose changes were also confirmed with western blotting.

Table 6 - Chromatin bound downregulated proteins

Protein IDs	Protein	Normalised H/L Chromatin	Normalised H/L whole cell	Unique peptides-Chromatin	Sequence coverage (%) Chromatin	Unique peptides-whole cell	Sequence coverage (%) whole cell	p-value
BCL7C_HUMAN; BCL7A_HUMAN	B-cell CLL/lymphoma 7 protein family member C	0.16	NA	2	10.1	NA	NA	1.028E-10
RT26_HUMAN	28S ribosomal protein S26	0.19	0.26	2	13.2	2	13.2	7.626E-09
UTP18_HUMAN	U3 small nucleolar RNA-associated protein 18 homolog	0.19	NA	3	9.5	NA	NA	6.5454E-09
E7ESL0_HUMAN; RM22_HUMAN	39S ribosomal protein L22	0.24	NA	6	32.5	NA	NA	1E-06
T126A_HUMAN; E9PI90_HUMAN	Transmembrane protein 126A	0.27	0.67	2	14.9	2	24.1	0.00012547
ASF1A_HUMAN	Histone chaperone ASF1A	0.29	0.29	2	21.1	2	25	1.0451E-05
SSU72_HUMAN; Q5SV20_HUMAN	RNA polymerase II subunit A C-terminal domain phosphatase SSU72	0.29	0.79	2	12.4	3	18.6	1.1783E-05
CHP1_HUMAN; F5GX29_HUMAN	Calcium-binding protein p22	0.30	NA	4	25.6	NA	NA	2.1408E-06
CLK3_HUMAN; B3KUU7_HUMAN	Dual specificity protein kinase CLK3	0.32	NA	2	4.7	NA	NA	2.1346E-06
CE290_HUMAN	Centrosomal protein of 290 kDa	0.33	1.19	3	1.2	3	1.2	8.021E-05
SCAM3_HUMAN	Secretory carrier-associated membrane protein 3	0.33	1.12	3	13	4	18.7	0.00010266
SHOC2_HUMAN	Leucine-rich repeat protein SHOC-2	0.34	NA	2	6	NA	NA	0.00016435
CDN2C_HUMAN; Q6ICV4_HUMAN	Cyclin-dependent kinase 4 inhibitor	0.34	0.41	4	33.9	3	29.2	3.3534E-07
MIP18_HUMAN	Mitotic spindle-associated MMXD complex subunit MIP18	0.35	1.03	5	56.4	2	26.4	9.8266E-06
NEK7_HUMAN; F5H3U7_HUMAN	Serine/threonine-protein kinase Nek7	0.35	NA	2	8.6	NA	NA	0.0009504
GPX8_HUMAN; E7ETY7_HUMAN	Probable glutathione peroxidase 8	0.38	0.36	2	11	3	15.8	6.7531E-11
RM04_HUMAN	39S ribosomal protein L4	0.40	0.60	3	19.3	3	19.3	1.9843E-09
PAF_HUMAN; A6NNU5_HUMAN	PCNA-associated factor (PAF)	0.41	0.35	2	33.3	3	43.2	0.00088341
RM55_HUMAN	39S ribosomal protein L55	0.42	1.17	2	18.8	3	30.5	0.00659988
RM02_HUMAN; C9IY40_HUMAN	39S ribosomal protein L2	0.43	NA	4	17.7	NA	NA	0.00261716
Q5TZN3_HUMAN; UBE2C_HUMAN	Ubiquitin carrier protein	0.43	0.47	4	26.8	4	41.3	0.00145884
RNC_HUMAN; E7EMP9_HUMAN	Ribonuclease 3	0.43	NA	2	2	NA	NA	0.00285436
RM39_HUMAN; C9JG87_HUMAN	39S ribosomal protein L39	0.44	NA	3	10.4	NA	NA	0.00364382
GPKOW_HUMAN	G patch domain and KOW motifs-containing protein	0.45	NA	2	8.6	NA	NA	0.00452211
EHD4_HUMAN	EH domain-containing protein 4	0.46	1.05	5	10.9	5	12.6	7.5075E-05
Q53Y97_HUMAN; TYSY_HUMAN	Thymidylate synthase	0.46	0.48	4	17.9	6	33.9	0.00603105
LXN_HUMAN	Latexin	0.46	0.97	2	12.2	2	12.2	0.01011166
DTD1_HUMAN	D-tyrosyl-tRNA(Tyr) deacylase 1	0.47	NA	2	14.8	NA	NA	0.00741801
UCK2_HUMAN; B4DGD3_HUMAN	Uridine-cytidine kinase 2	0.47	0.38	4	25.7	5	36	1.9815E-05
RM19_HUMAN	39S ribosomal protein L19	0.47	2.34	3	11	3	11	0.00797396
COMD5_HUMAN; E9PJE4_HUMAN	COMM domain-containing protein 5	0.47	NA	2	21.4	NA	NA	0.00850064
CHCH2_HUMAN; CHCH9_HUMAN	Coiled-coil-helix-coiled-coil-helix domain-containing protein 2	0.48	0.68	2	18.5	2	18.5	0.00269054
ISY1_HUMAN	Pre-mRNA-splicing factor ISY1 homolog	0.48	NA	3	16.1	NA	NA	0.00019331
E7ETS8_HUMAN; DPOE1_HUMAN	DNA polymerase epsilon catalytic subunit A	0.49	NA	2	2	NA	NA	0.01115172
ATG9A_HUMAN	Autophagy-related protein 9A	0.49	NA	2	2.7	NA	NA	0.00019318
D6MXU3_HUMAN; POMP_HUMAN	Proteasome maturation protein	0.49	NA	3	37.6	NA	NA	9.8955E-05
CS021_HUMAN	Uncharacterized protein C19orf21	0.50	0.62	6	14	9	38.7	0.00090272

Table 7 - Chromatin bound up-regulated proteins

Protein ID	Protein	Normalised H/L Chromatin	Normalised H/L whole cell	Unique peptides-Chromatin	Sequence coverage (%) Chromatin	Unique peptides-whole cell	Sequence coverage (%) whole cell	p-value
CENPF_HUMAN	Centromere protein F	1.91	NA	10	4.2	NA	NA	0.00731234
E9PNP3_HUMAN ;CK067_HUMAN	Uncharacterized protein GN=C11orf67	1.94	2.30	2	17.7	2	11.9	0.04082998
CRIPT_HUMAN	Cysteine-rich PDZ-binding protein	2.10	2.68	2	11.9	2	11.9	0.00055665
DNJB1_HUMAN; Q6FHS4_HUMAN	DnaJ homolog subfamily B member 1	2.16	2.42	10	40.3	9	31.8	0.00143784
Q68CM6_HUMAN; STXB1_HUMAN	Syntaxin-binding protein 1	2.18	NA	2	4.4	NA	NA	0.00653487
RHG17_HUMAN; C9IZD3_HUMAN	Rho GTPase-activating protein 17	2.18	NA	3	6.9	NA	NA	0.01880311
GBRL2_HUMAN; Q6FG91_HUMAN	Gamma-aminobutyric acid receptor-associated protein-like 2	2.19	1.78	3	29.1	4	40.2	0.00583013
PI3R4_HUMAN	Phosphoinositide 3-kinase regulatory subunit 4	2.27	NA	2	3.4	NA	NA	0.00364268
EPIPL_HUMAN	Epiplakin	2.34	2.40	30	62.6	28	57.3	0.00010228
AP3B1_HUMAN; E5RJ68_HUMAN	AP-3 complex subunit beta-1	2.35	1.05	6	7.7	4	5.4	0.00103692
CETN2_HUMAN	Centrin-2	2.36	2.20	3	36	5	50.6	1.1487E-05
ZO1_HUMAN	Tight junction protein ZO-1	2.37	1.90	4	3.3	3	2.6	1.0953E-08
CUL1_HUMAN; E7EWR0_HUMAN	Cullin-1	2.49	NA	2	3.6	NA	NA	0.00125469
ERD21_HUMAN	ER lumen protein retaining receptor 1	2.63	1.12	2	17	4	27.4	0.00017193
TRIP6_HUMAN	Thyroid receptor-interacting protein 6	2.64	2.39	4	13	2	9.9	0.00079334
E9PPU0_HUMAN	Uncharacterized protein GN=EPPK1	2.66	NA	2	46.6	NA	NA	0.00052193
DAD1_HUMAN; F5GXX5_HUMAN	Dolichyl-diphosphooligosaccharide--protein glycosyltransferase subunit DAD1	2.71	0.97	4	35.4	4	35.4	0.00130214
PHS_HUMAN	Pterin-4-alpha-carbinolamine dehydratase	2.84	0.86	3	38.5	3	38.5	0.00021955
F5H619_HUMAN; HTR5A_HUMAN	Uncharacterized protein GN=HEATR5A	2.86	NA	2	1.6	NA	NA	4.9627E-11
PLCB3_HUMAN	1-phosphatidylinositol-4,5-bisphosphate phosphodiesterase beta-3	2.98	1.19	6	7.3	9	11.3	1.2958E-05
DCUP_HUMAN; Q5T446_HUMAN	Uroporphyrinogen decarboxylase	3.00	1.24	2	13.1	3	23.4	1.5753E-11
UBE2S_HUMAN	Ubiquitin-conjugating enzyme E2 S	3.04	2.05	8	51.8	8	59.5	0.00812798
MAT1_HUMAN	CDK-activating kinase assembly factor MAT1	3.05	NA	2	11.3	NA	NA	8.1199E-05
E9PEY0_HUMAN; CE170_HUMAN	Centrosomal protein of 170 kDa	3.18	1.14	2	1.8	3	2.2	2.3332E-05
H10_HUMAN; F5H022_HUMAN	Histone H1.0	3.21	4.18	9	32	9	32	1.4306E-10
TSC2_HUMAN; E9PGN1_HUMAN	Tuberin	3.44	NA	2	1.2	NA	NA	1.213E-05
CYR61_HUMAN; Q6FI18_HUMAN	Protein CYR61	3.48	3.60	4	11	4	11	0.00201012

Table 7 (cont) - Chromatin bound up-regulated proteins

Protein ID	Protein	Normalised H/L Chromatin	Normalised H/L whole cell	Unique peptides-Chromatin	Sequence coverage (%) Chromatin	Unique peptides-whole cell	Sequence coverage (%) whole cell	p-value
ABCB6_HUMAN	ATP-binding cassette sub-family B member 6	4.13	NA	3	5.6	NA	NA	0.00037559
SC61G_HUMAN	Protein transport protein Sec61 subunit gamma	4.18	2.20	2	36.8	2	36.8	6.0416E-05
SCAFB_HUMAN	Protein SCAF11	4.54	NA	2	1.6	NA	NA	9.3765E-08
ASH1L_HUMAN	Probable histone-lysine N-methyltransferase ASH1L	4.59	NA	2	1.3	NA	NA	7.4939E-08
DHX36_HUMAN; F5GZS0_HUMAN	Probable ATP-dependent RNA helicase DHX36	4.98	1.20	3	5.6	3	5.5	0.00879812
Q8IWZ2_HUMAN; ANKH1_HUMAN	Ankyrin repeat and KH domain-containing protein 1	5.08	NA	2	4.1	NA	NA	9.3233E-09
MYO19_HUMAN; CB072_HUMAN	Myosin-XIX	5.29	NA	2	2.8	NA	NA	3.8803E-09
VAMP2_HUMAN	Vesicle-associated membrane protein 2	5.43	NA	2	35.3	NA	NA	2.5874E-09
MZT1_HUMAN	Mitotic-spindle organizing protein 1	5.51	3.12	4	58.5	2	39	0.00197458
Q5JP73_HUMAN; SKIV2_HUMAN	Helicase SKI2W	6.19	NA	3	3.8	NA	NA	0.00026281
BAG6_HUMAN; B0UX83_HUMAN;	Large proline-rich protein BAG6	6.77	1.30	4	3.7	11	15.1	3.0562E-12
RM52_HUMAN; A6NMQ8_HUMAN	39S ribosomal protein L52	8.45	NA	2	42.3	NA	NA	0.0001076
SLD5_HUMAN; E5RFF9_HUMAN	DNA replication complex GINS protein SLD5	9.35	NA	3	21.1	NA	NA	5.0702E-25
NDUS2_HUMAN	NADH dehydrogenase [ubiquinone] iron-sulfur protein 2	9.80	NA	2	4.3	NA	NA	2.1264E-11

5.3 Discussion

Acetylation lysine residues is one of 8 known histone post translational modifications (Kouzarides 2007; Tan, Luo et al. 2011). Acetylation of histones has been shown to be associated with activation of transcription, DNA synthesis and DNA repair (Kouzarides 2007). Most of the work pertaining to histone acetylation has been done studying its effects on transcription activation. Histone acetylation has been seen on the histones in nucleosomes at promoters of active genes and the level of acetylation has been shown to be positively correlated with transcription rates (MacDonald and Howe 2009). Lower levels of acetylation have been seen to exist throughout the genome.

Histone acetylation is brought about by histone acetyl transferase (HAT) complexes, which are divided into three families known as GNAT, MYST, and CBP/p300 (Sterner and Berger 2000). The complexes do not show much specificity, with some having overlapping targets. It has been shown that the HAT complexes interact with various transcriptional activators and acetylate the histones at promoters, leading to activation of transcription by binding of the TATA-box binding protein (TBP) (MacDonald and Howe 2009).

Most of the characterised sites for acetylation in histones are confined to the histone tails and can be recognised by bromo-domain containing proteins. Bromodomains are found in both the SWI/SNF and RSC (Remodels the Structure of Chromatin) chromatin- remodeling complexes (MacDonald and Howe 2009). These

complexes use ATP hydrolysis to alter chromatin structure by either removing, or sliding, the histones and thereby altering chromatin structure. Transcription activation is thought to be facilitated by the concerted activities of facilitating TBP protein binding and chromatin remodeling. Consequently, it has been shown in yeast that aberrant acetylation leads to activation from cryptic promoters within coding regions (Carrozza, Hassan et al. 2003).

De-acetylation is correlated with transcriptional repression. There are three classes of histone de-acetylases – the class I and class II de-acetylases, the class III NAD^+ dependent enzymes of the Sir family and class IV with a single member, HDAC11 (Bannister and Kouzarides 2011). These enzymes, like the acetylases, do not show high specificity to specific modification sites. Inhibition of de-acetylation leads to a corresponding increase in histone acetylation levels.

As mentioned above, acetylation has been shown to be associated with activation of transcription, DNA synthesis and DNA repair (Kouzarides 2007). All these processes require a decompacted chromatin conformation to allow transcription factors access to the chromatin. Increased histone acetylation has been shown to be associated with a decompacted chromatin structure. In experiments involving heterokaryons, fusion of human B lymphocytes, which have more compact chromatin, with mouse ES cells that have decompacted chromatin, led to the B lymphocyte nuclei increasing in size, with corresponding chromatin decompaction and increased histone acetylation (Piccolo, Pereira et al. 2011). Experiments with reconstituted nucleosome arrays have also shown that acetylated histones require higher

concentrations of polyvalent cations to compact the nucleosome arrays, when compared with control arrays (Tse, Sera et al. 1998). This shows a correlation between charge and compaction levels, as acetylation removes positive charge and hence leads to a net increase in the negative charge of the nucleosome arrays.

Trichostatin A is a drug that inhibits Class II Histone deacetylase complexes (HDACs) (Yoshida, Horinouchi et al. 1995). Inhibition of HDACs leads to increased acetylation of histones. This increase in acetylation upon treating cells with TSA has been shown previously to cause decompaction of chromatin (Toth, Knoch et al. 2004; Lleres, James et al. 2009). Acetylation of lysines will result in a decrease n the positive charge of the chromatin and can lead to decompaction, as seen from experiments with nucleosome arrays (Tse, Sera et al. 1998). However, it has also been shown that acetyl-lysines of the histone tails bind specific proteins (MacDonald and Howe 2009). Proteins like HP1, Polycomb repressor complex and the HMG family of proteins have all been shown to be affect chromatin structure, with the former two binding to specific histone modifications (Grewal and Jia 2007; Reeves 2010). Similarly, there could be proteins that affect chromatin compaction by either binding acetyl lysines, or through losing affinity for lysines upon acetylation of histones.

A SILAC based approach was used to identify proteins that could potentially affect chromatin structure by their affinity for binding acetyl lysine modified histones. HeLa cells were grown in media containing arginine and lysine, either with the normal 'light' isotopes of carbon and nitrogen (i.e. $^{12}C^{14}N$) (light), or 'heavy' isotopes of carbon and nitrogen L-[$^{13}C_6$,$^{15}N_4$]arginine and L-[$^{13}C_6$,$^{15}N_2$]lysine. Cells grown with the

light media were the control cells. Cells grown with heavy media were treated with 200ng/ml TSA for 12 hours.

TSA treatment of cells could lead to a number of effects within the cells, which may, or may not, influence chromatin structure. However, proteins influencing chromatin structure have a higher probability to be directly associated with chromatin. To identify proteins that have a higher relevance to this study, the total proteome and a chromatin enriched fraction were processed and analysed independently. The chromatin fraction was isolated using the SimpleChIP® Enzymatic Chromatin IP Kit (Cell Signalling ♯9002), as per manufacturer's instructions. In this technique, cells are fixed prior to extraction of the chromatin, which will minimise the potential loss of proteins with lower binding affinity to chromatin.

Mass spectrometry analysis of the protein samples led to the identification of 175,975 peptides corresponding to 3,219 proteins from the chromatin proteome and a total of 170,534 peptides corresponding to 3147 proteins from the whole cell lysate proteome. Of the identified peptides, 4,330 and 3,075 peptides mapped to histones were identified from the isolated chromatin and total cell lysate experiments respectively. This indicated that the chromatin fraction had 40% more peptides mapping to histones when compared to the whole cell lysate indicating enrichment for histones and thereby chromatin bound proteins.

To check for the efficiency of TSA treatment, peptides with acetylated lysines were identified, mapped to proteins and quantified as described above. Acetylated

peptides from the histones H3 and H2B were identified from both sets of experiments and acetylated peptides of histone H2A were additionally identified from the whole cell lysate. There were varying levels of increase in acetylation for the individual peptides, ranging from two to eleven fold (Table – 1, 2). However, the levels of most histones, including the ones for which acetylated peptides were identified, were of equal abundance in both sets of experiments. This indicated the TSA treatment has led to the increase in acetylation of histones without changing the total abundance of the histones after treatment with TSA.

As a negative control, acetyl-lysine peptides from the protein Small Nuclear Ribonucleoprotein F (SNRPF) were also identified and quantified from both sets of experiments (Table – 1, 2). There was no change in the levels of the acetylated peptide or of total protein showing that the increase in acetylation was not global.

For identification of proteins that change in concentration after treatment with TSA in the chromatin fraction, only those with a minimum of two unique peptides and identified in at least two of the three biological replicates were chosen and further analysed. The stringent conditions used increase the reliability of the results by reducing the number of potential false positives. The median fold changes (normalised H/L ratio) were calculated to be 1.0012 and 1.0311 for chromatin associated proteins, and lysate proteins, respectively, indicating that most proteins were not changing (Fig 32). Protein concentrations were considered to be significantly changed if the fold change of the proteins was at least two standard deviations away from the median. For proteins identified from isolated chromatin, a fold change (normalised H/L ratio) either greater than 1.90, or less than 0.52, and for

proteins identified from total cell lysate, either greater than 1.92, or less than 0.54, were considered to be significantly changed.

To check for the reproducibility of the fold changes for the proteins identified from the chromatin fraction, a student's t test was performed. The fold change values from the three biological replicates of each protein were compared with the values of all non-significant proteins (i.e. proteins that do not meet the two standard deviation criteria) and p values were obtained. A 0.05 p value cutoff was used in combination with a 2 standard deviation fold change to identify reproducible, changing proteins. A total of 41 proteins were found to be up regulated in the chromatin fraction of which 22 were also identified in the whole cell lysate. Eleven of these proteins were also upregulated while the other 11 were not significantly changed upon TSA treatment (Table 7). Of the 38 proteins found to be significantly down regulated in the chromatin fraction, 23 were also identified in the whole cell lysate, of which 8 proteins were significantly down regulated, 1 protein was significantly upregulated and 14 were not significantly changed upon TSA treatment (Table 6).

The proteins which change only in the chromatin fraction could be recruited to or away from the chromatin after TSA while the total cellular concentration remains unchanged. The proteins that change in both fraction are possibly regulated as part of gene expression or degradation pathways.

The decompaction of chromatin upon TSA treatment could possibly be brought about by proteins known to be associated with regulation of chromatin compaction. All the three isoforms of HP1 were identified from both protein fractions, while eight HMG protein isoforms were identified from the chromatin fraction and whole cell lysate. There was no significant change in the protein levels of these proteins with treatment with TSA showing that these proteins are probably not involved in causing decompaction after TSA treatment (Table – 4, 5).

From the list of proteins that were identified to be significantly changing, three proteins were selected, based on the availability of reagents, for confirmation by western blotting to validate of the results from mass spectrometry. Western blotting confirmed the results obtained from mass spectrometry showing a marked increase in Histone H1.0 after TSA treatment (Fig 33). Histone H1.0 is an isoform of Histone H1, which was shown to be upregulated 4.2 fold in the whole cell extract and 3.2 fold in the chromatin fraction. Histone H1 has seven somatic isoforms. H1.0 along with H1X are the two that are expressed in a replication independent manner (Terme, Sese et al. 2011) and upregulated in G_0 as cells enter contact inhibition, senescence, or differentiation (Th'ng, Sung et al. 2005). H1.0 is the shortest variant of histone H1, but has the highest density of basic amino acids and is known to accumulate in terminally differentiated cells (Terme, Sese et al. 2011). Mice with the H1.0 gene knocked out have been shown to be deficient for dendritic cells (Gabrilovich, Cheng et al. 2002). In a study with mouse fibroblasts, GFP tagged H1.0 was found to accumulate in the euchromatic regions of the nucleus with more decompacted chromatin and was the second fastest to recover in Fluorescence

Recovery After Photo-bleaching (FRAP) experiments (Th'ng, Sung et al. 2005). However, another study using atomic force microscopy has shown histone H1.0 causes higher compaction of nucleosome arrays along with H1.4 and H1.5 when compared with all isoforms of H1 (Clausell, Happel et al. 2009).

Epiplakin is a member of the plakin family. It has been shown to be associated with keratin and vimentin filaments in cells and an increase in filament association was observed under stress conditions (Spazierer, Raberger et al. 2008). Knock down of epiplakin leads to the disruption of these filament networks (Jang, Kalinin et al. 2005). It was also shown to be upregulated during Ca^{2+}-mediated differentiation of normal human epidermal keratinocytes (NHEKs) (Jang, Kalinin et al. 2005). Epiplakin was upregulated 2.4 fold (quantified from 406 peptides) in whole cell lysate and 2.3 fold (quantified from 535 peptides) in the Chromatin fraction. However, vimentin and keratin showed no significant changes, with fold change values close to 1 in both samples.

PCNA associated factor (PAF) was found to be down-regulated after TSA treatment by 0.35 fold (quantified from 5 peptides), in the whole cell lysate and 0.41 fold (quantified from 4 peptides) in the chromatin fraction, when compared with control levels. PAF has recently been shown to be a cell cycle regulated protein with highest expression during the G2/M phase (Emanuele, Ciccia et al. 2011) and has previously been shown to be increased in tumors (Yu, Huang et al. 2001). Thus the decrease of PAF in cells treated with TSA could also be a possible result of the cells being arrested predominantly in the G1 phase, as has been reported previously with TSA

treatment (Yoshida, Kijima et al. 1990; Kim, Ki et al. 2000). However, mitotic cells do show the highest compaction states and PAF could possibly be an effector of increasing chromatin compaction, which could also explain its downregulation upon decompaction of chromatin. Both Epiplakin, quantified from hundreds of peptides, and PAF, quantified from 5 peptides, showed an increase and decrease in protein levels, respectively when analysed with western blotting, confirming the reliability of mass spectrometry quantification (Fig 33).

The proteins that have been identified from this screen may either be directly involved with chromatin compaction, or else be due to secondary effects, like G1 arrest (Yoshida, Kijima et al. 1990; Kim, Ki et al. 2000). The list of proteins offers candidates that could modulate chromatin compaction. However, whether the changes are a cause, or a consequence, of chromatin decompaction have to be ascertained.

Of the proteins whose levels were significantly changed in the chromatin fraction, one protein, ASH1L, was found to contain a bromodomain. Bromodomains have been shown to bind acetyl-lysine. ASH1L was found to be significantly upregulated in the chromatin fraction upon TSA treatment. ASH1L is a methyl transferase that has been shown to be associated with active genes, where it methylates histone H3 at lysine 4, which is a mark of active transcription and associated with decompacted chromatin (Gregory, Vakoc et al. 2007). ASH1L was the only protein identified with a bromo domain among the significantly changed proteins.

The histone chaperone ASF1a was found to be downregulated in both the whole cell lysate and chromatin fractions. The mammalian HIRA/UBN1/ASF1a complex is a histone chaperone complex that is conserved from budding yeast (*Saccharomyces cerevisiae*) to humans. This complex preferentially deposits the histone variant H3.3 into chromatin in a DNA replication-independent manner and is implicated in diverse chromatin regulatory events from gene activation to heterochromatinization (Rai, Puri et al. 2011). ASF1A has also been shown to be required for the restoration of H3 lysine 56 acetylation, post UV induced DNA damage repair (Battu, Ray et al. 2011).

Two ubiquitin transferring proteins were also detected, i.e., UBE2S, which was upregulated, and UBE2C, which was down regulated. Both proteins have been shown to be components of the Anaphase promoting complex. UBE2S, although not essential, has been shown to promote mitotic exit and has been shown in vitro to elongate ubiquitin chains initiated by UBE2C (Garnett, Mansfeld et al. 2009). UBE2C has been shown to be required for progression of mitosis, with a dominant negative mutant, created by changing the catalytic cysteine to serine, causes cells to arrest in metaphase (Townsley, Aristarkhov et al. 1997). The UBE2S protein associated with mitotic exit, which is characterised by chromatin decompaction, was increased after TSA treatment, while the ubiquitin transferase associated with the progression of mitosis was decreased, although they have been shown to be part of the same complex.

The list of significantly changing proteins includes 8 mitochondrial ribosomal proteins, 7 of which belong to the larger 39S ribosomal subunit. Sub cellular

localisation data using immunofluorescence, for three of these proteins, i.e., 39S ribosomal protein L52, 39S ribosomal protein L2 and 39S ribosomal protein L55 can be seen in the protein atlas database (proteinatlas.org; (Uhlen, Oksvold et al. 2010). The former two proteins show nuclear localisation and might have additional unknown functions in the nucleus. Similarly, the two isoforms of ER lumen protein retaining receptor 1 also show nuclear staining (proteinatlas.org; (Uhlen, Oksvold et al. 2010).

However, TSA treatment could have secondary effects, which cause these changes in protein concentration and may not be associated with chromatin compaction. Experiments involving either siRNA knock-down, or overexpression studies, for the proteins identified in this proteomics screen could give more insights into the functions of these proteins and help to identify proteins that can influence chromatin structure. For example proteins that increase chromatin compaction by associating with chromatin, that are displaced by an increase in acetylation or proteins that bind chromatin with increased acetylation and decrease compaction could be identified.

Chapter 6

Discussion

DNA is made from just four monomer building blocks, i.e., dATP, dCTP, dGTP and dTTP and is the carrier of genetic information for all organisms, excluding RNA viruses. In eukaryotes, the DNA is wrapped around basic histones, which partially neutralises the charge of the negative poly-phosphate backbone of DNA. However, not all of this charge is neutralised, and there is still repulsion from the remaining negative charge of the phosphates in the DNA (Strick, Strissel et al. 2001). This repulsion causes the poly-nucleosome to remain decompacted. In defined nucleosome arrays it has been shown that this repulsion can be neutralised by the presence of polyvalent cations (Korolev, Allahverdi et al. 2010). The required concentration of polyvalent cations for chromatin compaction increased when the histones had post translational modifications like acetylation, which decreases the positive charge of histones (Tse, Sera et al. 1998).

The chromatin environment within the nucleus of a cell is different from in vitro assembled nucleosome arrays, having for example a number of associated factors like chromatin binding proteins, RNA, different combinations of histone variants and post translational modifications. However, studies from permeabilised cells using FLIM indicate that chromatin in vivo compacts in a similar manner to nucleosome arrays that lacks these associated factors. The increase in compaction of chromatin in permeabilised cells was maximal at 6-8mM of either of the divalent cations Mg^{2+} or Ca^{2+} (Fig – 12, 14), similar to what was observed in experiments with nucleosome arrays (Zheng, Lu et al. 2005). In the experimental system used by Zheng et al., they used crosslinking between nucleosome arrays to quantify inter-array associations, representing tertiary structures. The data from their experiments, although involving

a completely different methodology, correlated with the data obtained using the FLIM system. An increase in chromatin compaction was also seen with an increase in concentration of other polyvalent cations, like spermine and spermidine, in permeabilised cells (Fig – 15, 16). Increase in Ca^{2+} in intact cells also led to an increase in compaction (Fig 19).

The internal ionic environment of a cell will play a role in the compaction dynamics of the chromatin. It has been shown that there is an increase in concentration of chromatin bound calcium of mitotic cells (Strick, Strissel et al. 2001). The results obtained from experiments in this thesis along with those results suggests that the increase in calcium can be a major contributing factor for the formation of the condensed mitotic chromosomes. Similarly, polyamines have also been shown to be regulated in a cyclic manner through the cell cycle. It has been shown that the concentration of polyamines increases during two phases of the cell cycle, at the S phase and the G2/M phase transition (Alm and Oredsson 2009). At the S phase, new chromatin is being synthesized and this will result in increased amounts of chromatin, for the cell to maintain the compaction state of the chromatin, the factors required for the maintenance of compaction will also have to be increased. Similarly, during the G2/M phase transition, the cell condenses the chromatin to undergo cell division. As the increase in polyamines in increased in both the instances where the chromatin is increasing and when condensing, it could be associated with its maintenance. The experiments from this thesis show that the increase of polyamine concentration in permeabilised cells does indeed lead to the increase in chromatin compaction. The data from both experiments show that the

increase in compaction and also its maintenance requires changes in cation concentrations.

Similarly polyamines sperimine and spermidine were first crystallised from semen in 1678 by Anton van Leeuwenhoek and later found to be highly abundant in sperm cells. The compaction of chromatin in sperm cells is mainly attributed to the presence of the basic protamines that replace native histones. However, protamines are not conserved amongst all organisms, and yet highly compacted sperm chromatin is formed (Lewis, Saperas et al. 2004). Thus the compaction can also be attributed to the presence of polyamines which as I have demonstrated can compact chromatin even at much lower concentrations, when compared to divalent cations.

RNAse treatment led to the increase in compaction of permeabilised cells. This effect can be attributed to the decrease in repulsive negative charges upon the loss of the RNA. Transcription is known to be associated with regions of decompacted chromatin. Experiments in wheat have shown that the genes encoding glutenin are maintained in a compacted state and decompact upon activation (Wegel, Vallejos et al. 2005). However, it was also seen in the same study that transcription always preceded decompaction as compact region with active transcription were observed, but not vice versa. This along with the RNAse experiment suggests that a mechanism for transcription dependent decompaction could be facilitated by changes in the charge environment brought about by increased RNA concentrations.

In addition I also show evidence for more than one structural state of chromatin, one of which was more stable. The more stable compaction state, brought about at 2mM of either Mg^{2+} or Ca^{2+}, could correspond to the 30nm fiber, as nucleosome arrays form the 30nm fibre in vitro at the same concentration of Mg^{2+} (Luger and Hansen 2005). I am currently collaborating with the David Bazzet-Jones group to identify the structure formed at 2mM of Mg^{2+} in permeabilised cells using electron spectroscopic imaging studies (Bazett-Jones, Li et al. 2008). If proved to the 30nm structure, this will be the first ever report of visualisation of the 30nm structure in an intact nucleus, with exception of the echinoderm sperm chromatin. However, even if it is shown to be the 30nm fibre, it could still be an artifact of permeabilisation of the cell. Which would mean that the 30nm fibre is prevented from forming, or the native conditions of a cell does not favor the formation of the 30nm fibre.

ATP depletion results in global chromatin compaction (Fig 20). However, the mechanism by which this occurs is not known. I used ATP depletion as a model system to identify processes that maintain chromatin compaction. Processes like transcription and DNA replication, implicated in maintaining chromatin in a decompacted state (Mahy, Perry et al. 2002; Centore, Havens et al. 2010) are inhibited after ATP depletion. However, they are not functional in mitotic chromosomes. My results show that ATP depletion also leads to the compaction of mitotic chromosomes (Fig 23), showing that the increase in compaction brought about by ATP depletion is not solely a consequence of either inhibiting transcription or DNA replication. However, the possibility remains that other proteins, like the ATP dependent chromatin remodelers, might also be involved in maintaining

decompaction and further studies have to be done to study their potential involvement in maintaining decompaction.

At physiological pH ATP has a charge of -4. ATP, with a charge of -4, has been shown to bind polyamines with high affinity. This binding is stronger than that of polyamines binding to other negatively charged molecules, including RNA and DNA (Watanabe, Kusama-Eguchi et al. 1991). This suggests the possibility that upon the depletion of ATP, the binding of polyamines could be biased towards RNA and DNA. This binding will result in neutralising the charge of chromatin and thereby increase its compaction. Staining for spermine showed a change in localisation after ATP depletion (Fig 28). The effect was most observed in the loss of staining in the nucleolus. The nucleolus is the site of rRNA transcription, which accounts for 50% of the transcription in cells (Raska, Koberna et al. 2004). This would also indicate a higher turnover of ATP within the nucleolus which will be lost with ATP depletion. Considering the fact that spermine is required in much lower concentrations to induce compaction, when compared to divalent cations, it is possible a change in localisation of polyamines is responsible for most of the chromatin compaction caused by ATP depletion. This hypothesis is further corroborated with the experiments with the knockdown of APC, which has been shown to cause an increase in polyamine production(Rial, Meyskens et al. 2009). When APC was knocked down, there was an increase in the compaction of mitotic chromatin. I am currently working with the group of Alan Fairlamb (University of Dundee) to quantify changes in localisation of polyamines after ATP depletion in HeLa cells.

Having experimented with a system where the compaction of chromatin is increased, I decided to look for changes associated with a system wherein, chromatin in decompacted. TSA treatment leads to increased acetylation of histones (Fig 30). This causes neutralisation of the positive charge on the lysines of histones. This consequent increase in net negative charge will lead to decompaction of chromatin. However, acetyl lysines are known to bind proteins that carry a bromodomain. Similarly, chromodomain containing proteins bind methyl–lysine, HP1 which is known to be associated with compacted heterochromatin is one such chromodomain containing protein. This opens the possibility that in vivo, chromatin decompaction seen with increased acetylation (Fig 31) is also assisted by other proteins.

A SILAC based approach was used to identify proteins whose levels change after treatment with TSA. HeLa cells were used as the model system as SILAC protocols had been standardized for HeLa cells and basic processes like maintenance of chromatin compaction are most likely conserved among cell types. SILAC based proteomics were done with whole cell extracts and also with isolated chromatin. The isolated chromatin was fixed prior to extraction, as chromatin isolation would require the permeabilisation of cells in buffer systems, which can affect the compaction state of chromatin based on their ionic composition.

Comparison of the proteins identified from both lists will not only reveal proteins that have changed in overall concentration, but also identify proteins that have changes in their association with the chromatin. The latter proteins would have

change in the chromatin fraction, whereas remain unchanged in the whole cell lysate. This experiment revealed a list of 78 proteins (Table – 6, 7), of which only one protein, ASH1L, contained a bromodomain. ASH1L was significantly upregulated and is a methyl transferase, which methylates lysine 4 of histone H3, a mark of active transcription. The role of ASH1L and others from the list have to be further studied to identify which of these proteins, if any, can modulate chromatin compaction. Over expression and knockdown of proteins that have been identified from the analysis of TSA treated cells could lead to the identification of proteins involved in maintaining chromatin compaction.

In this thesis I have shown that changes in charge brought about either by addition of cations, or by removal of RNA alter chromatin compaction states. Changes in the ionic concentration possibly alter chromatin compaction on a global scale. This, however, will not explain the formation of distinct heterochromatic and euchromatin regions within the nucleus. The recruitment of specific protein complexes to specific regions of chromatin possibly marked my sequence or histone modifications could alter the local charge environment of the chromatin and cause the surrounding chromatin to adopt a given conformation.

Two recent studies have shown that proteins associated with compacted chromatin function by neutralising negative charge. In vitro experiments have shown that the subunit of the PRC1 complex, PSC, which induces compaction is highly basic (Grau, Chapman et al. 2011). The protein has been shown to have a domain that helps in dimerisation of the protein, and another domain which is highly basic and

unstructured. The latter domain has been shown to effect compaction of chromatin. Interestingly, the mouse protein also belonging to the PRC1 complex that caused the increase in compaction was not homologous to PSC protein from Drosophila (Grau, Chapman et al. 2011). However, the similarity between the two proteins was the presence of highly basic domains. Similarly the isolated N-terminal region of the telomere binding protein, TRF2, which induced highest compaction, was also shown to be the most basic part of the protein (Baker, Fu et al. 2011).

HMG proteins show the presence of a long negatively charged carboxy-terminal tail that serves a regulatory function (Gerlitz, Hock et al. 2009). Most functions they have been shown to regulate, like transcription activation, DNA repair require decompaction of chromatin. This the presence of more negative charge as with the incease with RNA will lead to an increase in negative charge in the local environment and could possibly lead to decompaction.

The study of chromatin compaction states could also help to improve our understanding of certain disease conditions. For example, ICF syndrome is a rare autosomal recessive disorder in which patients display immunodeficiency, mental retardation, developmental delay and instability of pericentric heterochromatin of chromosomes 1, 9 and 16 (Smeets, Moog et al. 1994). Hypomethylation of DNA was observed in these patients, with patients showing mutations in the DNMT3B gene and the chromatin showed an increase in DNase hypersensitivity, indicating decompacted chromatin (Hansen, Stoger et al. 2000). Mutations in the CREB-binding protein (CBP), an acetyl transferase that acetylates histones, have been shown to cause Rubinstein-Taybi syndrome (Hendrich and Bickmore 2001). Laminopathies are

a group of diseases that result from different mutations in the gene LMNA (Worman, Ostlund et al. 2010). The lamins, Lamin A and Lamin C, encoded by the gene, are associated with the nuclear envelope and interact with heterochromatin (Dechat, Pfleghaar et al. 2008). Histone deacetylase inhibitors have also been used in trials for the treatment of some cancers (Robey, Chakraborty et al. 2011).

With the role of chromatin compaction states being identified as being important in regulating gene expression, the experiments in this thesis could help in improve our understanding pathways and processes involved in maintenance of chromatin structure and consequently gene expression. With the implication of these pathways for disease mechanisms, a better understanding could also potentially lead to the identification of new drug targets and future therapies.

6.2 References

Adam, S. A. and L. Gerace (1991). "Cytosolic proteins that specifically bind nuclear location signals are receptors for nuclear import." Cell **66**(5): 837-847.

Ahmed, K., H. Dehghani, et al. (2010). "Global chromatin architecture reflects pluripotency and lineage commitment in the early mouse embryo." PloS one **5**(5): e10531.

Allahverdi, A., R. Yang, et al. (2011). "The effects of histone H4 tail acetylations on cation-induced chromatin folding and self-association." Nucleic acids research **39**(5): 1680-1691.

Alm, K. and S. Oredsson (2009). "Cells and polyamines do it cyclically." Essays in biochemistry **46**: 63-76.

Altaf, M., A. Auger, et al. (2009). "Connection between histone H2A variants and chromatin remodeling complexes." Biochemistry and Cell Biology **87**(1): 35-50.

Andersen, J. S., C. E. Lyon, et al. (2002). "Directed proteomic analysis of the human nucleolus." Current biology : CB **12**(1): 1-11.

Anderson, S. N., B. L. Cool, et al. (2004). "Microarrayed compound screening (microARCS) to identify activators and inhibitors of AMP-activated protein kinase." Journal of biomolecular screening **9**(2): 112-121.

Ayyanathan, K., M. S. Lechner, et al. (2003). "Regulated recruitment of HP1 to a euchromatic gene induces mitotically heritable, epigenetic gene silencing: a mammalian cell culture model of gene variegation." Genes & development **17**(15): 1855-1869.

Baker, A. M., Q. Fu, et al. (2011). "The telomere binding protein TRF2 induces chromatin compaction." PloS one **6**(4): e19124.

Banerjee, T. and D. Chakravarti (2011). "A peek into the complex realm of histone phosphorylation." Molecular and Cellular Biology **31**(24): 4858-4873.

Bannister, A. J. and T. Kouzarides (2005). "Reversing histone methylation." Nature **436**(7054): 1103-1106.

Bannister, A. J. and T. Kouzarides (2011). "Regulation of chromatin by histone modifications." Cell research **21**(3): 381-395.

Bastiaens, P. I. H. and A. Squire (1999). "Fluorescence lifetime imaging microscopy: Spatial resolution of biochemical processes in the cell." Trends in Cell Biology **9**(2): 48-52.

Battu, A., A. Ray, et al. (2011). "ASF1A and ATM regulate H3K56-mediated cell-cycle checkpoint recovery in response to UV irradiation." Nucleic acids research **39**(18): 7931-7945.

Bazett-Jones, D. P., R. Li, et al. (2008). "Elucidating chromatin and nuclear domain architecture with electron spectroscopic imaging." Chromosome research : an international journal on the molecular, supramolecular and evolutionary aspects of chromosome biology **16**(3): 397-412.

Becker, W. (2008). The Bh TCSPC Handbook.

Bloomfield, V. A. (1996). "DNA condensation." Current opinion in structural biology **6**(3): 334-341.

Boisvert, F. M., Y. Ahmad, et al. (2012). "A quantitative spatial proteomics analysis of proteome turnover in human cells." Molecular & cellular proteomics : MCP **11**(3): M111 011429.

Bolzer, A., G. Kreth, et al. (2005). "Three-dimensional maps of all chromosomes in human male fibroblast nuclei and prometaphase rosettes." PLoS biology **3**(5): e157.

Brown, K. E., J. Baxter, et al. (1999). "Dynamic repositioning of genes in the nucleus of lymphocytes preparing for cell division." Molecular cell **3**(2): 207-217.

Brown, K. E., S. S. Guest, et al. (1997). "Association of transcriptionally silent genes with Ikaros complexes at centromeric heterochromatin." Cell **91**(6): 845-854.

Bustin, M. (2001). "Chromatin unfolding and activation by HMGN* chromosomal protiens." Trends in Biochemical Sciences **26**(7): 431-437.

Carafoli, E. (1991). "Calcium pump of the plasma membrane." Physiological reviews **71**(1): 129-153.

Carrozza, M. J., A. H. Hassan, et al. (2003). "Assay of activator recruitment of chromatin-modifying complexes." Methods in enzymology **371**: 536-544.

Caterino, T. L. and J. J. Hayes (2007). "Chromatin structure depends on what's in the nucleosome's pocket." Nature structural & molecular biology **14**(11): 1056-1058.

Caudron-Herger, M., K. Muller-Ott, et al. (2011). "Coding RNAs with a non-coding function: maintenance of open chromatin structure." Nucleus **2**(5): 410-424.

Centore, R. C., C. G. Havens, et al. (2010). "CRL4(Cdt2)-mediated destruction of the histone methyltransferase Set8 prevents premature chromatin compaction in S phase." Molecular cell **40**(1): 22-33.

Chambeyron, S., N. R. Da Silva, et al. (2005). "Nuclear re-organisation of the Hoxb complex during mouse embryonic development." Development **132**(9): 2215-2223.

Chodaparambil, J. V., A. J. Barbera, et al. (2007). "A charged and contoured surface on the nucleosome regulates chromatin compaction." Nature structural & molecular biology **14**(11): 1105-1107.

Churchill, M. E. A. and M. Suzuki (1989). "'SPKK' motifs prefer to bind to DNA at A/T-rich sites." EMBO Journal **8**(13): 4189-4195.

Clapier, C. R. and B. R. Cairns (2009). "The biology of chromatin remodeling complexes." Annual review of biochemistry **78**: 273-304.

Clausell, J., N. Happel, et al. (2009). "Histone H1 subtypes differentially modulate chromatin condensation without preventing ATP-dependent remodeling by SWI/SNF or NURF." PloS one **4**(10): e0007243.

Comings, D. E. (1980). "Arrangement of chromatin in the nucleus." Human genetics **53**(2): 131-143.

Costa, S. and P. Shaw (2006). "Chromatin organization and cell fate switch respond to positional information in Arabidopsis." Nature **439**(7075): 493-496.

Cox, J. and M. Mann (2008). "MaxQuant enables high peptide identification rates, individualized p.p.b.-range mass accuracies and proteome-wide protein quantification." Nature biotechnology **26**(12): 1367-1372.

Cox, J., I. Matic, et al. (2009). "A practical guide to the MaxQuant computational platform for SILAC-based quantitative proteomics." Nature protocols **4**(5): 698-705.

Cremer, T. and M. Cremer (2010). "Chromosome territories." Cold Spring Harbor perspectives in biology **2**(3): a003889.

Croft, J. A., J. M. Bridger, et al. (1999). "Differences in the localization and morphology of chromosomes in the human nucleus." The Journal of cell biology **145**(6): 1119-1131.

Csernoch, L., J. C. Bernengo, et al. (1998). "Measurements of intracellular Mg2+ concentration in mouse skeletal muscle fibers with the fluorescent indicator mag-indo-1." Biophysical journal **75**(2): 957-967.

Dechat, T., K. Pfleghaar, et al. (2008). "Nuclear lamins: major factors in the structural organization and function of the nucleus and chromatin." Genes & development **22**(7): 832-853.

Dikovskaya, D., G. Khoudoli, et al. (2012). "The adenomatous polyposis coli protein contributes to normal compaction of mitotic chromatin." PloS one **7**(6): e38102.

Eagle, H. (1955). "The specific amino acid requirements of a human carcinoma cell (Stain HeLa) in tissue culture." The Journal of experimental medicine **102**(1): 37-48.

Eils, R., S. Dietzel, et al. (1996). "Three-dimensional reconstruction of painted human interphase chromosomes: active and inactive X chromosome territories have similar volumes but differ in shape and surface structure." The Journal of cell biology **135**(6 Pt 1): 1427-1440.

Eltsov, M., K. M. Maclellan, et al. (2008). "Analysis of cryo-electron microscopy images does not support the existence of 30-nm chromatin fibers in mitotic chromosomes in situ." Proceedings of the National Academy of Sciences of the United States of America **105**(50): 19732-19737.

Emanuele, M. J., A. Ciccia, et al. (2011). "Proliferating cell nuclear antigen (PCNA)-associated KIAA0101/PAF15 protein is a cell cycle-regulated anaphase-promoting complex/cyclosome substrate." Proceedings of the National Academy of Sciences of the United States of America **108**(24): 9845-9850.

Endale, M., S. D. Kim, et al. (2010). "Ischemia induces regulator of G protein signaling 2 (RGS2) protein upregulation and enhances apoptosis in astrocytes." American journal of physiology. Cell physiology **298**(3): C611-623.

Fan, J. Y., D. Rangasamy, et al. (2004). "H2A.Z alters the nucleosome surface to promote HP1alpha-mediated chromatin fiber folding." Molecular cell **16**(4): 655-661.

Fan, Y., T. Nikitina, et al. (2003). "H1 linker histones are essential for mouse development and affect nucleosome spacing in vivo." Molecular and cellular biology **23**(13): 4559-4572.

Fan, Y., A. Sirotkin, et al. (2001). "Individual somatic H1 subtypes are dispensable for mouse development even in mice lacking the H1(0) replacement subtype." Molecular and Cellular Biology **21**(23): 7933-7943.

Fashena, S. J., R. Reeves, et al. (1992). "A poly(dA-dT) upstream activating sequence binds high-mobility group I protein and contributes to lymphotoxin (tumor necrosis factor beta) gene regulation." Molecular and Cellular Biology **12**(2): 894-903.

Fenn, J. B., M. Mann, et al. (1989). "Electrospray ionization for mass spectrometry of large biomolecules." Science **246**(4926): 64-71.

Fierz, B., C. Chatterjee, et al. (2011). "Histone H2B ubiquitylation disrupts local and higher-order chromatin compaction." Nature chemical biology **7**(2): 113-119.

Finlan, L. E., D. Sproul, et al. (2008). "Recruitment to the nuclear periphery can alter expression of genes in human cells." PLoS genetics **4**(3): e1000039.

Fischle, W., Y. Wang, et al. (2003). "Molecular basis for the discrimination of repressive methyl-lysine marks in histone H3 by Polycomb and HP1 chromodomains." Genes & development **17**(15): 1870-1881.

Forster, T. (1949). "Experimentelle und theoretische untersuchung des zwischenmolekularen ubergangs von elektronenanregunsenergie." Z. Naturforsch. **4 A**: 321-327.

Furusawa, T., J. H. Lim, et al. (2006). "Down-regulation of nucleosomal binding protein HMGN1 expression during embryogenesis modulates Sox9 expression in chondrocytes." Molecular and Cellular Biology **26**(2): 592-604.

Gabrilovich, D. I., P. Cheng, et al. (2002). "H1(0) histone and differentiation of dendritic cells. A molecular target for tumor-derived factors." Journal of leukocyte biology **72**(2): 285-296.

Garnett, M. J., J. Mansfeld, et al. (2009). "UBE2S elongates ubiquitin chains on APC/C substrates to promote mitotic exit." Nature cell biology **11**(11): 1363-1369.

Gee, K. R., K. A. Brown, et al. (2000). "Chemical and physiological characterization of fluo-4 Ca(2+)-indicator dyes." Cell calcium **27**(2): 97-106.

Gerlitz, G., R. Hock, et al. (2009). "The dynamics of HMG protein-chromatin interactions in living cells." Biochemistry and Cell Biology **87**(1): 127-137.

Ghaemmaghami, S., W. K. Huh, et al. (2003). "Global analysis of protein expression in yeast." Nature **425**(6959): 737-741.

Gordon, F., K. Luger, et al. (2005). "The core histone N-terminal tail domains function independently and additively during salt-dependent oligomerization of nucleosomal arrays." The Journal of biological chemistry **280**(40): 33701-33706.

Grau, D. J., B. A. Chapman, et al. (2011). "Compaction of chromatin by diverse Polycomb group proteins requires localized regions of high charge." Genes & development **25**(20): 2210-2221.

Greaves, I. K., D. Rangasamy, et al. (2007). "H2A.Z contributes to the unique 3D structure of the centromere." Proceedings of the National Academy of Sciences of the United States of America **104**(2): 525-530.

Gregory, G. D., C. R. Vakoc, et al. (2007). "Mammalian ASH1L is a histone methyltransferase that occupies the transcribed region of active genes." Molecular and cellular biology **27**(24): 8466-8479.

Grewal, S. I. S. and S. Jia (2007). "Heterochromatin revisited." Nat Rev Genet **8**(1): 35-46.

Ha, H. C., N. S. Sirisoma, et al. (1998). "The natural polyamine spermine functions directly as a free radical scavenger." Proceedings of the National Academy of Sciences of the United States of America **95**(19): 11140-11145.

Haas, W., B. K. Faherty, et al. (2006). "Optimization and use of peptide mass measurement accuracy in shotgun proteomics." Molecular & cellular proteomics : MCP **5**(7): 1326-1337.

Hansen, J. C. (2002). "Conformational dynamics of the chromatin fiber in solution: determinants, mechanisms, and functions." Annual review of biophysics and biomolecular structure **31**: 361-392.

Hansen, J. C. and A. P. Wolffe (1992). "Influence of chromatin folding on transcription initiation and elongation by RNA polymerase III." Biochemistry **31**(34): 7977-7988.

Hansen, R. S., R. Stoger, et al. (2000). "Escape from gene silencing in ICF syndrome: evidence for advanced replication time as a major determinant." Human molecular genetics **9**(18): 2575-2587.

Hardy, S., P. â. Jacques, et al. (2009). "The euchromatic and heterochromatic landscapes are shaped by antagonizing effects of transcription on H2A.Z deposition." PLoS Genetics **5**(10).

Hargreaves, D. C. and G. R. Crabtree (2011). "ATP-dependent chromatin remodeling: Genetics, genomics and mechanisms." Cell Research **21**(3): 396-420.

Heitz, S. (1928). "Das Heterochromatin der Moose." Jahrb Wiss Bot **69**: 762–818.

Hendrich, B. and W. Bickmore (2001). "Human diseases with underlying defects in chromatin structure and modification." Human molecular genetics **10**(20): 2233-2242.

Hines, K. A., D. E. Cryderman, et al. (2009). "Domains of heterochromatin protein 1 required for Drosophila melanogaster heterochromatin spreading." Genetics **182**(4): 967-977.

Hirota, T., J. J. Lipp, et al. (2005). "Histone H3 serine10 phosphorylation by Aurora B causes HP1 dissociation from heterochromatin." Nature **438**(7071): 1176-1180.

Horowitz, R. A., D. A. Agard, et al. (1994). "The three-dimensional architecture of chromatin in situ: electron tomography reveals fibers composed of a continuously variable zig-zag nucleosomal ribbon." The Journal of cell biology **125**(1): 1-10.

Hsu, J. Y., Z. W. Sun, et al. (2000). "Mitotic phosphorylation of histone H3 is governed by Ipl1/aurora kinase and Glc7/PP1 phosphatase in budding yeast and nematodes." Cell **102**(3): 279-291.

Jacobs, S. A. and S. Khorasanizadeh (2002). "Structure of HP1 chromodomain bound to a lysine 9-methylated histone H3 tail." Science **295**(5562): 2080-2083.

Jacobson, R. H., A. G. Ladurner, et al. (2000). "Structure and function of a human TAFII250 double bromodomain module." Science **288**(5470): 1422-1425.

Jang, S. I., A. Kalinin, et al. (2005). "Characterization of human epiplakin: RNAi-mediated epiplakin depletion leads to the disruption of keratin and vimentin IF networks." Journal of cell science **118**(Pt 4): 781-793.

Joshi, A. A. and K. Struhl (2005). "Eaf3 chromodomain interaction with methylated H3-K36 links histone deacetylation to pol II elongation." Molecular Cell **20**(6): 971-978.

Joti, Y., T. Hikima, et al. (2012). "Chromosomes without a 30-nm chromatin fiber." Nucleus **3**(5): 0--1.

Kan, P. Y., T. L. Caterino, et al. (2009). "The H4 tail domain participates in intra- and internucleosome interactions with protein and DNA during folding and oligomerization of nucleosome arrays." Molecular and cellular biology **29**(2): 538-546.

Kan, P. Y., X. Lu, et al. (2007). "The H3 tail domain participates in multiple interactions during folding and self-association of nucleosome arrays." Molecular and cellular biology **27**(6): 2084-2091.

Karas, M. and F. Hillenkamp (1988). "Laser desorption ionization of proteins with molecular masses exceeding 10,000 daltons." Analytical chemistry **60**(20): 2299-2301.

Khalil, A., J. L. Grant, et al. (2007). "Chromosome territories have a highly nonspherical morphology and nonrandom positioning." Chromosome research : an international journal on the molecular, supramolecular and evolutionary aspects of chromosome biology **15**(7): 899-916.

Khorasanizadeh, S. (2004). "The nucleosome: from genomic organization to genomic regulation." Cell **116**(2): 259-272.

Khoudoli, G. A., P. J. Gillespie, et al. (2008). "Temporal profiling of the chromatin proteome reveals system-wide responses to replication inhibition." Current biology : CB **18**(11): 838-843.

Kim, Y. B., S. W. Ki, et al. (2000). "Mechanism of cell cycle arrest caused by histone deacetylase inhibitors in human carcinoma cells." The Journal of antibiotics **53**(10): 1191-1200.

Kimura H Fau - Cook, P. R. and P. R. Cook (2001). "Kinetics of core histones in living human cells: little exchange of H3 and H4 and." The Journal of cell biology **153**(7): 1341-1353.

Koehler, D., V. Zakhartchenko, et al. (2009). "Changes of higher order chromatin arrangements during major genome activation in bovine preimplantation embryos." Experimental cell research **315**(12): 2053-2063.

Kornberg, R. D. and J. O. Thomas (1974). "Chromatin structure; oligomers of the histones." Science **184**(4139): 865-868.

Korner, U., M. Bustin, et al. (2003). "Developmental role of HMGN proteins in Xenopus laevis." Mechanisms of Development **120**(10): 1177-1192.

Korolev, N., A. Allahverdi, et al. (2010). "Electrostatic origin of salt-induced nucleosome array compaction." Biophysical journal **99**(6): 1896-1905.

Kouzarides, T. (2007). "Chromatin modifications and their function." Cell **128**(4): 693-705.

Kumaran, R. I. and D. L. Spector (2008). "A genetic locus targeted to the nuclear periphery in living cells maintains its transcriptional competence." The Journal of cell biology **180**(1): 51-65.

Kwon, S. H. and J. L. Workman (2011). "The changing faces of HP1: From heterochromatin formation and gene silencing to euchromatic gene expression: HP1 acts as a positive regulator of transcription." BioEssays **33**(4): 280-289.

Lachner, M., R. J. O'Sullivan, et al. (2003). "An epigenetic road map for histone lysine methylation." Journal of cell science **116**(Pt 11): 2117-2124.

Lakowicz, J. R. (2006). Principles of Fluorescence Spectroscopy.

Lewis, J. D., N. Saperas, et al. (2004). "Histone H1 and the origin of protamines." Proceedings of the National Academy of Sciences of the United States of America **101**(12): 4148-4152.

Lleres, D., J. James, et al. (2009). "Quantitative analysis of chromatin compaction in living cells using FLIM-FRET." The Journal of cell biology **187**(4): 481-496.

Lleres, D., S. Swift, et al. (2007). "Detecting protein-protein interactions in vivo with FRET using multiphoton fluorescence lifetime imaging microscopy (FLIM)." Current protocols in cytometry / editorial board, J. Paul Robinson, managing editor ... [et al.] **Chapter 12**: Unit12 10.

Lomberk, G., D. Bensi, et al. (2006). "Evidence for the existence of an HP1-mediated subcode within the histone code." Nature cell biology **8**(4): 407-415.

Lu, X., S. N. Wontakal, et al. (2009). "Linker histone H1 is essential for Drosophila development, the establishment of pericentric heterochromatin, and a normal polytene chromosome structure." Genes & development **23**(4): 452-465.

Luger, K. and J. C. Hansen (2005). "Nucleosome and chromatin fiber dynamics." Current opinion in structural biology **15**(2): 188-196.

Luijsterburg, M. S., C. Dinant, et al. (2009). "Heterochromatin protein 1 is recruited to various types of DNA damage." The Journal of cell biology **185**(4): 577-586.

Lyon, M. F. (1962). "Sex chromatin and gene action in the mammalian X-chromosome." American journal of human genetics **14**: 135-148.

Macdonald, N., J. P. I. Welburn, et al. (2005). "Molecular basis for the recognition of phosphorylated and phosphoacetylated histone H3 by 14-3-3." Molecular Cell **20**(2): 199-211.

MacDonald, V. E. and L. J. Howe (2009). "Histone acetylation: where to go and how to get there." Epigenetics : official journal of the DNA Methylation Society **4**(3): 139-143.

Mahy, N. L., P. E. Perry, et al. (2002). "Gene density and transcription influence the localization of chromatin outside of chromosome territories detectable by FISH." The Journal of cell biology **159**(5): 753-763.

Mann, M. (2006). "Functional and quantitative proteomics using SILAC." Nature reviews. Molecular cell biology **7**(12): 952-958.

Martin, R. M., S. M. Gorisch, et al. (2007). "An unexpected link between energy metabolism, calcium, chromatin condensation and cell cycle." Cell cycle **6**(19): 2422-2424.

McCartney, B. M. and I. S. Nathke (2008). "Cell regulation by the Apc protein Apc as master regulator of epithelia." Current opinion in cell biology **20**(2): 186-193.

Meister, P., B. D. Towbin, et al. (2010). "The spatial dynamics of tissue-specific promoters during C. elegans development." Genes & development **24**(8): 766-782.

Merika, M. and D. Thanos (2001). "Enhanceosomes." Current Opinion in Genetics and Development **11**(2): 205-208.

Muthuswami, R., L. D. Mesner, et al. (2000). "Phosphoaminoglycosides inhibit SWI2/SNF2 family DNA-dependent molecular motor domains." Biochemistry **39**(15): 4358-4365.

Narita, M., V. Krizhanovsky, et al. (2006). "A Novel Role for High-Mobility Group A Proteins in Cellular Senescence and Heterochromatin Formation." Cell **126**(3): 503-514.

Nathke, I. S., C. L. Adams, et al. (1996). "The adenomatous polyposis coli tumor suppressor protein localizes to plasma membrane sites involved in active cell migration." The Journal of cell biology **134**(1): 165-179.

Nissen, M. S., T. A. Langan, et al. (1991). "Phosphorylation by cdc2 kinase modulates DNA binding activity of high mobility group I nonhistone chromatin protein." Journal of Biological Chemistry **266**(30): 19945-19952.

Ohta, S., J. C. Bukowski-Wills, et al. (2010). "The protein composition of mitotic chromosomes determined using multiclassifier combinatorial proteomics." Cell **142**(5): 810-821.

Olsen, J. V., J. C. Schwartz, et al. (2009). "A dual pressure linear ion trap orbitrap instrument with very high sequencing speed." Molecular and Cellular Proteomics **8**(12): 2759-2769.

Ong, S. E., B. Blagoev, et al. (2002). "Stable isotope labeling by amino acids in cell culture, SILAC, as a simple and accurate approach to expression proteomics." Molecular & cellular proteomics : MCP **1**(5): 376-386.

Orsi, G. A., P. Couble, et al. (2009). "Epigenetic and replacement roles of histone variant H3.3 in reproduction and development." International Journal of Developmental Biology **53**(2-3): 231-243.

Owen-Hughes, T., R. T. Utley, et al. (1999). Analysis of Nucleosome Disruption by ATP-Driven Chromatin Remodeling Complexes. **119:** 319-331.

Parada, L. A., P. G. McQueen, et al. (2004). "Tissue-specific spatial organization of genomes." Genome biology **5**(7): R44.

Persson, L. (2009). "Polyamine homoeostasis." Essays in biochemistry **46**: 11-24.

Piccolo, F. M., C. F. Pereira, et al. (2011). "Using heterokaryons to understand pluripotency and reprogramming." Philosophical transactions of the Royal Society of London. Series B, Biological sciences **366**(1575): 2260-2265.

Rai, T. S., A. Puri, et al. (2011). "Human CABIN1 is a functional member of the human HIRA/UBN1/ASF1a histone H3.3 chaperone complex." Molecular and cellular biology **31**(19): 4107-4118.

Rando, O. J. (2012). "Combinatorial complexity in chromatin structure and function: revisiting the histone code." Current opinion in genetics & development **22**(2): 148-155.

Raska, I., K. Koberna, et al. (2004). "The nucleolus and transcription of ribosomal genes." Biology of the cell / under the auspices of the European Cell Biology Organization **96**(8): 579-594.

Reeves, R. (2010). "Nuclear functions of the HMG proteins." Biochimica et biophysica acta **1799**(1-2): 3-14.

Reeves, R. and L. Beckerbauer (2001). "HMGI/Y proteins: Flexible regulators of transcription and chromatin structure." Biochimica et Biophysica Acta - Gene Structure and Expression **1519**(1-2): 13-29.

Reeves, R., T. A. Langan, et al. (1991). "Phosphorylation of the DNA-binding domain of nonhistone high-mobility group I protein by cdc2 kinase: Reduction of binding affinity." Proceedings of the National Academy of Sciences of the United States of America **88**(5): 1671-1675.

Reeves, R. and M. S. Nissen (1990). "The A¬ ∑ T-DNA-binding domain of mammalian high mobility group I chromosomal proteins. A novel peptide motif for recognizing DNA structure." Journal of Biological Chemistry **265**(15): 8573-8582.

Reichel, C., J. Mathur, et al. (1996). "Enhanced green fluorescence by the expression of an Aequorea victoria green fluorescent protein mutant in mono- and

dicotyledonous plant cells." Proceedings of the National Academy of Sciences of the United States of America **93**(12): 5888-5893.

Rial, N. S., F. L. Meyskens, et al. (2009). "Polyamines as mediators of APC-dependent intestinal carcinogenesis and cancer chemoprevention." Essays in biochemistry **46**: 111-124.

Robey, R. W., A. R. Chakraborty, et al. (2011). "Histone deacetylase inhibitors: emerging mechanisms of resistance." Molecular pharmaceutics **8**(6): 2021-2031.

Rogakou, E. P., D. R. Pilch, et al. (1998). "DNA double-stranded breaks induce histone H2AX phosphorylation on serine 139." The Journal of biological chemistry **273**(10): 5858-5868.

Ruegg, U. T. and G. M. Burgess (1989). "Staurosporine, K-252 and UCN-01: potent but nonspecific inhibitors of protein kinases." Trends in pharmacological sciences **10**(6): 218-220.

Sancho, M., E. Diani, et al. (2008). "Depletion of human histone H1 variants uncovers specific roles in gene expression and cell growth." PLoS Genetics **4**(10): e1000227.

Scheffer, M. P., M. Eltsov, et al. (2011). "Evidence for short-range helical order in the 30-nm chromatin fibers of erythrocyte nuclei." Proceedings of the National Academy of Sciences of the United States of America **108**(41): 16992-16997.

Schneider, R. and R. Grosschedl (2007). "Dynamics and interplay of nuclear architecture, genome organization, and gene expression." Genes & development **21**(23): 3027-3043.

Schwartz, Y. B. and V. Pirrotta (2008). "Polycomb complexes and epigenetic states." Current opinion in cell biology **20**(3): 266-273.

Schwarz, P. M. and J. C. Hansen (1994). "Formation and stability of higher order chromatin structures. Contributions of the histone octamer." The Journal of biological chemistry **269**(23): 16284-16289.

Schwoebel, E. D., T. H. Ho, et al. (2002). "The mechanism of inhibition of Ran-dependent nuclear transport by cellular ATP depletion." The Journal of cell biology **157**(6): 963-974.

Sehgal, P. B., J. E. Darnell, Jr., et al. (1976). "The inhibition by DRB (5,6-dichloro-1-beta-D-ribofuranosylbenzimidazole) of hnRNA and mRNA production in HeLa cells." Cell **9**(3): 473-480.

Shaner, N. C., R. E. Campbell, et al. (2004). "Improved monomeric red, orange and yellow fluorescent proteins derived from Discosoma sp. red fluorescent protein." Nature Biotechnology **22**(12): 1567-1572.

Sharma, S., T. K. Kelly, et al. (2010). "Epigenetics in cancer." Carcinogenesis **31**(1): 27-36.

Shav-Tal, Y., X. Darzacq, et al. (2004). "Dynamics of single mRNPs in nuclei of living cells." Science **304**(5678): 1797-1800.

Shiloh, Y., E. Shema, et al. (2011). "RNF20-RNF40: A ubiquitin-driven link between gene expression and the DNA damage response." FEBS letters **585**(18): 2795-2802.

Shogren-Knaak, M., H. Ishii, et al. (2006). "Histone H4-K16 acetylation controls chromatin structure and protein interactions." Science **311**(5762): 844-847.

Simpson, R. T., F. Thoma, et al. (1985). "Chromatin reconstituted from tandemly repeated cloned DNA fragments and core histones: a model system for study of higher order structure." Cell **42**(3): 799-808.

Smeets, D. F., U. Moog, et al. (1994). "ICF syndrome: a new case and review of the literature." Human genetics **94**(3): 240-246.

Snyder, R. D. (1989). "Polyamine depletion is associated with altered chromatin structure in HeLa cells." The Biochemical journal **260**(3): 697-704.

Solovei, I., M. Kreysing, et al. (2009). "Nuclear architecture of rod photoreceptor cells adapts to vision in mammalian evolution." Cell **137**(2): 356-368.

Spazierer, D., J. Raberger, et al. (2008). "Stress-induced recruitment of epiplakin to keratin networks increases their resistance to hyperphosphorylation-induced disruption." Journal of cell science **121**(Pt 6): 825-833.

Stack, S. M., D. B. Brown, et al. (1977). "Visualization of interphase chromosomes." Journal of cell science **26**: 281-299.

Sterner, D. E. and S. L. Berger (2000). "Acetylation of histones and transcription-related factors." Microbiology and molecular biology reviews : MMBR **64**(2): 435-459.

Strick, R., P. L. Strissel, et al. (2001). "Cation-chromatin binding as shown by ion microscopy is essential for the structural integrity of chromosomes." The Journal of cell biology **155**(6): 899-910.

Suto, R. K., M. J. Clarkson, et al. (2000). "Crystal structure of a nucleosome core particle containing the variant histone H2A.Z." Nature structural biology **7**(12): 1121-1124.

Talbert, P. B. and S. Henikoff (2010). "Histone variants--ancient wrap artists of the epigenome." Nature reviews. Molecular cell biology **11**(4): 264-275.

Tan, M., H. Luo, et al. (2011). "Identification of 67 histone marks and histone lysine crotonylation as a new type of histone modification." Cell **146**(6): 1016-1028.

Tanabe, H., S. Muller, et al. (2002). "Evolutionary conservation of chromosome territory arrangements in cell nuclei from higher primates." Proceedings of the National Academy of Sciences of the United States of America **99**(7): 4424-4429.

Telenius, H., A. H. Pelmear, et al. (1992). "Cytogenetic analysis by chromosome painting using DOP-PCR amplified flow-sorted chromosomes." Genes, chromosomes & cancer **4**(3): 257-263.

Terme, J. M., B. Sese, et al. (2011). "Histone H1 variants are differentially expressed and incorporated into chromatin during differentiation and reprogramming to pluripotency." The Journal of biological chemistry **286**(41): 35347-35357.

Th'ng, J. P., R. Sung, et al. (2005). "H1 family histones in the nucleus. Control of binding and localization by the C-terminal domain." The Journal of biological chemistry **280**(30): 27809-27814.

Toth, K. F., T. A. Knoch, et al. (2004). "Trichostatin A-induced histone acetylation causes decondensation of interphase chromatin." Journal of cell science **117**(Pt 18): 4277-4287.

Townsley, F. M., A. Aristarkhov, et al. (1997). "Dominant-negative cyclin-selective ubiquitin carrier protein E2-C/UbcH10 blocks cells in metaphase." Proceedings of the National Academy of Sciences of the United States of America **94**(6): 2362-2367.

Treanor, B., P. M. Lanigan, et al. (2006). "Microclusters of inhibitory killer immunoglobulin-like receptor signaling at natural killer cell immunological synapses." The Journal of cell biology **174**(1): 153-161.

Tremethick, D. J. (2007). "Higher-order structures of chromatin: the elusive 30 nm fiber." Cell **128**(4): 651-654.

Trinkle-Mulcahy, L., J. Andersen, et al. (2006). "Repo-Man recruits PP1 gamma to chromatin and is essential for cell viability." The Journal of cell biology **172**(5): 679-692.

Trojer, P. and D. Reinberg (2007). "Facultative heterochromatin: is there a distinctive molecular signature?" Molecular cell **28**(1): 1-13.

Tse, C., T. Sera, et al. (1998). "Disruption of higher-order folding by core histone acetylation dramatically enhances transcription of nucleosomal arrays by RNA polymerase III." Molecular and cellular biology **18**(8): 4629-4638.

Uhlen, M., P. Oksvold, et al. (2010). "Towards a knowledge-based Human Protein Atlas." Nature biotechnology **28**(12): 1248-1250.

Van Attikum, H., O. Fritsch, et al. (2004). "Recruitment of the INO80 complex by H2A phosphorylation links ATP-dependent chromatin remodeling with DNA double-strand break repair." Cell **119**(6): 777-788.

van Holde, K. (1989). Chromatin, Springer Verlag, New York.

van Holde, K. and J. Zlatanova (1995). "Chromatin higher order structure: chasing a mirage?" The Journal of biological chemistry **270**(15): 8373-8376.

van Holde, K. and J. Zlatanova (2007). "Chromatin fiber structure: Where is the problem now?" Seminars in cell & developmental biology **18**(5): 651-658.

Vishwanath, K., W. Zhong, et al. (2006). "Fluorescence quenching by polystyrene microspheres in UV-visible and NIR tissue-simulating phantoms." Optics express **14**(17): 7776-7788.

Wallace, H. M., A. V. Fraser, et al. (2003). "A perspective of polyamine metabolism." The Biochemical journal **376**(Pt 1): 1-14.

Wallrabe, H. and A. Periasamy (2005). "Imaging protein molecules using FRET and FLIM microscopy." Current Opinion in Biotechnology **16**(1 SPEC. ISS.): 19-27.

Wang, H., O. Bloom, et al. (1999). "HMG-1 as a late mediator of endotoxin lethality in mice." Science **285**(5425): 248-251.

Wang, H., L. Wang, et al. (2004). "Role of histone H2A ubiquitination in Polycomb silencing." Nature **431**(7010): 873-878.

Wang, H., L. Zhai, et al. (2006). "Histone H3 and H4 ubiquitylation by the CUL4-DDB-ROC1 ubiquitin ligase facilitates cellular response to DNA damage." Molecular Cell **22**(3): 383-394.

Watanabe, S., K. Kusama-Eguchi, et al. (1991). "Estimation of polyamine binding to macromolecules and ATP in bovine lymphocytes and rat liver." The Journal of biological chemistry **266**(31): 20803-20809.

Wegel, E., R. Koumproglou, et al. (2009). "Cell type-specific chromatin decondensation of a metabolic gene cluster in oats." The Plant cell **21**(12): 3926-3936.

Wegel, E., R. H. Vallejos, et al. (2005). "Large-scale chromatin decondensation induced in a developmentally activated transgene locus." Journal of cell science **118**(Pt 5): 1021-1031.

Weiss, M., S. Schrimpf, et al. (2010). "Shotgun proteomics data from multiple organisms reveals remarkable quantitative conservation of the eukaryotic core proteome." Proteomics **10**(6): 1297-1306.

Widom, J. (1998). "Structure, dynamics, and function of chromatin in vitro." Annual review of biophysics and biomolecular structure **27**: 285-327.

Woodcock, C. L. (2006). "Chromatin architecture." Current opinion in structural biology **16**(2): 213-220.

Woodcock, C. L. and R. P. Ghosh (2010). "Chromatin higher-order structure and dynamics." Cold Spring Harbor perspectives in biology **2**(5): a000596.

Worman, H. J., C. Ostlund, et al. (2010). "Diseases of the nuclear envelope." Cold Spring Harbor perspectives in biology **2**(2): a000760.

Yankulov, K., K. Yamashita, et al. (1995). "The transcriptional elongation inhibitor 5,6-dichloro-1-beta-D-ribofuranosylbenzimidazole inhibits transcription factor IIH-associated protein kinase." The Journal of biological chemistry **270**(41): 23922-23925.

Yoshida, M., S. Horinouchi, et al. (1995). "Trichostatin A and trapoxin: Novel chemical probes for the role of histone acetylation in chromatin structure and function." BioEssays **17**(5): 423-430.

Yoshida, M., M. Kijima, et al. (1990). "Potent and specific inhibition of mammalian histone deacetylase both in vivo and in vitro by trichostatin A." The Journal of biological chemistry **265**(28): 17174-17179.

Yu, P., B. Huang, et al. (2001). "p15(PAF), a novel PCNA associated factor with increased expression in tumor tissues." Oncogene **20**(4): 484-489.

Yuan, W., T. Wu, et al. (2012). "Dense chromatin activates Polycomb repressive complex 2 to regulate H3 lysine 27 methylation." Science **337**(6097): 971-975.

Zhao, K., E. Kas, et al. (1993). "SAR-dependent mobilization of histone H1 by HMG-I/Y in vitro: HMG-I/Y is enriched in H1-depleted chromatin." EMBO Journal **12**(8): 3237-3247.

Zheng, C., X. Lu, et al. (2005). "Salt-dependent intra- and internucleosomal interactions of the H3 tail domain in a model oligonucleosomal array." The Journal of biological chemistry **280**(39): 33552-33557.